



UNIVERSITÄT DUISBURG-ESSEN
FAKULTÄT FÜR MATHEMATIK

Risk Averse Shape Optimization - Risk Measures and Stochastic Orders

Von der Fakultät Mathematik der
Universität Duisburg-Essen

genehmigte Dissertation zur Erlangung eines
Doktorgrades (Dr. rer. nat.)

von

Martin Pach

aus Duisburg

Referent: Prof. Dr. Rüdiger Schultz

Korreferent: Prof. Dr. Martin Rumpf

Datum der mündlichen Prüfung: 17.12.2013

Acknowledgements

I owe a lot to my supervisor Prof. Dr. Rüdiger Schultz. It was up to him that i developed that passion for mathematics when i started as a freshman at the University of Duisburg-Essen. No less grateful i'm to Prof. Dr. Martin Rumpf who introduced me to the fascinating topic of shape optimization besides numerical mathematics. Their guidance and invaluable advice gave me the ability to work on this challenging but extremely fascinating topic. It was a great chance to work on different areas of mathematics. The frequent opportunities to visit external conferences were very inspiring and a strong motivation to try out something new. Also, i'm very grateful to my many colleagues during the last years for the many helpful discussions and support: Uwe Gotzes, Dimitri Drapkin, Claudia Stangl, Harald Held, Ralf Gollmer, Charlotte Henkel (for proofreading), and Benedict Geihe. I would also like to thank the organizers and members of the priority program SPP-1253 as meetings and conferences have always been a source of inspiration.

Finally and naturally, I thank my family for unconditional support.

This work has been supported by the German science foundation (DFG) priority program SPP-1253: Optimization with Partial Differential Equations as the project Multi-Scale Shape Optimization under Uncertainty, a joint project between Prof. Dr. Sergio Conti, and Prof. Dr. Martin Rumpf, both at University of Bonn, and Prof. Dr. Rüdiger Schultz, University of Duisburg-Essen. The Faculty of Mathematics at the University of Duisburg-Essen provided financial support besides the DFG project.

Zusammenfassung

Thema der vorliegenden Arbeit ist risikoaverse Formoptimierung. Gewöhnliche Formoptimierung umfasst jene Art von Problemen, bei denen die zu optimierende Variable die Form eines Objekts ist. Hier ist das Objekt ein elastischer Körper auf den eine Kraft einwirkt. Basierend auf den Konzepten der Sensitivitätsanalyse bezüglich Form und Topologie wird ein Algorithmus konstruiert, der den elastischen Körper bezüglich seiner elastischen Eigenschaften und dem dabei insgesamt gebrauchten Volumen sukzessiv verbessert. Das Resultat ist eine Struktur, die auf die wirkende Kraft so stabil wie möglich reagiert und dabei möglichst geringes Volumen hat. Diese Art von Problemen benötigen effiziente numerische Löser für die zugrundeliegenden partiellen Differentialgleichungen (hier ist dies das Modell der linearen Elastizität). Dazu werden unterschiedliche Finite Elemente Methoden sowie Ansätze zur Gittergenerierung benutzt. Mit den sogenannten Levelset Methoden wird die Entwicklung der Struktur numerisch beschrieben.

Unsicherheit kommt dann ins Spiel, wenn die berücksichtigten Kräfte als zufällig angenommen werden. So kann nun das elastische Verhalten des Körpers als Zufallsvariable angesehen werden, die von der Form abhängt. In einem ersten Ansatz wird die Form bezüglich verschiedener Risikomaße optimiert, die vor allem in Modellen der (Finanz-) Ökonomie zum Einsatz kommen. Solche Risikomaße definieren unterschiedliche Bewertungen von Risiko, welches einer Zufallsvariable anhängt. Risikoneutrale und risikoaverse Modelle werden zur Formoptimierung benutzt.

Eine neue Perspektive eröffnet sich, wenn *stochastic dominance relations* zur Risikobewertung herangezogen werden. Diese definieren eine Halbordnung auf dem Raum der Zufallsvariablen und ermöglichen es, diese in Relation zu stellen. Ausgehend von einem Benchmark, welches eine gewisse Güte für das Verhalten unter Einwirkung der zufälligen Kräfte beschreibt, kann eine Menge von Formen identifiziert werden, deren Verhalten unter Einwirkung der Kräfte nicht schlechter als das Benchmark ist. Aus dieser Menge werden dann Formen nach einem weiteren Kriterium, z.B. möglichst geringes Volumen, ausgewählt. Auf diese Art und Weise werden Formen mit geringem Volumen gefunden, die aber dennoch die zuvor gestellten Anforderungen erfüllen.

Die vorliegende Arbeit ist eine thematische Weiterentwicklung, Verbesserung und Neuimplementierung meiner Diplomarbeit "Levelsetverfahren in der Shapeoptimierung".

Abstract

In this thesis, risk averse shape optimization of elastic structures is at issue. Shape optimization, in general, deals with the type of problems where the variable to be optimized is the geometry or the shape of a domain. Here, the domain represents an elastic body which is subjected to a force applied. Relying on the concepts of *shape* and *topology sensitivity analysis* an algorithm is implemented which successively improves the elastic body concerning the elastic response and the total volume. Eventually, this procedure results in a body which is, on the one hand, as stiff as possible regarding the force applied and, on the other hand, whose volume is as small as possible. Solving such problems numerically requires an efficient solver for the underlying partial differential equation (here the linearized elasticity model). To this end, different finite element methods and mesh generation approaches are applied. Level set methods are employed to realize the evolution of the elastic body in the discrete setting.

Uncertainty is then introduced by considering the force applied to be random. Thus, the elastic body can be interpreted as a parameter defining a random variable. In a first approach risk measures, which are well-known in economics, are proposed to assess random variables. *Risk measures* give a notion of risk associated with random variables. Risk neutral and risk averse models are discussed and used to optimize over a class of shapes.

A new perspective arises when *stochastic dominance relations* are employed for the assessment of risk. They define an order on the space of random variables and allow to compare these to each other directly. Taking a benchmark random variable associated with a required behavior under uncertainty, a set of acceptable shapes can be identified by comparison to this benchmark. An additional criterion, e.g. minimal volume, is used to select shapes from this set. In that way, shapes with low volume are found which still meet the prescribed requirements.

This work is a thematic advancement, improvement, and complete re-implementation of my diploma thesis "Levelsetverfahren in der Shapeoptimierung" .

Contents

1	Introduction	1
2	Shape Optimization Problem	5
2.1	Linearized Elasticity Model	5
2.2	Shape Sensitivity	11
2.3	Topological Sensitivity	28
2.4	Level-Set-Methods	33
2.5	Solution Algorithm	40
2.6	Numerical Settings	41
2.6.1	Common Settings	44
2.6.2	A Two-scale Approach	46
2.6.3	A Hint to Stochastic: The Two-load Case	47
3	Stochastic Shape Optimization Models	50
3.1	Mean Risk Models	52
3.1.1	Stochastic Programming Perspective	54
3.1.2	Two-Stage Stochastic Programming Perspective	54
3.1.3	Incorporating Stochastic Loadings	55
3.1.4	Results for Mean Risk Models	57
3.2	Stochastic Dominance Models	68
3.2.1	Solution Algorithm	78
3.2.2	Results for Optimization with Stochastic Dominance Constraints	79
4	Final Remarks - State of the Art	95
	References	97

List of Symbols

- $D \subset \mathbb{R}^n$ Working domain containing all admissible domains \mathcal{O} .
- $J(\mathcal{O}) = J(\phi)$ Shape-differentiable objective function.
- U_{ad} The set of all admissible domains.
- Γ^0 Part of the boundary to be optimized.
- Γ_D Homogeneous Dirichlet boundary conditions.
- Γ_N Inhomogeneous Neumann boundary conditions.
- \mathbb{R}^n n-dimensional Euclidian space.
- \mathcal{O} Domain (or shape) representing an elastic body.
- $\epsilon(u)$ Linearized strain tensor.
- \mathcal{A} Stress tensor of the linearized elasticity model.
- ω Random state with finite number of realizations ω_i .
- ϕ Level set function defining the domain \mathcal{O} .
- π Vector of probabilities corresponding to ω .

1 Introduction

The present thesis has two main parts. Shape optimization on the one hand and stochastic programming on the other. A link between those two fields is established by reformulating a shape optimization problem involving uncertainty as a Two-Stage Stochastic Linear Program, see chapter 3. Then, to the best of our knowledge, we introduce a new aspect to shape optimization under uncertainty, namely risk assessment via risk measures and dominance relations, known from finance and operations research.

The term shape or topology optimization is related to those type of problems, where the variable to optimize is the geometry (or shape) of a domain. From a general point of view, this can be seen as an optimal control problem [35], where the domain takes the role of the control variable.

While shape optimization 'only' aims at finding an optimal shape of a domain, topology optimization, in addition, seeks for an optimal topology of the latter. We will just use the term shape optimization, meaning both methods in combination.

There is a broad range of applications in science and industrial engineering for this type of optimization, such as mathematical image registration [91, 106], inverse problems [38], optimal design [130], aerospace design [88, 144, 145] or structural mechanics [6, 29, 85, 111] just to mention a few. Within the last decade this field of research has drawn a lot of attention. Significant progress has been made from an analytical point of view and regarding the numerical implementation, see [66, 161]. The increase in available computing power has boosted applications to even large-scale problems.

Stochastic programming, on the other hand, is strongly related to economics, decision making, and operations research, see the monographs [31, 55, 60, 102, 131, 139]. Within the past century, it has become a substantial subfield of mathematical programming with applications to finance [136], transport problems or energy distribution in networks [171]. In general, stochastic programming comprises problems involving uncertain data, or parameters, in a linear or non-linear setting. When the underlying data are only known to be in certain boundaries, this leads to the field called robust optimization. Whereas, if the data follows a probability distribution, which is known, the problem is labeled stochastic optimization problem.

We rely on a solid knowledge of two-stage stochastic linear programming models and we will transfer concepts for handling uncertainty from this field to shape optimization.

In this thesis, we deal with shape optimization of elastic structures subjected to forces which are considered to be uncertain, i.e., they follow a probability distribution. We consider a linearized elasticity model, that is discussed in section 2.1.

The prototype of a deterministic shape optimization reads as

$$\min\{J(\mathcal{O}) : \mathcal{O} \in \mathcal{U}_{\text{ad}}\} \quad (1.1)$$

where $J : \mathcal{U}_{\text{ad}} \mapsto \mathbb{R}$ is a so-called shape functional, representing a certain quality of the domain (shape) $\mathcal{O} \subset \mathbb{R}^d$ ($d=2,3$). \mathcal{U}_{ad} is the set of admissible shapes. Usually, these are required to have some boundary regularity and are contained in a so-called working domain $D \subset \mathbb{R}^d$. A classical choice for J is the elastic energy, the so-called

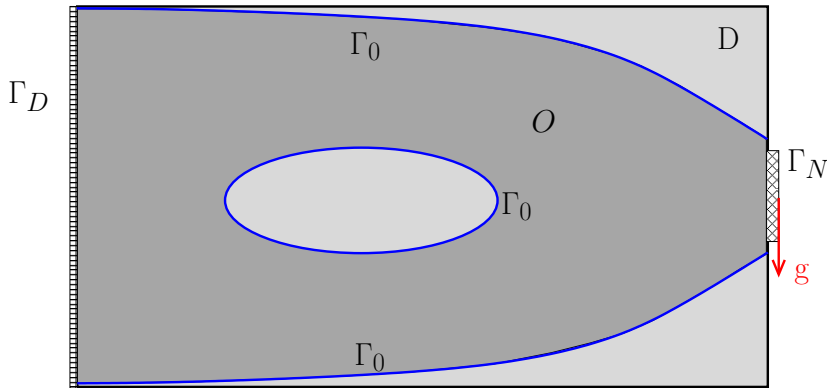


Figure 1.1: The configuration of a shape optimization problem is depicted. This is a typical setting for the optimization of an elastic structure and frequently considered in literature. Thus, it serves well as a benchmark test to check the correctness of the optimization algorithm. We see the working domain D and the shape \mathcal{O} contained in it. The boundary to the left is supposed to be Dirichlet boundary (Γ_D) and the part of the boundary on the right (Γ_N) is of Neumann type and subject to the force g . These parts of the boundary are fixed during the optimization process. The remaining part of $\partial\mathcal{O}$ (Γ_0) is to be optimized. This setting results in a cantilever like structure, see Fig. (2.14).

compliance functional, which is a measure for the overall elastic energy contained in the body \mathcal{O} , as a result of forces applied to it. Minimizing the compliance functional J yields a shape which responds as rigidly as possible when forces are applied.

Usually, analytical solutions are not available for shape optimization problems. Therefore, these are solved numerically using gradient descent methods. The shape and topology sensitivity analyses (see section 2.2 and section 2.3) provide information how to improve a given shape by the so-called *shape gradient* and *topological gradient*. Doing so, a sequence of shapes with decreasing values of the functional J is generated iteratively.

The evaluation of the functional J , as well as the computation of the *shape* and *topological gradient*, require the solution of the underlying elasticity model for each iteration step. Thus, solving the PDE constitutes the main part of the computational effort and an efficient and accurate numerical solver is crucial for the optimization process, see section 2.6.

Shape optimization models involving uncertainties have been investigated for different applications, for example, in aerodynamic design [98,143]. and structural design as well, [7, 8, 11, 20, 25, 48, 107]. There, uncertainties with respect to geometry, material properties, and loadings are considered. Mostly, these models are based on an expected-value (Multiload case) optimization or robust (worst case) optimization approach. We enrich the selection of existing approaches with a new type: models for assessment of risk via risk-measures and dominance relations.

As said, we consider the situation when the forces (loadings) applied are random variables. Then the functional $J(\mathcal{O})$ becomes a real-valued random variable, too. Thus, \mathcal{O} can be seen as a parameter defining the random variable $J(\mathcal{O}, \omega)$, where ω denotes the random state. So, seeking an optimal \mathcal{O} is equivalent to seeking an "optimal" random variable $J(\mathcal{O}, \omega)$. And this calls for a proper ranking of random variables.

A first choice, of course, is a ranking according to the expected value, which is risk neutral. Results discussed in Subsection 2.6.3 demonstrate the advantage of this model in the presence of uncertainty.

But, this approach completely ignores the variability of random variables. For instance, if for some reason, realizations of $J(\mathcal{O}, \omega)$ above a certain threshold are unacceptable, the need for refined models arises. In the field of stochastic programming, risk-measures for a broad range of applications are studied, see the monographs [64, 114, 127, 153]. We proposed assessment of risk according to the *expected excess* and *excess probability* models in previous works, [51, 52, 90]. In these, so-called risk-averse models, assessment of risk is assigned to a statistical parameter $\eta \in \mathbb{R}$ ($\eta > 0$), which serves as the threshold mentioned above. While the expected-excess model considers how much a random variable exceeds η in the mean, the excess-probability model takes account of the probability that η is exceeded. These models are at issue in section 3.1.

A different perspective is obtained, when we employ stochastic orders for the formulation of an optimization problem under uncertainty. Stochastic orders are an established issue in the theory of decision making under risk, see [59, 120–122, 134]. They define (partial) orders on the space of distribution functions, and allow to compare random variables by comparison of the corresponding distribution functions.

With this tools at hand, we proceed as follows:

Suppose a benchmark random variable is prescribed, then, instead of heading directly for "best" random variables, ranking by stochastic orders enables to identify a set of "acceptable" random variables by comparing those to the benchmark. This viewpoint allows for more flexibility. For instance, rather than requiring that $J(\mathcal{O}, \omega)$ must not exceed the deterministic value of, say, 50 (that would be the threshold η), we might wish to allow for values up to 60, on the one hand, and to require that 35 not to be exceeded with 40% and 40 with 90% probability, on the other hand. In this way, risk

aversion is not governed by 'just a real number' but by a benchmark, which allows to include distribution information.

By this pre-selection, we have identified a set \mathcal{S}_{acc} of shapes \mathcal{O} , each representing a random variable $J(\mathcal{O}, \omega)$, whose elastic behavior under uncertainty meets the particular requirements. From this set \mathcal{S}_{acc} we can choose according to an additional criterion, for instance: shapes with low volume are preferable.

Then the objective would be the volume, which is to be minimized over the set \mathcal{S}_{acc} , each member \mathcal{O} representing a random variable $J(\mathcal{O}, \omega)$, which is acceptable in the above sense.

This new approach gives a different notion of how to treat risk in the context of shape optimization. We will conclude with a discussion of the latter in section 3.2.

2 Shape Optimization Problem

2.1 Linearized Elasticity Model

As stated before, we focus on the elastic response of the body \mathcal{O} to be optimized. Thus a brief review of the underlying elasticity model will be given. In this work, we restrict our considerations to the basic model of linearized elasticity. Furthermore, we assume the body \mathcal{O} to consist of an isotropic, homogeneous material. Let $\mathcal{O} \subset \mathbb{R}^d$ ($d = 2$ or 3) be an open bounded set whose boundary is split into two disjunct parts

$$\partial\mathcal{O} = \Gamma_N \cup \Gamma_D \quad \Gamma_N \cap \Gamma_D = \emptyset$$

with Dirichlet boundary conditions on Γ_D and Neumann boundary conditions on Γ_N . The body \mathcal{O} is subjected to volume forces denoted by \mathbf{f} and boundary loads denoted by \mathbf{g} . The transformation \mathcal{O} undergoes is described by the deformation

$$\phi : \mathcal{O} \rightarrow \mathbb{R}^d$$

or in terms of displacement \mathbf{u} (cf. Fig. (2.1)).

$$\mathbf{u} : \mathcal{O} \rightarrow \mathbb{R}^d, \quad \phi = \mathbb{I} + \mathbf{u}$$

In elasticity theory, the Cauchy-Green strain tensor

$$\mathbf{C} := \nabla\phi^T \cdot \nabla\phi$$

is decisive for the local modification in length. The deviation from the identity defined as

$$\mathbf{E} := (\mathbf{C} - \mathbb{I})$$

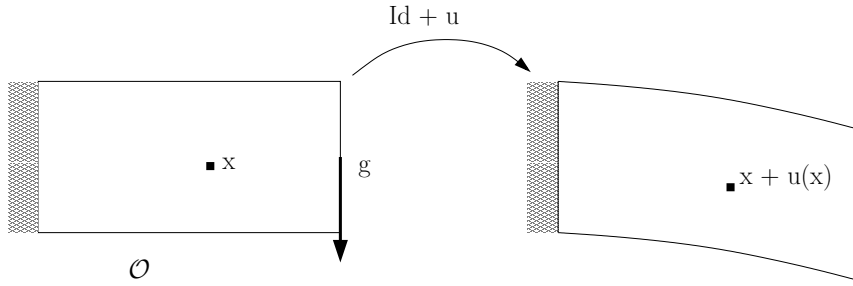


Figure 2.1: Illustration of the displacement u caused by a surface force g .

defines the strain. In matrices notation E reads as

$$E_{ij} := \frac{1}{2} (u_{i,j} + u_{j,i}) + \frac{1}{2} \sum_k u_{k,i} \cdot u_{k,j}$$

In linearized elasticity theory, the terms of quadratic order in E are truncated and a symmetric approximation is obtained

$$\epsilon_{ij} := \frac{1}{2} (u_{i,j} + u_{j,i}) \quad (2.1)$$

which in this thesis will be referred to as the linearized strain tensor $\epsilon = \epsilon(u)$. This is a first linearization; a further linearization arises by taking Hooke's linear material law as a basis, obtaining the following linear relation between the stress and strain tensors \mathcal{A} and $\epsilon(u)$, respectively.

$$\mathcal{A}(\epsilon(u)) := 2\mu\epsilon(u) + \lambda(\text{tr}\epsilon(u))\mathbb{I} \quad (2.2)$$

Here, μ and λ are the so called Lamé-coefficients which represent the material properties of the body \mathcal{O} . A scalar product on the space of tensors is given by

$$\mathcal{A} : \mathcal{B} = \sum_{i,j=1}^3 \mathcal{A}_{ij} \mathcal{B}_{ij} = \text{tr} [\mathcal{A}^T \mathcal{B}] \quad (2.3)$$

for $(d \otimes d)$ -tensors \mathcal{A}, \mathcal{B} .

To sum up, in linearized elasticity, only terms of first order of the displacement u are considered, both in the kinematic and material laws.

A crucial axiom in mechanics is that, in state of equilibrium, all forces and moment of forces sum up to zero. This includes volume and surface forces. The following variational formulation reflects this principle. Let $\mathcal{E}_{\text{elast}}(u)$ the elastic energy, i.e.,

$$\mathcal{E}_{\text{elast}}(u) := \int_{\mathcal{O}} \left[\frac{1}{2} \cdot \mathcal{A}(\epsilon(u)) : \epsilon(u) - f \cdot u \right] dx - \int_{\partial\mathcal{O}} g \cdot u \, d\nu \quad (2.4)$$

then the minimizer u

$$u = \arg \min_v \mathcal{E}_{\text{elast}}(v)$$

is the solution of the Lamé partial differential equation

$$\begin{aligned} -\operatorname{div}(\mathcal{A}(\epsilon(u))) &= f && \text{in } \mathcal{O} \\ u &= 0 && \text{on } \Gamma_D \\ \mathcal{A}(\epsilon(u)) \cdot n &= g && \text{on } \Gamma_N \end{aligned} \quad (2.5)$$

in case of homogeneous Dirichlet Boundary Conditions on Γ_D .

In what follows we will derive this in a more formal setting. Recall the notation of Sobolov spaces

$$H^{m,p}(\mathcal{O}) := \{v \in L^p(\mathcal{O}, \mathbb{R}) : \partial^\alpha v \in L^p(\mathcal{O}, \mathbb{R}) \forall |\alpha| \leq m\}$$

for $m \in \mathbb{N}_0$ and $1 \leq p < \infty$ and a multi index α with $\partial^\alpha v$ denoting the corresponding partial derivative (in the sense of distributions), see further [3,10,73]. Where $L^p(\mathcal{O}, \mathbb{R})$ denotes the Lebesgue-spaces. Equipped with the norm

$$\|v\|_{m,p}(\mathcal{O}) := \left(\int_{\mathcal{O}} \sum_{|\alpha| \leq m} |\partial^\alpha v|^p dx \right)^{\frac{1}{p}}$$

$H^{m,p}(\mathcal{O})$ is a Banach space. If $p = 2$, the space $H^{m,2}(\mathcal{O})$ is a Hilbert space with the inner product

$$(u, v)_{H^{m,2}(\mathcal{O})} = \int_{\mathcal{O}} \sum_{|\alpha| \leq m} \partial^\alpha u(x) \cdot \overline{\partial^\alpha v(x)} dx$$

It is customary to write $H^m(\mathcal{O})$ instead of $H^{m,2}(\mathcal{O})$ and $\|v\|_p$ instead of $\|v\|_{m,p}(\mathcal{O})$. For vector-valued functions we introduce the notation $H^m(\mathcal{O})^d$ which means each component is in $H^m(\mathcal{O})$. As we will derive (2.5) in its weak form, $p=1$ will provide sufficient regularity although in (2.5) second order derivatives occur. Dealing only with homogeneous Dirichlet boundary conditions, we define the solution space as :

$$H_{\Gamma_D}^1(\mathcal{O})^d := \{v \in H^1(\mathcal{O})^d : v|_{\Gamma_D} = 0\}$$

If we assume \mathcal{O} to be bounded with a Lipschitz boundary, then expression $v|_{\Gamma_D} = 0$ is well defined due to the trace theorem for Sobolov spaces. For the rest of this chapter we will use the notation $\mathcal{V} := H^m(\mathcal{O})^d$.

Lemma 2.1 (Korn's inequality). Let $\mathcal{O} \subset \mathbb{R}^d$ be an open bounded domain with a piecewise smooth boundary $\partial\mathcal{O}$. Furthermore $\Gamma_D \subset \partial\mathcal{O}$ is required to have a positive

$(d-1)$ -dimensional (Lebesgue) measure. Then there exists a constant $c := c(\mathcal{O}, \Gamma_D) > 0$ such that

$$\int_{\mathcal{O}} \epsilon(v) : \epsilon(v) \, dx \geq c \cdot \|v\|_1^2 \quad \forall v \in H_{\Gamma_D}^1(\mathcal{O})^d$$

holds.

Proof :

See [33, p. 290].

In the sequel, we sketch a proof of existence for a solution $u \in H_{\Gamma_D}^1(\mathcal{O})^d$ to the weak formulation of problem (2.5). The intrigued reader is referred to [33, 50] for a more detailed discussion. A weak formulation (as variational problem) only yields weak solutions, but on the other hand opens up possibilities for numerical treatment. Before we start we recall Green's formula for tensor products.

Lemma 2.2 (Green's formula). For $v \in H^1(\mathcal{O})^d$ and the symmetric tensor $\mathcal{A}(\epsilon(v)) := 2\mu\epsilon(v) + \lambda(\text{tr}\epsilon(v))\mathbb{I}$ it holds

$$-\int_{\mathcal{O}} \text{div}\mathcal{A}(\epsilon(v)) \cdot v \, dx = \int_{\mathcal{O}} \mathcal{A}(\epsilon(v)) : \epsilon(v) \, dx - \int_{\partial\mathcal{O}} \mathcal{A}(\epsilon(v))n \cdot v \, d\nu$$

Proof :

For sake of readability we write \mathcal{A} instead of $\mathcal{A}(\epsilon(v))$ and use Einstein's convention (repeated index notation). The outer normal of $\partial\mathcal{O}$ is denoted by n .

$$\begin{aligned} -\int_{\mathcal{O}} \text{div}\mathcal{A} \cdot v \, dx &= -\int_{\mathcal{O}} \mathcal{A}_{ij,j} v_i \, dx \\ &= -\frac{1}{2} \int_{\mathcal{O}} \mathcal{A}_{ij,j} v_i + \mathcal{A}_{ij,i} v_j \, dx \\ &= \frac{1}{2} \int_{\mathcal{O}} \mathcal{A}_{ij} v_{i,j} + \mathcal{A}_{ij} v_{j,i} \, dx - \frac{1}{2} \int_{\partial\mathcal{O}} (\mathcal{A}_{ij} v_i)n_j + (\mathcal{A}_{ij} v_j)n_i \, d\nu \\ &= \int_{\mathcal{O}} \mathcal{A}_{ij} \frac{1}{2}(v_{i,j} + v_{j,i}) \, dx - \int_{\partial\mathcal{O}} (\mathcal{A}_{ij} v_i)n_j \, d\nu \\ &= \int_{\mathcal{O}} \mathcal{A}_{ij} \epsilon(v)_{ij} \, dx - \int_{\partial\mathcal{O}} v \mathcal{A} n \, d\nu \\ &= \int_{\mathcal{O}} \mathcal{A} : \epsilon(v) \, dx - \int_{\partial\mathcal{O}} \mathcal{A}n \cdot v \, d\nu \end{aligned}$$

□

Now we return to the strong formulation (2.5). Let $f \in L^2(\mathcal{O})^d$ and $g \in \mathcal{V}$, furthermore let $\lambda > 0$, $\mu > 0$. Then multiplying equation 1 in (2.5) with $v \in \mathcal{V}$ and integrating over \mathcal{O} yields

$$\begin{aligned}
& - \int_{\mathcal{O}} \operatorname{div}(\mathcal{A}(\epsilon(u))) \cdot v \, dx = \int_{\mathcal{O}} f \cdot v \, dx \\
\Leftrightarrow & \int_{\mathcal{O}} \mathcal{A}(\epsilon(u)) : \epsilon(v) \, dx - \int_{\partial\mathcal{O}} \mathcal{A}(\epsilon(u))n \cdot v \, d\nu = \int_{\mathcal{O}} f \cdot v \, dx \\
\Leftrightarrow & \int_{\mathcal{O}} \mathcal{A}(\epsilon(u)) : \epsilon(v) \, dx = \int_{\mathcal{O}} f \cdot v \, dx + \int_{\partial\mathcal{O}} \mathcal{A}(\epsilon(u))n \cdot v \, d\nu \\
\Leftrightarrow & \int_{\mathcal{O}} \mathcal{A}(\epsilon(u)) : \epsilon(v) \, dx = \int_{\mathcal{O}} f \cdot v \, dx + \int_{\partial\mathcal{O}} g \cdot v \, d\nu
\end{aligned}$$

Identifying the left hand side as a bilinear form $a(u, v) := \int_{\mathcal{O}} \mathcal{A}(\epsilon(u)) : \epsilon(v) \, dx$ and the right hand side as a linear functional $L(v) := \int_{\mathcal{O}} f \cdot v \, dx + \int_{\partial\mathcal{O}} g \cdot v \, d\nu$, we can summarize the weak formulation of (2.5) in the equation:

$$a(u, v) = L(v) \quad \forall v \in \mathcal{V} \quad (2.6)$$

If there exist an $u \in \mathcal{V}$ fulfilling (2.6) it is called a weak solution. For proving existence and uniqueness we want to apply the Lax-Milgram theorem. Thus it is required the bilinear form $a(u, v)$ to be coercive and bounded, and the linear functional $L(v)$ to be bounded. For the functional L we get by the Cauchy-Schwartz inequality

$$\begin{aligned}
|L(v)| &= \left| \int_{\mathcal{O}} f \cdot v \, dx + \int_{\partial\mathcal{O}} g \cdot v \, d\nu \right| \\
&\leq \|f\|_{L^2(\mathcal{O})} \cdot \|v\|_{H^1(\mathcal{O})} + \|g\|_{L^2(\partial\mathcal{O})} \cdot \|v\|_{L^2(\partial\mathcal{O})}
\end{aligned}$$

Having in mind the continuity of the trace operator

$$\|v|_{\partial\mathcal{O}}\|_{L^2(\partial\mathcal{O})} \leq c(\mathcal{O})\|v\|_{H^1(\mathcal{O})}$$

we eventually get

$$\begin{aligned}
|L(v)| &\leq \|f\|_{L^2(\mathcal{O})} \cdot \|v\|_{H^1(\mathcal{O})} + c(\mathcal{O})\|g\|_{H^1(\mathcal{O})} \cdot \|v\|_{H^1(\mathcal{O})} \\
&= (\|f\|_{L^2(\mathcal{O})} + c(\mathcal{O})\|g\|_{H^1(\mathcal{O})}) \cdot \|v\|_{H^1(\mathcal{O})}
\end{aligned}$$

Boundedness of the bilinear form $a(u, v)$ is obtained directly by the Cauchy-Schwartz inequality:

$$\begin{aligned}
|a(u, v)| &= \left| \int_{\mathcal{O}} \mathcal{A}(\epsilon(u)) : \epsilon(v) \, dx \right| \\
&\leq \|u\|_{H^1(\mathcal{O})} \cdot \|v\|_{H^1(\mathcal{O})}
\end{aligned}$$

It remains to show that $a(\cdot, \cdot)$ is coercive.

$$\begin{aligned}
|a(v, v)| &= \left| \int_{\mathcal{O}} \mathcal{A}(\epsilon(v)) : \epsilon(v) \, dx \right| \\
&= \left| \int_{\mathcal{O}} (2\mu\epsilon(v) + \lambda(\text{tr}\epsilon(v))\mathbb{I}) : \epsilon(v) \, dx \right| \\
&= \left| \int_{\mathcal{O}} 2\mu\epsilon(v) : \epsilon(v) + \lambda(\text{tr}\epsilon(v))\mathbb{I} : \epsilon(v) \, dx \right| \\
&= \left| \int_{\mathcal{O}} 2\mu\epsilon(v) : \epsilon(v) + \lambda(\text{tr}\epsilon(v))^2 \, dx \right| \\
&\geq \left| \int_{\mathcal{O}} 2\mu\epsilon(v) : \epsilon(v) \, dx \right| \\
&\geq 2\mu c \|v\|_{H^1(\mathcal{O})}^2
\end{aligned}$$

The last estimation is due to Korn's inequality. The Lax-Milgram theorem then guarantees existence and uniqueness of a weak solution u for (2.6). For a more detailed discussion we refer to [33]. Later in this thesis, shape optimization with linearized elasticity will be pursued. Therefore, we discuss an analytical framework for shape derivatives, preparing subsequent numerical considerations.

2.2 Shape Sensitivity

Shape optimization signifies those type of problems, where the variable to optimize is the geometry of a structure or domain. Contrary to optimization in Hilbert spaces, this class of optimization problems requires special techniques. Therefore, we will discuss the concept of shape derivatives, which provides information of how to change (or vary) a domain to improve it.

A general formulation of a shape optimization problem reads as

$$\min\{J(\mathcal{O}) : \mathcal{O} \in U_{ad}\}$$

where U_{ad} is a class of admissible domains and $J : \mathcal{O} \mapsto \mathbb{R}$ a cost functional to be minimized over U_{ad} . A first observation indicates that the class U_{ad} in general does not have any linear or convex structure. Thus, it is difficult to identify necessary optimality conditions known from optimization in real vector spaces or Hilbert spaces. These conditions give information about the behavior of the objective in a neighborhood of a local optimum and usually are obtained by a so-called variational approach. For instance, the gradient of a real valued function would provide such information. Due to the lack of a vector space structure of the class of admissible shapes U_{ad} , a first step is to define a characterization of the neighborhood of a domain \mathcal{O} .

Definition 2.3 (Local Variations). Let $V \in C^1(\mathbb{R}^d, \mathbb{R}^d)$ be a vector field. We define the map :

$$T(s, x) := x + sV(x) \quad \forall x \in \mathbb{R}^d, \quad s \geq 0$$

Then for s sufficiently small, the map

$$T(s, \cdot) : \mathbb{R}^d \rightarrow \mathbb{R}^d, \quad x \mapsto x + sV(x) \quad \forall x \in \mathbb{R}^d, \quad s \geq 0$$

is a local C^1 -diffeomorphism. This follows from the fact that

$$(\mathbb{I} + sV) \in C^1(\mathbb{R}^d, \mathbb{R}^d) \quad , \quad \text{and} \quad \lim_{s \searrow 0} \det(\mathbb{I} + sV) = 1,$$

and applying the inverse function theorem. Thus, for every open bounded domain \mathcal{O} there exists a $s_0 > 0$ such that $T_{s_0}(\cdot)$ is a diffeomorphism and it holds $\mathcal{O}_{s_0} = T_{s_0}(\mathcal{O})$. Whereas $T_s(\mathcal{O})$ can be read as

$$T_s(\mathcal{O}) := \{T_s(x) : \forall x \in \mathcal{O}\}$$

with $T_s(x) := T(s, x) \quad \forall x \in \mathcal{O}$.

This type of variation is referred to as *perturbation of identity*. See [58] and [167]

for further details. Another approach for variations of a domain \mathcal{O} is referred to as *velocity (speed) method* which is applicable in more general settings. Again, we consider a vector field V and look at the solution $x : \mathbb{R}^+ \times \mathbb{R}^d \rightarrow \mathbb{R}^d$ for the initial value problem

$$\begin{aligned} \dot{x}(s, \bar{x}) &= V(x(s, \bar{x})) & \forall s \geq 0 \\ x(0, \bar{x}) &= \bar{x} & \forall \bar{x} \in \mathbb{R}^d \end{aligned}$$

for which a unique solution exists if V is Lipschitz continuous, that is $V \in C^{0,1}(\mathbb{R}^d, \mathbb{R}^d)$. Then the Picard-Lindelöf theorem ensures solvability. Variations of \mathcal{O} are generated by the mapping $T_s : \mathbb{R}^d \rightarrow \mathbb{R}^d$, i.e.,

$$T_s(\bar{x}) := x(s, \bar{x}) \quad \forall s \geq 0 \quad \forall \bar{x} \in \mathbb{R}^d$$

Thus, variations \mathcal{O}_s of \mathcal{O} are described as $\mathcal{O}_s := T_s(\mathcal{O})$.

Remark 2.4. In most settings, both types of variations, *velocity method* and *perturbation of identity*, provide the same results for first order shape derivatives. As we will see later, shape derivatives, in our considerations, only depend on restrictions $V|_{\partial\mathcal{O}}$ of vector fields to the boundary $\partial\mathcal{O}$ of \mathcal{O} . But there are settings in which this no longer holds, e.g., \mathcal{O} being a subset of a submanifold of \mathbb{R}^d . See [58] for a detailed discussion on this topic. In this case, shape derivatives obtained by the two different methods do not coincide.

Such cases will not be considered, thus, the *perturbation of identity* is sufficient for the construction of variations.

Definition 2.5 (Shape derivative). Let $V \in C^1(\mathbb{R}^d, \mathbb{R}^d)$ be a vector field and $T_s(\cdot)$ as defined above ($s > 0$). Then, the functional J has an *Eulerian semiderivative* at \mathcal{O} in direction V if the limit

$$\lim_{s \searrow 0} \frac{J(T_s(\mathcal{O})) - J(\mathcal{O})}{s} = \lim_{s \searrow 0} \frac{J(\mathcal{O}_s) - J(\mathcal{O})}{s} \quad (2.7)$$

exists. It will be denoted by $dJ(\mathcal{O}, V)$. Assume J has a derivative at \mathcal{O} in all directions $V \in \mathcal{V} := C^1(\mathbb{R}^d, \mathbb{R}^d)$ and the map

$$V \mapsto dJ(\mathcal{O}, V) : \mathcal{V} \rightarrow \mathbb{R}$$

is linear and continuous. Then this map will be referred to as the *shape differential* or *shape gradient*, denoted by $dJ(\mathcal{O})$, of J in the topological dual space \mathcal{V}' of \mathcal{V} .

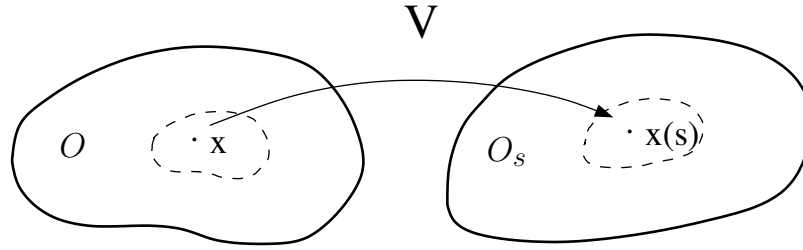


Figure 2.2: Deformation of \mathcal{O} by the vector field V .

A short example will illustrate how these variations lead to shape derivatives.

Example 2.6.

Let $V \in C^1(\mathbb{R}^d, \mathbb{R}^d)$ and suppose the boundary of \mathcal{O} is sufficiently smooth, that is at least a Lipschitz boundary. A more general situation is considered in [57]. For a given function $\vartheta \in C^1(\mathbb{R}^d, \mathbb{R}^d)$, we define the shape functional

$$J(\mathcal{O}) = \int_{\mathcal{O}} \vartheta(x) dx.$$

J is differentiable at \mathcal{O} in direction V and the derivative takes the form:

$$\begin{aligned} dJ(\mathcal{O}, V) &= \int_{\mathcal{O}} \operatorname{div}(V(x)\vartheta(x)) dx \\ &= \int_{\partial\mathcal{O}} V(x) \cdot n(x)\vartheta(x) d\nu \end{aligned}$$

.

Proof :

The map $T_s(\cdot)$ is for s sufficient small a C^1 -diffeomorphism with $T_s(\mathcal{O}) = \mathcal{O}_s$.

$$J(\mathcal{O}_s) = \int_{\mathcal{O}_s} \vartheta(x) dx = \int_{\mathcal{O}} \vartheta(T_s^{-1}(x)) |\det DT_s(x)| dx$$

$DT_s(x)$ being the Jacobian of $T_s(\cdot)$ with respect to x . Furthermore, it holds

$$\begin{aligned} dJ(\mathcal{O}, V) &= \left. \frac{\partial J(\mathcal{O}_s)}{\partial s} \right|_{s=0} = \left. \frac{\partial}{\partial s} \int_{\mathcal{O}} \vartheta(T_s(x)) |\det DT_s(x)| dx \right|_{s=0} \\ &= \int_{\mathcal{O}} \left. \frac{\partial}{\partial s} (\vartheta(T_s(x)) |\det DT_s(x)|) \right|_{s=0} dx \end{aligned}$$

$$\begin{aligned}
&= \int_{\mathcal{O}} \frac{\partial}{\partial s} (\vartheta(T_s(x))) \Big|_{s=0} |\det DT_0(V)(x)| \\
&\quad + \vartheta(T_0(V)(x)) \frac{\partial}{\partial s} (|\det DT_s(x)|) \Big|_{s=0} dx \\
&= \int_{\mathcal{O}} \frac{\partial}{\partial s} (\vartheta(T_s(x))) \Big|_{s=0} \\
&\quad + \vartheta(x) \frac{\partial}{\partial s} (|\det DT_s(x)|) \Big|_{s=0} dx \tag{2.8}
\end{aligned}$$

. Considering Taylor's formula of $T_s(\cdot)$ with respect to s , it is

$$\begin{aligned}
T_s(x) &= T_0(x) + \frac{\partial}{\partial s} T_s(x) \Big|_{s=0} s + o(s^2) \\
&= \mathbb{I} + V(x) s + \sigma(s^2).
\end{aligned}$$

So we have the following expression for the Jacobian of $T_s(x)$

$$DT_s(x) = \mathbb{I} + DV(x) s + \sigma(s^2).$$

Next, we apply the following relation to (2.8)

$$\frac{\partial}{\partial s} (\det DT_s(x)) \Big|_{s=0} = \operatorname{tr}(DV(x)) = \operatorname{div}(V(x))$$

Finally, the shape derivative takes the form

$$\begin{aligned}
dJ(\mathcal{O}, V) &= \int_{\mathcal{O}} \frac{\partial}{\partial s} (\vartheta(T_s(x))) \Big|_{s=0} + \vartheta(x) \operatorname{div}(V(x)) dx \\
&= \int_{\mathcal{O}} \nabla \vartheta(x) \frac{\partial}{\partial s} (T_s(x)) \Big|_{s=0} + \vartheta(x) \operatorname{div}(V(x)) dx \\
&= \int_{\mathcal{O}} \nabla \vartheta(x) V(x) + \vartheta(x) \operatorname{div}(V(x)) dx \\
&= \int_{\mathcal{O}} \operatorname{div}(V(x) \vartheta(x)) dx \\
&= \int_{\partial \mathcal{O}} V(x) \cdot n(x) \vartheta(x) d\nu
\end{aligned}$$

with n denoting the outer normal of \mathcal{O} .

This rather simplistic example gives just an idea how to generate shape differentials since the functional J does not depend on a solution of a state equation, e.g., the solution of the elasticity model discussed in the preceding chapter. In that situation, the calculation gets more subtle as one has to deal with the variation of the state solution as well. For instance, consider the compliance of the body \mathcal{O} as shape functional J to be optimized. It is

$$J(\mathcal{O}) = \int_{\mathcal{O}} \mathcal{A}(\epsilon(u)) : \epsilon(u) dx \quad (2.9)$$

which is a measure for the strain energy contained within \mathcal{O} , and u is the solution to the linearized elasticity model (2.5). Thus, the shape functional becomes

$$J(\mathcal{O}) := J(\mathcal{O}, u(\mathcal{O}))$$

and the derivative in definition 2.5 then reads as

$$\lim_{s \searrow 0} \frac{J(\mathcal{O}_s) - J(\mathcal{O})}{s} = \lim_{s \searrow 0} \frac{J(\mathcal{O}_s, u(\mathcal{O}_s)) - J(\mathcal{O}, u(\mathcal{O}))}{s} = \lim_{s \searrow 0} \frac{J(\mathcal{O}_s, u_s) - J(\mathcal{O}, u_0)}{s}$$

with u_s being the solution to (2.5) on \mathcal{O}_s . So, the crucial part for the computation of a shape differential is the asymptotic behavior of u_s as s tends to zero. And the question arises whether continuity or differentiability of u_s or at least of the shape functional can be established. This will be at issue in the subsequent discussion.

Linearized Elasticity as state constraint

Shape sensitivity calculus has been widely analyzed and there are different approaches to proof continuity and differentiability of shape functionals. See, e.g., the monographs [58, 86, 104, 164]. One approach, maybe the most commonly used, is referred to as the *reduced gradient method*. It is based on a straight forward formal differentiation of the reduced functional $J(\mathcal{O}, u(\mathcal{O}))$ using the chain rule. As a consequence, shape differentiability of the state u with respect to \mathcal{O} has to be provided.

We may rely of an alternative approach based on the concept of a Lagrangian formulation. Here, the state equation and its dual are realized in a weak formulation as side constraints of a Lagrangian functional. The shape derivative of the functional J then coincides with the derivative of the Lagrangian with respect to \mathcal{O} . Thus, it is not necessary to compute the above mentioned derivative of the state u .

Since we consider the linearized elasticity model as state equation, there will be a short interlude assembling some lemma and auxiliary calculations which will be helpful for the calculations of shape derivatives.

So, recall the linearized elasticity model (2.5):

$$\begin{aligned} -\operatorname{div}(\mathcal{A}(\epsilon(u))) &= f && \text{in } \mathcal{O} \\ u &= 0 && \text{on } \Gamma_D \\ \mathcal{A}(\epsilon(u)) \cdot n &= g && \text{on } \Gamma_N \end{aligned} \quad (2.10)$$

with $u \in H_{\Gamma_D}^1(\mathcal{O})^d$, $f \in L^2(\mathcal{O})^d$ and $g \in H^1(\mathcal{O})^d$.

Then some properties of the stress tensor \mathcal{A} are assembled in the following corollary.

Corollar 2.7. For the stress tensor \mathcal{A} and the strain tensor $\epsilon(u)$ from (2.2) and (2.1) sufficient smooth it holds $\forall \vartheta, \varphi \in H^1(\mathcal{O})^d$:

$$\begin{aligned} \text{(i)} \quad \int_{\Omega} \mathcal{A}\epsilon(\vartheta) : \epsilon(\varphi) \, dx &= \int_{\Omega} \operatorname{div}(\mathcal{A}\epsilon(\vartheta)) \cdot \varphi \, dx + \int_{\partial\Omega} \mathcal{A}\epsilon(\vartheta) \cdot n \cdot \varphi \, d\nu \\ \text{(ii)} \quad \mathcal{A}(\epsilon(\vartheta)) : \epsilon(\varphi) &= \mathcal{A}(\epsilon(\varphi)) : \epsilon(\vartheta) \end{aligned}$$

Proof :

(i) For the sake of readability, Einstein notation is used and we write \mathcal{A} instead of $\mathcal{A}\epsilon(\vartheta)$

$$\begin{aligned} \int_{\Omega} \mathcal{A} : \epsilon(\varphi) \, dx &= \frac{1}{2} \int_{\Omega} \mathcal{A}_{ij}(\varphi_{ij} + \varphi_{ji}) \, dx \\ &= -\frac{1}{2} \int_{\Omega} \mathcal{A}_{ij,j} \varphi_i + \mathcal{A}_{ij,i} \varphi_j \, dx + \frac{1}{2} \int_{\partial\Omega} \mathcal{A}_{ij}(\varphi_i n_j + \varphi_j n_i) \, d\nu \\ &= - \int_{\Omega} \operatorname{div}(\mathcal{A}) \cdot \varphi \, dx + \int_{\partial\Omega} \varphi \cdot \mathcal{A} \cdot n \, d\nu \end{aligned}$$

(ii) With the definition of the scalar product (2.3) in mind we have

$$\begin{aligned} \mathcal{A}(\epsilon(\vartheta)) : \epsilon(\varphi) &= \lambda \operatorname{tr}(\epsilon(\vartheta)) \mathbb{I} : \epsilon(\varphi) + 2\mu \epsilon(\vartheta) : \epsilon(\varphi) \\ &= \lambda \operatorname{tr}(\epsilon(\vartheta)) \operatorname{tr}(\epsilon(\varphi)) + 2\mu \operatorname{tr}(\epsilon(\vartheta) \cdot \epsilon(\varphi)) \\ &= \lambda \operatorname{tr}(\epsilon(\varphi)) \mathbb{I} : \epsilon(\vartheta) + 2\mu \epsilon(\varphi) : \epsilon(\vartheta) \\ &= \mathcal{A}(\epsilon(\varphi)) : \epsilon(\vartheta) \end{aligned}$$

Following the idea of (2.6) we take account of a boundary functional, which will be very useful later in this chapter.

Lemma 2.8.

Let $V \in C^1(\mathbb{R}^d, \mathbb{R}^d)$ and suppose the boundary of \mathcal{O} is of class C^2 . Then h denotes the mean curvature of $\partial\mathcal{O}$ and n the outer normal. For a given function $\vartheta \in C^1(\mathbb{R}^d, \mathbb{R}^d)$ we define the shape functional

$$J(\mathcal{O}) = \int_{\partial\mathcal{O}} \vartheta \, d\nu$$

then J is differentiable at \mathcal{O} in direction V and the derivative takes the form:

$$dJ(\mathcal{O}, V) = \int_{\partial\mathcal{O}} \left(\frac{\partial\vartheta}{\partial n} + \vartheta h \right) n \cdot V \, d\nu$$

Proof :

Start with a simple reformulation using Green's formula

$$\begin{aligned} J(\mathcal{O}) &= \int_{\partial\mathcal{O}} \vartheta \, d\nu \\ &= \int_{\partial\mathcal{O}} \vartheta \, n \cdot n \, d\nu \\ &= \int_{\mathcal{O}} \operatorname{div}(\vartheta n) \, dx \end{aligned}$$

using example 2.6 yields

$$\begin{aligned} dJ(\mathcal{O}, V) &= \int_{\partial\mathcal{O}} \operatorname{div}(\vartheta n) \, n \cdot V \, d\nu \\ &= \int_{\partial\mathcal{O}} (\vartheta_{,i} n_i + \vartheta n_{i,i}) \, n \cdot V \, d\nu \\ &= \int_{\partial\mathcal{O}} (\nabla\vartheta \cdot n + \vartheta \operatorname{div}(n)) \, n \cdot V \, d\nu \\ &= \int_{\partial\mathcal{O}} \left(\frac{\partial\vartheta}{\partial n} + \vartheta h \right) \, n \cdot V \, d\nu. \end{aligned}$$

Here again Einstein notation was used.

□

Remark 2.9. With (2.6) and (2.8) at hand, derivatives for the volume and the surface area can be easily derived. These terms will be useful to realize a volume or surface

penalization in shape optimization problems. For a volume penalization term we have

$$J(\mathcal{O}) = \int_{\mathcal{O}} dx \quad \Rightarrow \quad dJ(\mathcal{O}, V) = \int_{\partial\mathcal{O}} n \cdot V \, d\nu$$

and for surface penalization we get

$$J(\mathcal{O}) = \int_{\partial\mathcal{O}} d\nu \quad \Rightarrow \quad dJ(\mathcal{O}, V) = \int_{\partial\mathcal{O}} h n \cdot V \, d\nu$$

We will now derive the shape derivatives for a class of functionals which comprises the functionals we focus on in our numerical computations.

Lemma 2.10.

Consider a domain $\mathcal{O} \in \mathbb{R}^d$ and a vector field $V : \mathbb{R}^d \rightarrow \mathbb{R}^d$ satisfying conditions in Definition 2.3. Furthermore, let the the data f and g comply with the requirements ensuring existence for the linearized elasticity model (2.5). Then the functionals as defined below

(I)

$$J_1(\mathcal{O}) = \int_{\mathcal{O}} \mathcal{A}(\epsilon(u)) : \epsilon(u) \, dx = \int_{\mathcal{O}} f \cdot u \, dx + \int_{\Gamma_N} g \cdot u \, d\nu \quad (2.11)$$

(II)

$$J_2(\mathcal{O}) = \int_{\mathcal{O}} |u - u_0|^2 \, dx \quad (2.12)$$

have the shape derivatives :

(I)

$$\begin{aligned} dJ_1(\mathcal{O}, V) = & \int_{\Gamma_N} \left(2 \left[\frac{\partial(g \cdot u)}{\partial n} + hg \cdot u + f \cdot u \right] - \mathcal{A}\epsilon(u) : \epsilon(u) \right) V \cdot n \, d\nu \\ & + \int_{\Gamma_D} (\mathcal{A}\epsilon(u) : \epsilon(u)) V \cdot n \, d\nu \end{aligned} \quad (2.13)$$

(II)

$$\begin{aligned}
dJ_2(\mathcal{O}, V) &= \int_{\Gamma_N} (|u - u_0|^2 + \mathcal{A}(\epsilon(u)) : \epsilon(p) - p \cdot f) V \cdot n \, d\nu \\
&\quad + \int_{\Gamma_N} h V \cdot n \, d\nu \\
&\quad - \int_{\Gamma_N} \left(\frac{\partial(g \cdot p)}{\partial n} + hg \cdot p \right) V \cdot n \, d\nu \\
&\quad - \int_{\Gamma_D} (-|u - u_0|^2 + \mathcal{A}(\epsilon(u)) : \epsilon(p) + p \cdot f) V \cdot n \, d\nu
\end{aligned} \tag{2.14}$$

where p denotes the adjoint state defined as the solution to

$$\begin{aligned}
-\operatorname{div}(\mathcal{A}(\epsilon(p))) &= -2(u - u_0) && \text{in } \mathcal{O} \\
p &= 0 && \text{on } \Gamma_D \\
\mathcal{A}(\epsilon(p)) \cdot n &= 0 && \text{on } \Gamma_N
\end{aligned} \tag{2.15}$$

Proof :

We will prove the above statements both at once by considering a general objective functional.

$$J(\mathcal{O}) = \int_{\mathcal{O}} j(x, u(x)) \, dx + \int_{\Gamma_N} l(x, u(x)) \, d\nu \tag{2.16}$$

with differentiable functions $j : \mathbb{R} \times \mathbb{R}^3 \rightarrow \mathbb{R}$ and $l : \mathbb{R} \times \mathbb{R}^3 \rightarrow \mathbb{R}$. Now we follow an approach well known from control theory. We introduce the general functional F

$$F(\mathcal{O}, \varphi) = \int_{\mathcal{O}} j(x, \varphi(x)) \, dx + \int_{\Gamma_N} l(x, \varphi(x)) \, d\nu$$

such that $F(\mathcal{O}, u) = J(\mathcal{O})$ holds. By introducing a Lagrange multiplier ψ , the so called adjoint state, we construct a Lagrangian functional.

$$\mathcal{L}(\mathcal{O}, \varphi, \psi) = F(\mathcal{O}, \varphi) + dE(\mathcal{O}, \varphi; \psi) \tag{2.17}$$

The state equation is now realized as a side constraint in its variational form. It is

$$E(\mathcal{O}, \varphi) := \mathcal{E}_{\text{elast}}(\varphi) = \int_{\mathcal{O}} \left[\frac{1}{2} \cdot \mathcal{A}(\epsilon(\varphi)) : \epsilon(\varphi) - f \cdot \varphi \right] \, dx - \int_{\partial\mathcal{O}} g \cdot \varphi \, d\nu,$$

and the variation of the elastic energy in direction ψ reads as

$$\begin{aligned} dE(\mathcal{O}, \varphi; \psi) &:= \left. \frac{d}{dt} E(\mathcal{O}, \varphi + t\psi) \right|_{t=0} \\ &= \int_{\mathcal{O}} [\mathcal{A}(\epsilon(\varphi)) : \epsilon(\psi) - f \cdot \psi] dx - \int_{\partial\mathcal{O}} g \cdot \psi d\nu. \end{aligned}$$

As we have to ensure that the Dirichlet Boundary Conditions are fulfilled, the Lagrangian as in (2.17) is adjusted by adding an additional term and the Lagrangian finally takes the form:

$$\begin{aligned} \mathcal{L}(\mathcal{O}, \varphi, \psi) &= \int_{\mathcal{O}} j(x, \varphi(x)) dx + \int_{\Gamma_N} l(x, \varphi(x)) d\nu \\ &+ \underbrace{\int_{\mathcal{O}} \mathcal{A}\epsilon(\varphi) : \epsilon(\psi) - \psi \cdot f dx - \int_{\Gamma_N} \psi \cdot g d\nu}_{dE(\mathcal{O}, \varphi; \psi)} \\ &- \underbrace{\int_{\Gamma_D} \psi \cdot \mathcal{A}\epsilon(\varphi) \cdot n + \varphi \cdot \mathcal{A}\epsilon(\psi) \cdot n d\nu}_{\text{additional term}} \quad \varphi, \psi \in H^1(\mathbb{R}^d)^d. \end{aligned} \tag{2.18}$$

Then, we observe for the objective

$$J(\mathcal{O}) = \min_{\varphi \in H^1(\mathbb{R}^d)^d} \sup_{\psi \in H^1(\mathbb{R}^d)^d} \mathcal{L}(\mathcal{O}, \varphi, \psi) \tag{2.19}$$

due to the fact that it holds

$$\sup_{\psi \in H^1(\mathbb{R}^d)^d} \mathcal{L}(\mathcal{O}, \varphi, \psi) = \begin{cases} F(\mathcal{O}, u(\mathcal{O})), & \text{if } \varphi = u(\mathcal{O}) \\ +\infty, & \text{if } \varphi \neq u(\mathcal{O}) \end{cases} \tag{2.20}$$

This can easily be justified by taking account of the linearity of $dE(\mathcal{O}, \varphi; \psi)$. The Lagrangian \mathcal{L} is convex and continuous with respect to φ and concave and continuous with respect to ψ . Moreover, the Sobolov space $H^1(\mathbb{R}^d)^d$ is convex and closed. Following [65] \mathcal{L} has a saddle point if and only if the saddle point equations have a solution, that is

$$p \in H^1(\mathbb{R}^d)^d, \quad d\mathcal{L}(\mathcal{O}, u, p; 0, \psi) = 0 \quad \forall \psi \in H^1(\mathbb{R}^d)^d \tag{2.21}$$

$$u \in H^1(\mathbb{R}^d)^d, \quad d\mathcal{L}(\mathcal{O}, u, p; \varphi, 0) = 0 \quad \forall \varphi \in H^1(\mathbb{R}^d)^d \tag{2.22}$$

If we take (2.21) as a starting point, we obtain by using Corollary 2.7

$$\begin{aligned}
d\mathcal{L}(\mathcal{O}, u, p; 0, \psi) &= \int_{\mathcal{O}} \mathcal{A}\epsilon(u) : \epsilon(\psi) - \psi \cdot f \, dx - \int_{\Gamma_N} \psi \cdot g \, d\nu \\
&\quad - \int_{\Gamma_D} \psi \cdot \mathcal{A}\epsilon(u) \cdot n + u \cdot \mathcal{A}\epsilon(\psi) \cdot n \, d\nu \\
&= - \int_{\mathcal{O}} (\operatorname{div} \mathcal{A}\epsilon(u) + f) \psi \, dx \\
&\quad + \int_{\Gamma_N} (\mathcal{A}\epsilon(u)n - g) \psi \, d\nu \\
&\quad - \int_{\Gamma_D} \psi \cdot \mathcal{A}\epsilon(u) \cdot n + u \cdot \mathcal{A}\epsilon(\psi) \cdot n \, d\nu
\end{aligned}$$

First, choose $\psi \in C_0^\infty(\mathcal{O})$ with compact support within \mathcal{O} the fundamental lemma of the calculus of variations yields

$$-\operatorname{div} \mathcal{A}\epsilon(u) = f \quad \text{in } \mathcal{O}$$

then, considering $\psi \in H_D^1(\mathcal{O})$ we get

$$\mathcal{A}\epsilon(u)n = g \quad \text{on } \Gamma_N$$

and finally by varying $\mathcal{A}\epsilon(\psi) \cdot n$ on Γ_D the Dirichlet Boundary Conditions are established. See [73] for a detailed justification of the last argument. Thus, u is the unique solution of the elasticity model (2.5).

Proceeding with (2.22), we observe that p is the solution of the adjoint equation (2.15).

$$\begin{aligned}
d\mathcal{L}(\mathcal{O}, u, p; \varphi, 0) &= \int_{\mathcal{O}} \frac{d}{dy} j(x, u(x)) \varphi \, dx + \int_{\Gamma_N} \frac{d}{dy} l(x, u(x)) \varphi \, d\nu \\
&\quad + \int_{\mathcal{O}} \mathcal{A}\epsilon(\varphi) : \epsilon(p) \, dx \\
&\quad - \int_{\Gamma_D} p \cdot \mathcal{A}\epsilon(\varphi) \cdot n + \varphi \cdot \mathcal{A}\epsilon(p) \cdot n \, d\nu \\
&= \int_{\mathcal{O}} \left(-\operatorname{div} \mathcal{A}\epsilon(p) + \frac{d}{dy} j(x, u(x)) \right) \psi \, dx
\end{aligned}$$

$$\begin{aligned}
& + \int_{\Gamma_N} \left(\mathcal{A}\epsilon(p)n - \frac{d}{dy}l(x, u(x)) \right) \psi \, d\nu \\
& - \int_{\Gamma_D} p \cdot \mathcal{A}\epsilon(\varphi) \cdot n + \varphi \cdot \mathcal{A}\epsilon(p) \cdot n \, d\nu
\end{aligned}$$

With the same arguments as above, we identify p as the unique solution to the adjoint equation

$$\begin{aligned}
-\operatorname{div}(\mathcal{A}(\epsilon(p))) &= -\frac{d}{dy}j(x, u(x)) \quad \text{in } \mathcal{O} \\
p &= 0 \quad \text{on } \Gamma_D \\
\mathcal{A}(\epsilon(p)) \cdot n &= \frac{d}{dy}l(x, u(x)) \quad \text{on } \Gamma_N
\end{aligned}$$

Coming back to (2.19), we have found

$$J(\mathcal{O}) = \mathcal{L}(\mathcal{O}, u, p)$$

Then, the shape derivative of J is given by the derivative of \mathcal{L} with respect to the vector field V .

$$dJ(\mathcal{O}, V) = \frac{d}{dV}\mathcal{L}(\mathcal{O}, u, p)$$

This is a crucial result provided by the *shape sensitivity analysis*. For a comprehensive discussion the reader is referred to [45,53,115,128,158] and in particular to [58]. Having in mind 2.6 and 2.8, we can continue

$$\begin{aligned}
\frac{d}{dV}\mathcal{L}(\mathcal{O}, u, p) &= \int_{\partial\mathcal{O}} (j(x, u(x)) + \mathcal{A}(\epsilon(u)) : \epsilon(p) - p \cdot f) V \cdot n \, d\nu \\
& + \int_{\Gamma_N} \left(\frac{\partial l(x, u(x))}{\partial n} + hl(x, u(x)) \right) V \cdot n \, d\nu \\
& - \int_{\Gamma_N} \left(\frac{\partial(g \cdot p)}{\partial n} + hg \cdot p \right) V \cdot n \, d\nu \\
& - \int_{\Gamma_D} \left(\frac{\partial}{\partial n} (u \cdot \mathcal{A}(\epsilon(p)) \cdot n + p \cdot \mathcal{A}(\epsilon(u)) \cdot n) \right) V \cdot n \, d\nu \\
& - \int_{\Gamma_D} \left(h (u \cdot \mathcal{A}(\epsilon(p)) \cdot n + p \cdot \mathcal{A}(\epsilon(u)) \cdot n) \right) V \cdot n \, d\nu.
\end{aligned}$$

Due to the fact that it is $u = p = 0$ on Γ_D it can easily be shown that on Γ_D it holds:

$$\begin{aligned} & \frac{\partial}{\partial n} \left(u \cdot \mathcal{A}(\epsilon(p)) \cdot n + p \cdot \mathcal{A}(\epsilon(u)) \cdot n \right) \\ & + h \left(u \cdot \mathcal{A}(\epsilon(p)) \cdot n + p \cdot \mathcal{A}(\epsilon(u)) \cdot n \right) = 2 \mathcal{A}(\epsilon(u)) : \epsilon(p) \end{aligned}$$

So, we have

$$\begin{aligned} dJ(\mathcal{O}; V) &= \int_{\Gamma_N} (j(x, u(x)) + \mathcal{A}(\epsilon(u)) : \epsilon(p) - p \cdot f) V \cdot n \, d\nu \\ &+ \int_{\Gamma_N} \left(\frac{\partial l(x, u(x))}{\partial n} + hl(x, u(x)) \right) V \cdot n \, d\nu \\ &- \int_{\Gamma_N} \left(\frac{\partial (g \cdot p)}{\partial n} + hg \cdot p \right) V \cdot n \, d\nu \\ &- \int_{\Gamma_D} (-j(x, u(x)) + \mathcal{A}(\epsilon(u)) : \epsilon(p) + p \cdot f) V \cdot n \, d\nu. \end{aligned}$$

The derivatives of the shape functionals in (2.13) and (2.14) are obtained by an appropriate choice of j and l . To justify (2.13) set

$$j := f \cdot u \quad l := g \cdot u$$

. It turns out that in this case we get the relation

$$p = -u$$

for the primal and dual state. So, the functional J_1 is self adjoint and has the derivative

$$\begin{aligned} dJ_1(\mathcal{O}, V) &= \int_{\Gamma_N} \left(2 \left[\frac{\partial (g \cdot u)}{\partial n} + hg \cdot u + f \cdot u \right] - \mathcal{A}\epsilon(u) : \epsilon(u) \right) V \cdot n \, d\nu \\ &+ \int_{\Gamma_D} (\mathcal{A}\epsilon(u) : \epsilon(u)) V \cdot n \, d\nu \end{aligned}$$

For (2.14) it is

$$j := |u - u_0|^2 \quad l := 0$$

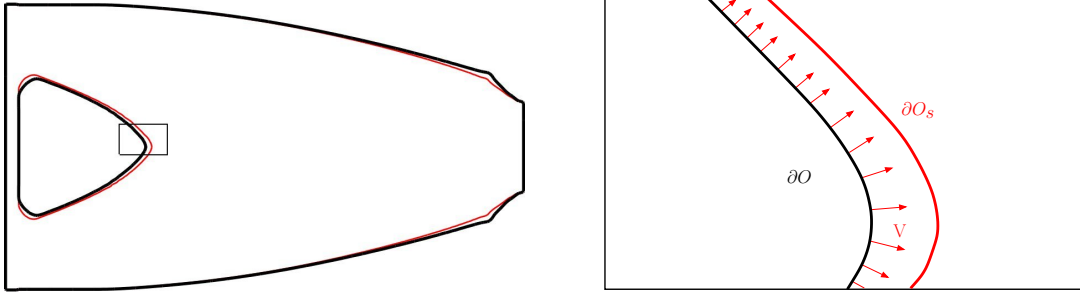


Figure 2.3: A small variation of the boundary induced by a vector field V according to Definition 2.3. On the left: the old (black) and the updated (red) domains. On the right: a zoom displays the velocity field V .

and we get the dual state equation (2.15) for p and finally for the derivative of J_2

$$\begin{aligned}
 dJ_2(\mathcal{O}, V) &= \int_{\Gamma_N} (|u - u_0|^2 + \mathcal{A}(\epsilon(u)) : \epsilon(p) - p \cdot f) V \cdot n \, d\nu \\
 &\quad + \int_{\Gamma_N} h V \cdot n \, d\nu \\
 &\quad - \int_{\Gamma_N} \left(\frac{\partial(g \cdot p)}{\partial n} + hg \cdot p \right) V \cdot n \, d\nu \\
 &\quad - \int_{\Gamma_D} (-|u - u_0|^2 + \mathcal{A}(\epsilon(u)) : \epsilon(p) + p \cdot f) V \cdot n \, d\nu
 \end{aligned}$$

□

Remark 2.11 (Zolesio-Hadamard Structure Theorem).

We observe that shape derivatives for the above functionals are represented by boundary integral expressions. In fact, these define a vector distribution $\mathcal{G}(\mathcal{O})$ in \mathcal{V}' , the so-called *shape gradient*. As a matter of fact, if J is a shape-differentiable functional with *shape gradient* $\mathcal{G}(\mathcal{O})$, then the support of $\mathcal{G}(\mathcal{O})$ is contained in $\partial\mathcal{O}$. This is implied by the well known Zolésio-Hadamard *structure theorem*, see [58]. It generalizes previous work from Hadamard and Zolésio to a wider range of shape functionals.

At this point, we formulate the actual shape optimization problem. Usually, one of the shape functions in Lemma 2.10 plus a volume penalization term is considered

as an objective function.

$$\min\{J(\mathcal{O}) + \alpha \int_{\mathcal{O}} dx : \mathcal{O} \in U_{ad}\} \quad (2.23)$$

The second term can be seen as a regularization term with the Lagrange parameter $\alpha \in \mathbb{R}$ ($\alpha > 0$). For instance, when we consider the compliance as the objective J , it can easily be shown, that the derivative of J in direction of vector fields V with $\langle V(x), n \rangle > 0$ is negative. Thus, the optimization process (here minization of J) without volume penalization would generate shapes with increasing volume until the whole working domain D is filled. So, an optimization would not reveal any structure and would be meaningless.

Algorithm 2.12 (Gradient Descent). Using information provided by shape derivatives of the objective $J(\mathcal{O})$, a sketch of a very first optimization algorithm reads as follows:

1. Choose an initial shape \mathcal{O}_0 and parameters for step size and volume penalization.
2. For $k \geq 0$ solve the elasticity system (2.5) for the current shape \mathcal{O}_k to obtain solutions u_k and p_k
3. Compute the steepest descent direction (that is a velocity field V) using (2.10) and perform a line search along this until a new shape \mathcal{O}_{k+1} with $J(\mathcal{O}_{k+1}) < J(\mathcal{O}_k)$ is found. That means, we consider slightly different shapes caused by a variation of the boundary along the vector field V , see Fig. (2.3). Return to step 2 unless some abort criterion is fulfilled.

Example results for using this algorithm are illustrated in Fig. (2.4) and Fig. (2.5).

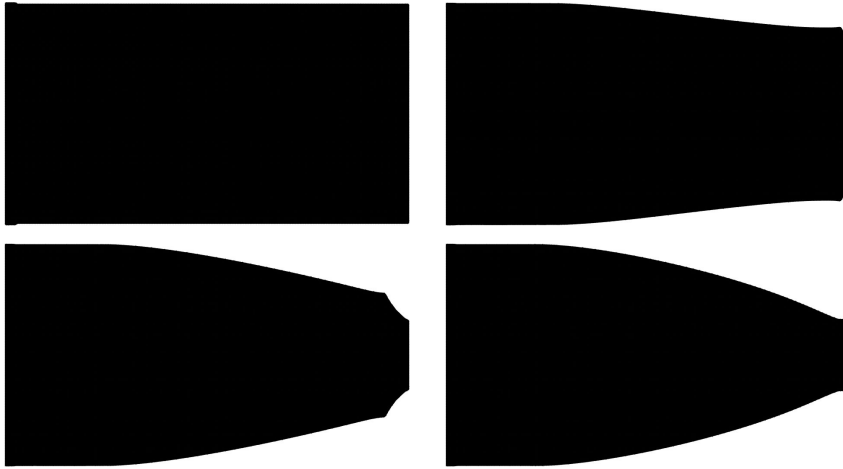


Figure 2.4: First example for optimization of a cantilever like structure using algorithm 2.12. This cantilever setting is maybe the most illustrated one in literature, and serves well as a benchmark problem. Here, the whole working domain D is taken as the initial shape. We suppose homogeneous Dirichlet boundary conditions on the left boundary and inhomogeneous Neumann boundary conditions on one part of the boundary to the right. Both parts remain fixed. See the configuration in Fig. (1.1). We consider a surface force g of to 5.5 and a volume penalization with $\alpha = 1.4$. The sequence displays iterations 0, 10, 20 and 32 .

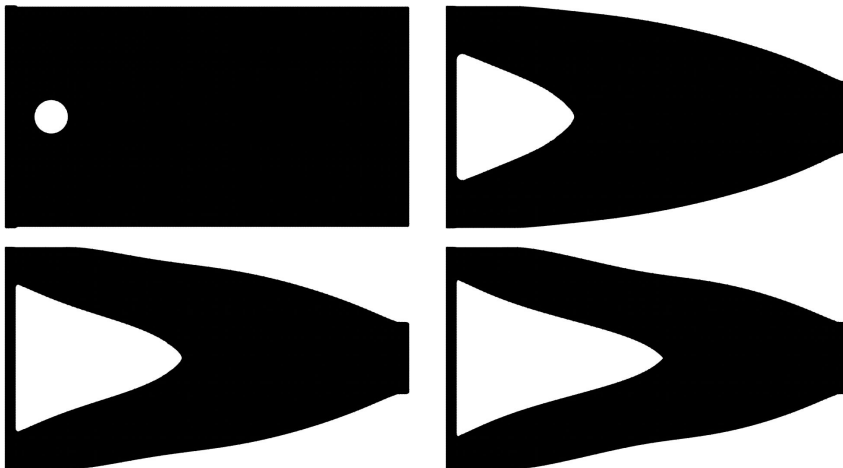


Figure 2.5: Second example with the same configuration as in Fig. (2.4) but with a different initial shape. The resulting shape differs significantly from that one obtained in the first example. The sequence shows iterations 0, 30, 50 and 157.

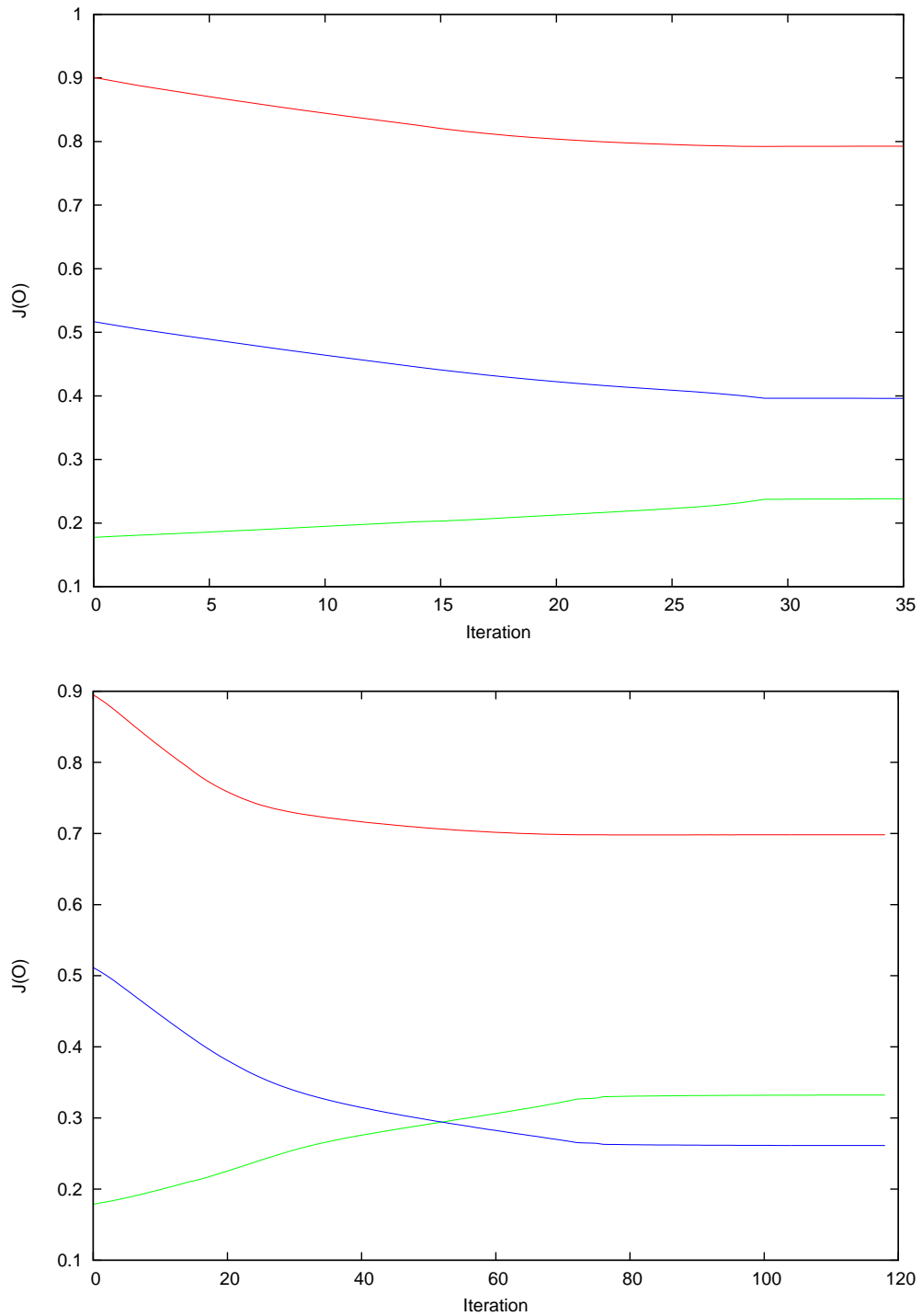


Figure 2.6: Functions graphs for the optimization processes according to Fig. (2.4) (top) and Fig. (2.5) (bottom). The compliance is colored green, the volume blue and the total value of shape function J is colored red.

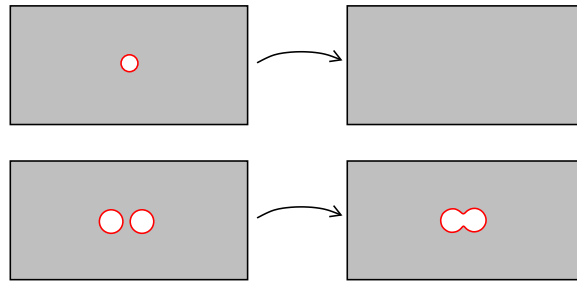


Figure 2.7: Types of topological changes that are possible using only shape derivatives and level set methods. The shape gradient provides information how to move the boundary. In practice, this is done by making a step $t > 0$. If then one of above situation occurs, the level set approach can process the new boundary information.

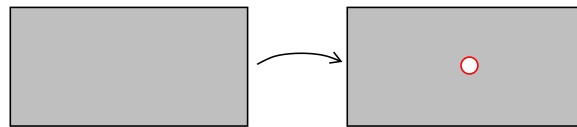


Figure 2.8: This type of topological change is impossible without additional information besides the shape sensitivity analysis. The shape gradient only provides information for already existing boundaries how to move, and thus, gives no hint where to place a hole. Once this information is available, the change in the topology can easily be performed by modifying the level set function.

2.3 Topological Sensitivity

Finding optimal shapes using only shape derivatives suffers a major drawback as it does not include the problem of finding an optimal topology of shapes. As we have seen, shape derivatives rely on variations of the boundary of a given domain which do not change the topology of this. Thus, changes of the topology like the occurrence or disappearance of a small cavity are not covered by methods discussed in the preceding chapter, see Fig. (2.7). Whereas in numerical practice, merging or disappearing holes can easily be tackled when using level set methods (this will be at issue in the succeeding chapter), the occurrence of new holes represents a totally different problem and leads to the so-called *topological sensitivity analysis*, see Fig. (2.8). There, information is provided how to change the topology of a given domain in order to improve a shape functional.

In general, solving shape optimization problems the way we do, i.e., applying a gradient descent method, is prone to find local minima instead of global ones. A remedy to this effect would be a reliable method for changing the topology, as this enables to 'escape' bad local minima to find better ones. The impact on the resulting shape

found by our optimization process is significant. See the different results using only shape derivatives on the one hand Fig. (2.4) Fig. (2.5), and using both, shape and topological derivatives, on the other hand, shown in Fig. (2.9).

Topological sensitivity has been extensively studied in the past decade, and today is incorporated in a broad range of applications, e.g. inverse problems, imaging [37, 97, 106] and especially structural or mechanical design [6, 72, 74, 77, 164]. In fact, topology sensitivity has been investigated for various types of (systems of) differential equations as state constraint [13, 15, 16, 99, 117]. For a comprehensive survey see the recently published monograph [161]. The term *topology optimization* comprises different approaches for structural optimization, whereas a well established aside the above mentioned, is based on *homogenization theory*, see the pioneer work of Murat and Tartar [116] and subsequent improvements [5, 28]. Here, an extended idea of a domain underlies the theoretical and practical work. A domain is considered to have a density continuously ranging from zero (void) to one (solid), in contrast to a description via a characteristic function being either zero or one. This relaxed interpretation enables the implementation of efficient algorithms, e.g. the well known SIMP method (Solid Isotropic Material with Penalization) see [26, 28, 29], which are sufficient in many practical problems. Despite these advantages, this approach suffers the drawback that resultant domains consist of composite materials, which may have no physical meaning. To get around this, penalization and filter methods for the material density are applied to enforce sharp interfaces between void and solid material, or keep the material physically justifiable.

However, we follow a strategy where the domain under consideration is represented via a level set function, that is we have a sharp interface between void and solid material. Thus, a method that indicates where to change a given topology is essential. As a first practical implementation, in 1994, Schumacher introduced the so-called *Bubble Method* [72] which creates holes in a domain according to some criterion. Later, this principal was taken up by Sokolowski and Zochowski (1999) [163] and Guillaume and Masmoudi (2001) [77], and they developed the concept of *topological derivative* or *topological asymptotic*. Here, the sensitivity of a shape functional J , defined on given domain \mathcal{O} , is calculated when a small hole is drilled. This is performed as follows: Consider a fixed model hole w in \mathbb{R}^d , w being open and smooth bounded around a center point $x_0 \in \mathcal{O}$. Then, for $\rho > 0$ we get the rescaled hole w_ρ

$$w_\rho = x_0 + \rho w$$

and thus, the perforated domain $\mathcal{O}_\rho = \mathcal{O} \setminus w_\rho$. Then, the asymptotic behavior of

$J(\mathcal{O}_\rho)$ as ρ tends to zero is of interest and existence of the following limit is questioned.

$$\lim_{\rho \searrow 0} \frac{J(\mathcal{O}) - J(\mathcal{O}_\rho)}{|w_\rho|}$$

Of course, in the case where the shape functional studied, depends on the solution u_ρ of a boundary value problem (defined on the domain \mathcal{O}_ρ), an asymptotic analysis of the solution u_ρ with respect to ρ (u_ρ being the solution on \mathcal{O}_ρ) is essential. In this connection, the reader is referred to various sources [54, 63, 75, 100, 112, 159, 160] for a detailed discussion on methods for constructing asymptotic expansions for partial differential equations. It is worth mentioning that some ideas can be traced back to the early 20th century, see Prandtl (1904) [129]. Results of these works underly the concept of the so-called *topological derivative*, see for instance [74, 163]. The topological derivative is obtained when an asymptotic expansion of the cost functional J is considered.

$$J(\mathcal{O}_\rho) = J(\mathcal{O}) + f(\rho)D_T J + \mathcal{R}(f(\rho))$$

Whereby f is a non-negative function such that it is $\lim_{\rho \searrow 0} f(\rho) = 0$ and $\mathcal{R}(f(\rho))$ contains all higher order terms than $f(\rho)$, that is $\mathcal{R}(f(\rho)) = o(f(\rho))$. The term $D_T J$ denotes the topological derivative located at the point x . At first sight, one might think this calculation has to be done for each $x \in \mathcal{O}$, but it turns out that exploiting information of the corresponding adjoint state, enables to compute the topological derivative in the whole domain \mathcal{O} simultaneously.

First we take a look at the topological derivative of the volume functional, as an illustrative example.

Lemma 2.13. The topological derivative of the volume functional $V(\mathcal{O}) = \int_{\mathcal{O}} dx$ is

$$D_T V(x) = -|w|.$$

Proof : Suppose $d = 2$ then for $\rho > 0$ it holds

$$\begin{aligned} V(\mathcal{O}_\rho) &= \int_{\mathcal{O}_\rho} dx \\ &= \int_{\mathcal{O}} dx - \int_{w_\rho} dx \\ &= V(\mathcal{O}) - \rho^2 \int_w dx \\ &= V(\mathcal{O}) - \rho^2 |w| \end{aligned}$$

Then we identify $f(\rho) = \rho^2$ and $D_T V = -|w|$.

□

This result meets the reader's expectations. Likewise we obtain the topological derivative for the surface functional. For sake of simplicity, from now on let w be the unit ball B_1 . Then it is

$$S(\mathcal{O}_\rho) = \int_{\mathcal{O}_\rho} d\nu = \rho \int_{\mathcal{O}_1} d\nu = \rho 2\pi .$$

Thus we get

$$S(\mathcal{O}_\rho) = S(\mathcal{O}_0) + \rho 2\pi$$

and we find $f = p$ and $D_T S = 2\pi$.

Recalling our genuine shape functionals, which depend on the solution u to the state equation,

(I)

$$J_1(\mathcal{O}) = \int_{\mathcal{O}} \mathcal{A}(\epsilon(u)) : \epsilon(u) dx = \int_{\mathcal{O}} f \cdot u dx + \int_{\Gamma_N} g \cdot u d\nu \quad (2.24)$$

(II)

$$J_2(\mathcal{O}) = \int_{\mathcal{O}} |u - u_0|^2 dx \quad (2.25)$$

we need to specify which boundary conditions are valid on the emerging boundary ∂B_ρ , as these are affecting the topological derivative. For our purpose we choose homogeneous Neumann boundary conditions. Eventually, we obtain the following topological derivatives in dimension $d = 2$:

Theorem 2.14. Assume for simplicity that $f = 0$ and u is the solution of (2.5). For any $x \in \mathcal{O}$ the topological derivatives of J_1 and J_2 take the form :

$$D_T J_1(x) = \frac{\pi(\lambda + 2\mu)}{2\mu(\lambda + \mu)} \{4\mu \mathcal{A}\epsilon(u) \cdot \epsilon(u) + (\lambda - \mu) \operatorname{tr}(\mathcal{A}\epsilon(u)) \operatorname{tr}(\epsilon(u))\}(x)$$

$$D_T J_2(x) = \frac{\pi}{2} |u(x) - u_0(x)|^2 -$$

$$\frac{\pi(\lambda + 2\mu)}{2\mu(\lambda + \mu)} \{4\mu \mathcal{A}\epsilon(u) \cdot \epsilon(p) + (\lambda - \mu) \operatorname{tr}(\mathcal{A}\epsilon(u)) \operatorname{tr}(\epsilon(p))\}(x)$$

For proofs the reader is referred to [77] and [164].

With this additional information we improve algorithm 2.12 so that it does not depend on the topology of the initial shape.

Algorithm 2.15.

1. Set parameters for step size control and volume penalization. Choose the whole working domain as initial shape \mathcal{O}_0
2. For $k \geq 0$ solve the elasticity system (2.5) for \mathcal{O}_k to obtain u_k and p_k
3. (a) For $(k \bmod 10) \neq 0$: Compute the steepest descent direction and perform a line search according to the step size control.
 (b) For $(k \bmod 10) = 0$: Compute the topological sensitivity and change the topology.

Return to step 2 unless some abort criterion is fulfilled.

The sequence of shapes illustrated in Fig. (2.9) demonstrates the advantages of using this improved algorithm. It indicates the optimization process to be robust and to yield reliable results.

Remark 2.16 (Change of topology).

The topological gradient calculated in theorem (2.14) provides pointwise information how the objective J changes if a small hole is created at a point $x \in \mathcal{O}$. Being aware of the fact that creating holes for more than just one point might not result in a decrease of the objective J , this approach would accelerate the optimization process enormously. Therefore, we define a threshold η_{top} and cut out every point $x \in \mathcal{O}$ for which the topological gradient $D_T J(x)$ is smaller than η_{top} . Let $top_{min} = \arg \min_{x \in \mathcal{O}} D_T J(x)$ and a step size $\tau_{top} = 0.1$, then we set $\eta_{top} = (1 - \tau_{top}) \cdot top_{min}$. If, after performing the topological change, the objective J has not decreased, the procedure is repeated with $\tau_{top}^{new} = 0.5 \tau_{top}$. This is done until the objective has decreased, or $\tau_{top} < 0.001$ and no topological change is performed.

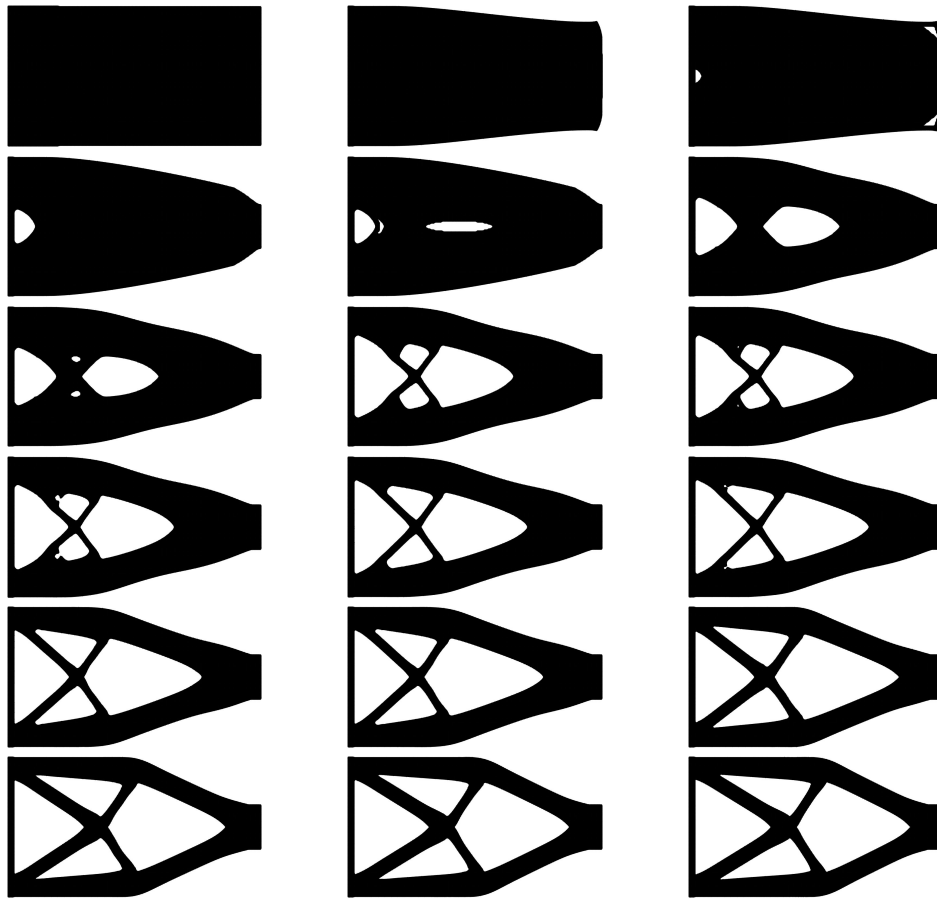


Figure 2.9: A sequence of shapes for optimization with the topological derivative. The configuration is similar to the one in Fig. (2.4), that is volume penalization $\alpha = 1.4$ and surface force $g = 5.5$. Depicted (from top left to down right) are iterations 0,10,11, 21,22,32, 33,43,44, 45,55,56, 67,68,100, 150,200, and 233. Topological changes are performed after step 10, 21, 32, 44, 55, 67. After that point, topological changes do not improve the current shape anymore and, therefore, are omitted.

2.4 Level-Set-Methods

The aim of this chapter is to motivate the use of level set methods in context of shape optimization. These techniques have proven to be very useful in a rather broad range of applications including mathematical image processing, computational physics, and engineering and yet in shape optimization, too. See [9, 152, 172]. In general, level set methods, first introduced by Osher and Sethian [125], are numerical techniques for tracking the evolution of interfaces and boundaries. They provide some eminent advantages compared to other approaches for the representation of interfaces. Contrary to most techniques used for interface representation, e.g. parametrization techniques, handling of topological changes like merging boundaries or nucleation of holes is performed in a simple way. In the preceding chapter, 'derivatives of shapes', that is small

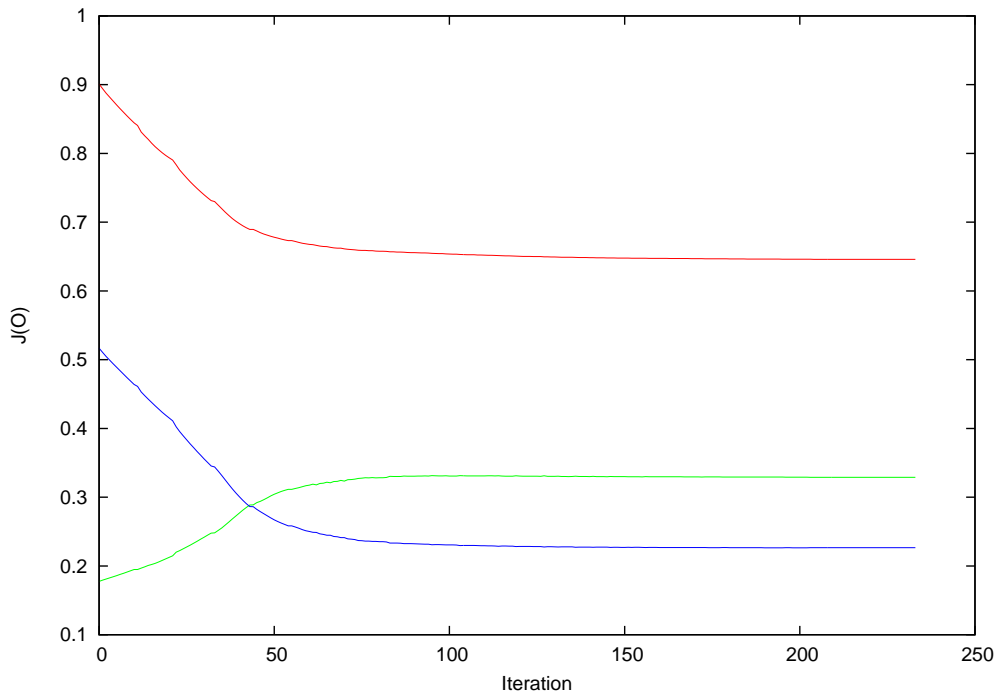


Figure 2.10: Function graph for the sequence of shapes depicted in Fig. (2.9). The total value of J is colored in red, the volume in blue and the compliance in green. An additional improvement is obtained, i.e., less volume with a smaller total value of J for the final shape. Compare the function graph in Fig. (2.6).

variations of the boundaries to improve a shape functional, were introduced. These shape derivatives are described by vector fields which indicate the evolution of the boundary. We will give an overview of different methods necessary for this boundary evolution.

Boundary representation via level sets.

Interface representation via level sets is based on the embedding of the interface as the zero level of a higher dimensional level set function. This means a fundamental shift in how one views interfaces, namely replacing an explicit description by an implicit one. Consider a function $\phi : \mathbb{R}^d \rightarrow \mathbb{R}$, the so called level set function, with non vanishing gradient, $\nabla\phi \neq 0$. Then we simply identify \mathcal{O} and $\partial\mathcal{O}$ as :

$$\begin{aligned} \phi(x) &= 0 & x &\in \partial\mathcal{O} \\ \phi(x) &< 0 & x &\in \mathcal{O} \\ \phi(x) &> 0 & x &\notin \mathcal{O} \end{aligned}$$

Fig. (2.11) illustrates this relation between \mathcal{O} and ϕ . Of course, this representation via ϕ is not unique. For example choose $a \in \mathbb{R}^+$, then $a \cdot \phi(x)$ is another representation

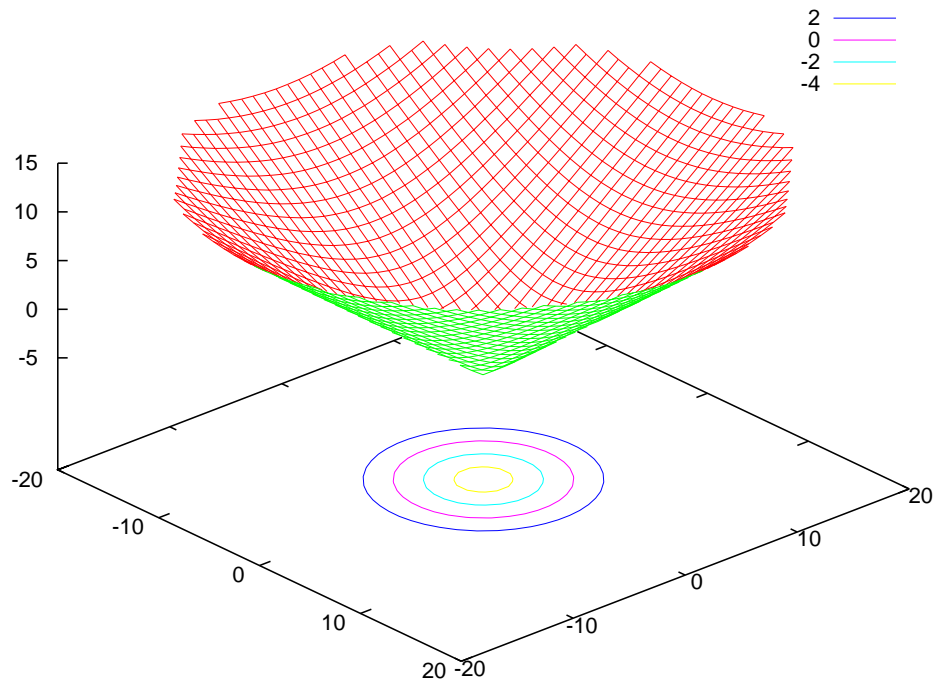


Figure 2.11: Different level-sets of the function $\phi(x) = |x| - 5$, $x \in \mathbb{R}^2$. Each can be interpreted as the boundary of a circle with different radius.

of \mathcal{O} . We will see later that level set functions close to a *signed distance function*, that is $|\nabla\phi(x)| \approx 1 \quad \forall x \in \mathbb{R}^d$, are to prefer due to stability reasons.

Furthermore, geometric quantities of the boundary $\partial\mathcal{O}$ can also be expressed in terms of the level set function. For the outer normal n of $\partial\mathcal{O}$, we have

$$n = \frac{\nabla\phi}{|\nabla\phi|}$$

and for the mean curvature, denoted by h , it holds:

$$h = \operatorname{div}(n) = \operatorname{div}\left(\frac{\nabla\phi}{|\nabla\phi|}\right)$$

Now, we can focus on the evolution of the level set function ϕ as this implicitly describes the evolution of \mathcal{O} .

Level set equation

Evolution of the level set function ϕ is incorporated by introducing a fictitious time t and redefining ϕ as a time dependent function $\phi(t, x)$. Thus, we obtain time dependency of $\mathcal{O}(t)$ by

$$\mathcal{O}(t) := \{x \in \mathbb{R}^d : \phi(t, x) \leq 0\}$$

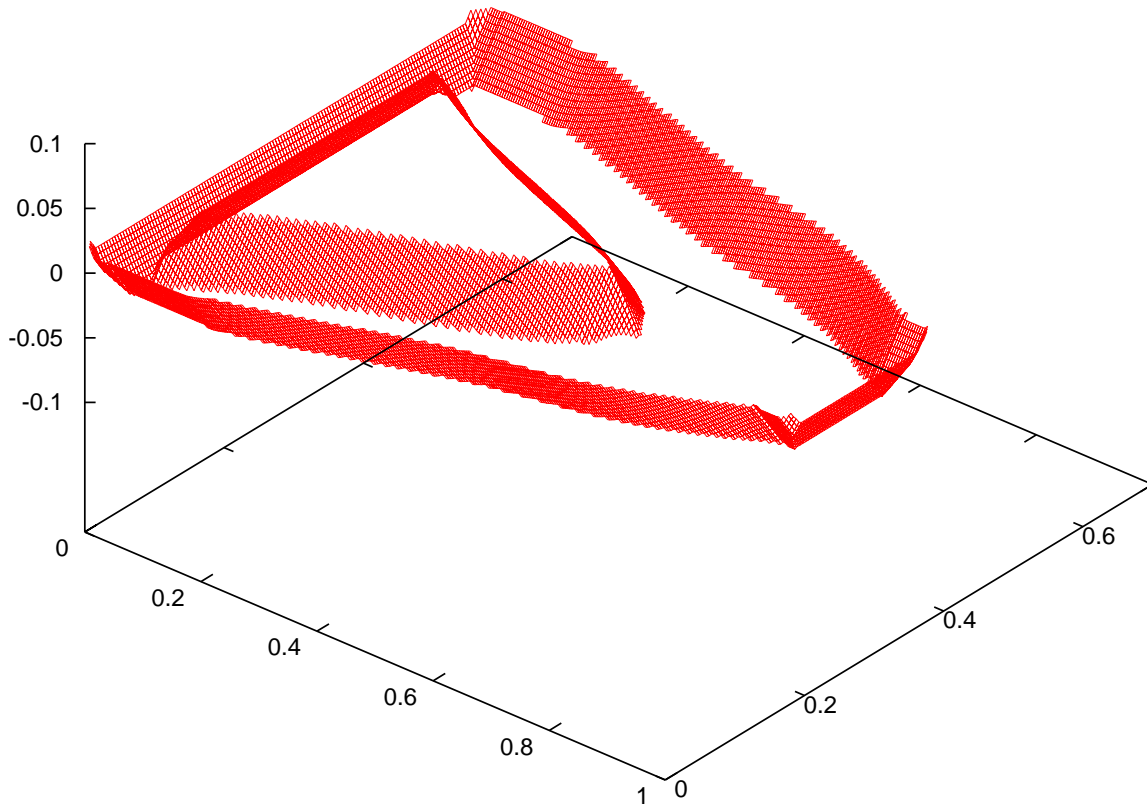


Figure 2.12: Here, the level set function ϕ for the final shape \mathcal{O} in Fig. (2.5) is depicted. The zero level of ϕ corresponds to $\partial\mathcal{O}$. ϕ is a signed distance function, that is, $\phi(x) = \pm \text{dist}(x, \partial\mathcal{O})$. Of course, ϕ only needs to be a signed distance function in a narrow band around the zero level. We use a bandwidth of 6 times h , where h is the element size of the underlying finite element discretization, see the next section 2.6.

$$\partial\mathcal{O}(t) := \{x \in \mathbb{R}^d : \phi(t, x) = 0\}$$

For a given vector field (velocity field) $V : \mathbb{R}^d \rightarrow \mathbb{R}^d$ sufficiently smooth we consider the evolution of the iso levels $\phi(x) = c$, for fixed $c \in \mathbb{R}$. Let $x_0 \in \mathbb{R}^d$ with $\phi(0, x_0) = c$, then we define the initial value problem for the trajectory $x(t) : \mathbb{R} \rightarrow \mathbb{R}^d$

$$\begin{aligned} x(0) &= x_0 \\ \dot{x}(t) &= V(x(t)) \end{aligned}$$

where $\dot{x}(t)$ is the derivative with respect to t . With the required regularity of V , the Picard-Lindelöf theorem ensures unique solvability. We obtain a Hamilton-Jacobian type equation by

$$\frac{\partial}{\partial t} \phi(t, x(t)) = 0 \quad (2.26)$$

$$\Leftrightarrow \dot{\phi}(t, x(t)) + \nabla\phi(t, x(t)) \cdot \dot{x}(t) = 0 \quad (2.27)$$

$$\Leftrightarrow \dot{\phi}(t, x(t)) + V(x(t)) \cdot n |\nabla\phi(t, x(t))| = 0 \quad (2.28)$$

Equation (2.28) is also referred to as level set equation. It relates variations of the level set function to variations of the iso-levels in normal direction according to a velocity field.

Extension velocities

As we have seen above, the variation of the level set function can be computed straight forward according to (2.28) if a velocity field is given a priori. This is not always the case. In many practical applications one has to deal with the situation when a velocity field is only defined on one iso-level, as it is in the case of shape optimization. One main result in the previous chapter is the boundary representation of the shape derivative. Thus, one has to find a way to extend the given velocity field given on the zero level to all level sets or at least to a *narrow band* around the zero level set. We follow [2, 150] and find that it is a good choice to define an extended vector field according to

$$\begin{aligned} \nabla V_{ext} \cdot \nabla\phi &= 0 \quad \text{in } \mathbb{R}^d \\ V_{ext} &= F \quad \text{on } \partial\mathcal{O} \end{aligned}$$

which means a constant extension along the normal direction of $\partial\mathcal{O}$. If we take a look at

$$\begin{aligned} \frac{\partial}{\partial t} \|\nabla\phi\|^2 &= \frac{\partial}{\partial t} (\nabla\phi \cdot \nabla\phi) \\ &= 2\nabla\phi \cdot \frac{\partial}{\partial t} (\nabla\phi) \\ &= -2\nabla\phi \cdot (\nabla V_{ext} \|\nabla\phi\| + \nabla(\|\nabla\phi\|) V_{ext}) \end{aligned}$$

the last term is zero if $|\nabla\phi| = 1$ and because of $\nabla V_{ext} \cdot \nabla\phi = 0$. That means the derivative of the norm of $\nabla\phi(t)$ is zero and it is $\|\nabla\phi(t)\| = 1$, $t > 0$. So $\phi(t)$ remains a signed distance function. Thus, the iso-levels maintain an even distance which prevents from developing shocks and rarefactions as discussed in [146–148]. We will see later that the expression of the shape derivative in terms of level set function gives good reason for conserving this property of ϕ .

Re-initialization

First, in the initialization step for $t = 0$, the level set function is constructed as a signed distance function to the boundary of \mathcal{O} .

$$\begin{aligned}\phi(x) &= 0 & x \in \partial\mathcal{O} \\ \phi(x) &= -\text{dist}(\mathcal{O}, x) & x \in \mathcal{O} \\ \phi(x) &= +\text{dist}(\mathcal{O}, x) & x \notin \mathcal{O}\end{aligned}$$

After evolving to some point $t > 0$, the level set function may, for some reason, not be similar to a signed distance function anymore. Then, a new signed distance function is created preserving the boundary information of ϕ and the process is continued setting $t = 0$.

$$\phi_{new}(x) = 0, \quad \forall x \in \{x \in \mathbb{R}^d : \phi(x) = 0\}, \quad \|\nabla\phi_{new}\| = 1$$

This procedure is referred to as re-initialization. For the construction of the signed distance function we solve the Eikonal equation

$$\|\nabla T\|V = 1 \quad T = 0 \text{ on } \partial\mathcal{O} \tag{2.29}$$

with unit speed $V = 1$. $T(x)$ can be considered as the arrival time of the expanding front $\partial\mathcal{O}$. Contrary to the level set equation (2.28), this is a boundary value problem and strictly requires $V > 0$. But therefore it offers fast and efficient algorithms for a numerical solution. We rely on the so-called Fast Marching Method based on an upwind scheme. See [123, 124, 149, 175] for a detailed introduction to this topic.

Shape derivative in level set formulation

Due to the relation in (2.28) it is possible to reformulate the shape calculus completely in a level set framework. If we rewrite the objective function $J(\mathcal{O})$

$$J(\phi) := J(\{x \in \mathbb{R}^d : \phi(x) < 0\}) = J(\mathcal{O})$$

and consider variations of the function ϕ according to

$$\phi(t, x) = \phi(x) + t\psi(x) \quad \Rightarrow \quad \left. \frac{\partial}{\partial t} \phi(t, x) \right|_{t=0} = \psi(x)$$

we obtain by (2.28)

$$\begin{aligned}\psi(x) &= -V(x) \cdot n |\nabla\phi(x)| \\ \Leftrightarrow -\psi(x) |\nabla\phi(x)|^{-1} n &= V(x)\end{aligned}$$

Thus, we can identify the derivative of J at ϕ in direction ψ as

$$dJ(\phi, \psi) := dJ(\mathcal{O}, -\psi(x)|\nabla\phi(x)|^{-1} n)$$

Note that for ϕ being a signed distance function, the above simply reads as

$$dJ(\phi, \psi) := dJ(\mathcal{O}, -\psi(x) n) \quad (2.30)$$

whereas ϕ being far away from a signed distance function will cause numerical problems.

Regularized gradient

To solve shape optimization problems, we propose a gradient descent method according to

$$\dot{\phi}(t) = -\text{grad}_{\mathcal{G}}J(\phi)$$

with respect to a metric \mathcal{G} on the Hilbert space θ of variations of the level set function ϕ . A discussion on different choices of \mathcal{G} can be found in [36, 38, 56, 123, 151]. We choose a weighted $H^{1,2}$ -metric according to

$$\mathcal{G}(\phi, \psi) = (\phi, \psi)_{L^2} + \frac{\sigma^2}{2}(\nabla\phi, \nabla\psi)_{L^2} = \int_D \phi\psi + \frac{\sigma^2}{2}\nabla\phi \cdot \nabla\psi \, dx$$

with $\sigma > 0$. Of course, the space θ has to be restricted to functions with sufficient regularity, say $\theta \subset C_0^1(D)$. We now obtain $\text{grad}_{\mathcal{G}}J(\phi)$ by solving

$$\mathcal{G}(\text{grad}_{\mathcal{G}}J(\phi), \psi) = dJ(\phi, \psi) \quad \forall \psi \in \theta \quad (2.31)$$

which is equivalent to solving the equation

$$\left(\mathbb{I} + \frac{\sigma^2}{2}\Delta\right) \text{grad}_{\mathcal{G}} = dJ(\phi)$$

in the sense of distributions. With this at hand, we follow a time discrete, regularized gradient scheme

$$\mathcal{G}(\phi^{k+1} - \phi^k, \psi) = -\tau dJ(\phi, \psi) \quad k \in \mathbb{N} \quad (2.32)$$

to generate a sequence of level set functions ϕ^k . At each time step, we apply Armijo's rule to control the step size τ . Thus, a level set function ϕ^{k+1} is accepted if

$$J(\phi^{k+1}) \leq J(\phi^k) - q \tau \mathcal{G}(\text{grad}_{\mathcal{G}}J(\phi^k), \text{grad}_{\mathcal{G}}J(\phi^k)) \quad q \in (0, 1) \quad (2.33)$$

is fulfilled, that means the objective J decreases sufficiently. If this requirement is

violated, the step size τ is set to $b \cdot \tau$, with $0 < b < 1$. In our implementation we set $q = 0.9$ and $b = 0.5$.

2.5 Solution Algorithm

We now have all ingredients to formulate the actual optimization algorithm.

Algorithm 2.17.

Beforehand, parameters have to be set:

- Specify the objective J , especially volume penalization α and surface penalization β .
- Define a maximal number of iterations $0 < Num_{iter} \in \mathbb{N}$; such a rough abort criterion is necessary due to numerical errors in the calculation of the shape derivative. We can not expect the derivative to be zero at the end of the process. In general, shape optimization problems do not have an analytical solution. Although, a numerical implementation is always just a relaxation of the original problem, existence of a minimizer is given only in rare cases.
- Set parameters q and b for the Armijo step size control, and an initial step size t_0
- Determine the frequency of topological changes n_{top}
- As initial shape choose the working domain D .

For $k = 0$ until $k = Num_{iter}$ do :

1. solve the elasticity system (2.5) (and if necessary it's dual system) for ϕ_k to obtain u_k and p_k
2. (a) For $(k \bmod n_{top}) \neq 0$: Compute the gradient direction $grad_{\mathcal{G}}J(\phi^k)$ according to (2.31), generate ϕ_{k+1} as described in (2.32) and find an acceptable step size t_k in (2.33).
 - (b) For $(k \bmod n_{top}) = 0$: Compute the topological gradient (2.14) and check whether or not a change of topology decreases the objective J , see Remark 2.16.
3. The updated level set function ϕ_{k+1} is re-initialized according to (2.29) to prevent errors in the calculation of the next gradient direction $grad_{\mathcal{G}}J(\phi^{k+1})$, see (2.30). Set $k := k + 1$ and return to step 1 unless $k = Num_{iter}$.

2.6 Numerical Settings

An efficient and accurate method for solving the state equation is of eminent importance for solving shape optimization problems. Since for each iteration step the state equation (in our case this is a vector valued system of partial differential equations (2.5)) needs to be solved, this constitutes the major part of the computational effort. Our discretization relies on a linear finite element method based on a quadratic grid defined on the working domain $D = [0, 1]^2$. To resolve the boundary in an adequate way, we use two different approaches. The first one is based on the so-called *composite finite elements* discretization. Here, each square is divided into two triangles. On this triangular grid we consider the space \mathcal{V}_h of piecewise affine continuous basis functions. $h = 2^{-l}$ denotes the side length of each square where $l \in \mathbb{N}^+$ is the grid depth. A shape $\mathcal{O}_h \subset D$ is then represented by a discrete level set function $\phi_h \in \mathcal{V}_h$. As described above, the boundary of \mathcal{O}_h is given by the zero level of ϕ_h which defines a finite polygon. Contrary to homogenization approaches and the SIMP-method [5, 26, 28, 29, 116], we deal with a solid-void material interface. Therefore, we need to adjust the finite element space \mathcal{V}_h for squares, which are intersected by the polygon $\partial\mathcal{O}_h$. Suppose $\theta_i \in \mathcal{V}_h$ to be a basis function on such a square. Then we define a vector-valued *composite finite element* basis function $\theta_{ij}^{cfe}(x) = e_j \chi_{\mathcal{O}_h}(x) \theta_i(x)$, where $e_1 = (1, 0), e_2 = (0, 1)$ are the basis vectors of \mathbb{R}^2 and $\chi_{\mathcal{O}_h}$ is the indicator function of \mathcal{O}_h . Altogether, those modified basis functions generate the *composite finite element* space \mathcal{V}_h^{cfe} . This approach has been introduced by Hackbusch and Sauter [82]. Here, the advantage is that degrees of freedom remain at the vertices of the original grid. Due to the uniform structure, it is possible to implement very efficient multigrid solvers. See [142] and further developments in [110]. Even elliptic boundary value problems with discontinuous coefficients across a given interface can be handled. This discretization approach underlies results computed in section 3.1.4 and is implemented the numerical software library *Quocmesh* which has been developed by the working group of Prof. M. Rumpf at the university of Bonn.

Although, this approach works fine in practice for shape optimization [51, 52, 90] we can not completely exclude that a truncation of the basis functions as described above, has a disturbing effect on the shape gradient. According to 2.11, the shape gradient has support on the boundary, so we need the solution u of the state equation to be as precise as possible on $\partial\mathcal{O}$. Therefore, we implemented a second approach to handle boundary conditions. Here, the boundary is fully resolved by an adapted grid, and so a truncation of basis functions is avoided.

Mesh generation for arbitrary domains is a great challenge and has been intensively investigated in different contexts, see [17, 19, 22, 30, 62, 110, 132, 138, 154, 157].

A very impressive, and thus inspiring, achievement is the triangular mesh generator developed by Jonathan Shewchuk [156]. Here, for a given polygonal boundary a tri-

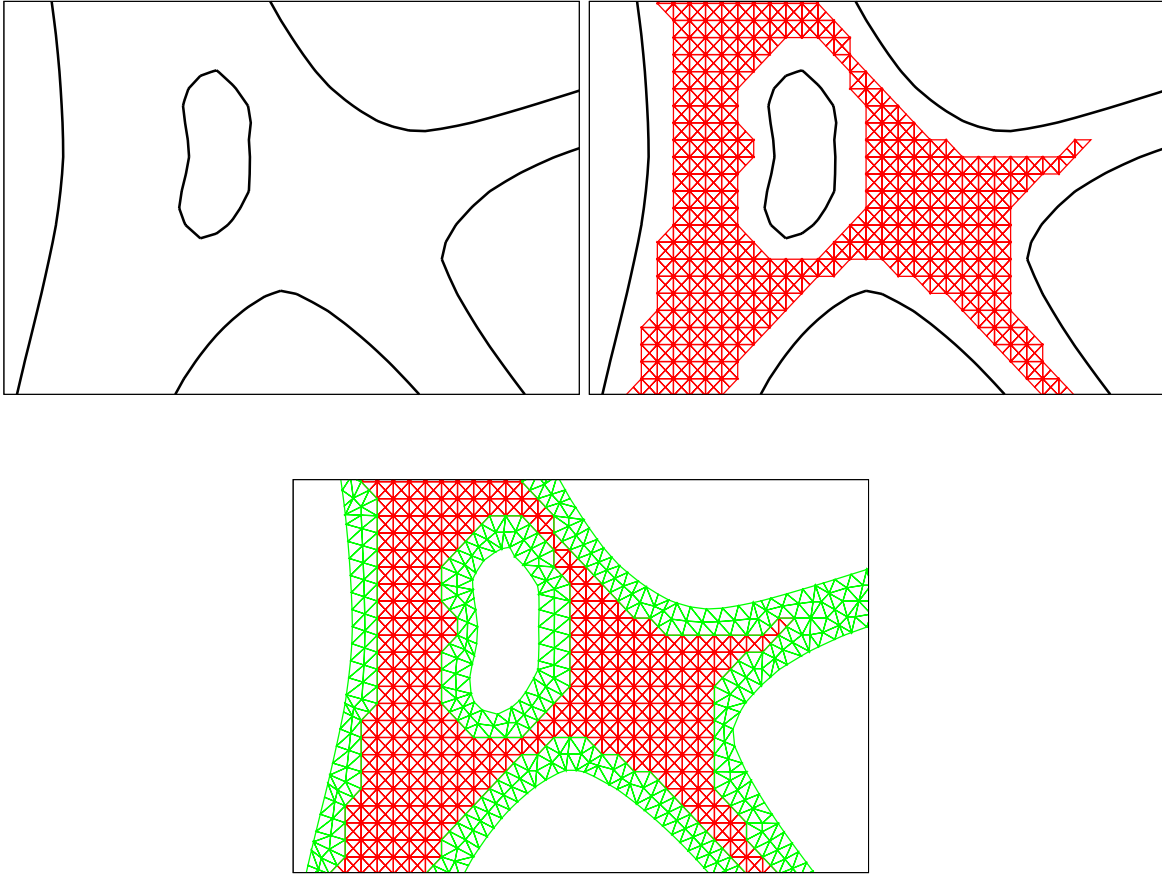


Figure 2.13: The process of constructing a hybrid grid resolving of the domain $\mathcal{O} = \{x \in \mathbb{R}^2 : \phi(x) < 0\} =: [\phi < 0]$ is illustrated. After identifying the polygon $[\phi = 0] := \partial\mathcal{O}$ (upper left side), the information about the distance of each grid point to the boundary, which is provided implicitly as ϕ is a signed distance function, is used to generate a semi-uniform grid inside \mathcal{O} (upper right side). Finally, an adapted grid resolving the boundary $[\phi = 0]$ is constructed.

angulation is generated with restrictions to the maximum angle or the size of each triangle. This avoids rounding errors caused by 'bad' finite elements, which would result in a ill-conditioned system matrix for a Ritz-Galerkin discretization. But, the obtained triangular mesh is not uniform. Thus, one has to deal with an increased expense in data-management, since information for each element needs to be stored. To get around this, we tried to combine advantages of both mesh types: low effort for data-management using a uniform grid on the one hand, and a good boundary approximation using an adapted grid on the other hand. How this is done is illustrated in (Fig. 2.13). We will briefly describe the process of our mesh generation. First the polygons, which compose $\partial\mathcal{O}_h$, are generated by evaluating the discrete level set function ϕ_h given on the uniform grid of squares. ϕ_h is a signed distance function, and therefore provides information about the distance to the boundary of each node of the

grid. Then, based on this information, all nodes with a minimum distance bigger than $1.5 h$ to the boundary are identified. These remain fixed and a semi-uniform grid, consisting of triangles, is constructed. In the last step, an unstructured triangulation is generated which contains the boundary nodes and the nodes of the semi-uniform grid near to the boundary. In doing so, we want the triangles to be as good as possible in the sense of aforementioned rounding errors. Up to now, this is done just in a heuristic way and in few situations yields obtuse angles. But in the majority of cases we obtain triangles with the desired properties, and thus, this approach serves well for our purpose.

This is not yet finished and further improvements regarding adaptive refinement, domain decomposition and multigrid methods are a future ambition.

This approach is used for the computation of results in the subsequent section and section 3.2.2.

2.6.1 Common Settings

We now demonstrate how this works in practice. First a selection of common settings is displayed. Compliance is the objective J to be optimized under a single load configuration.

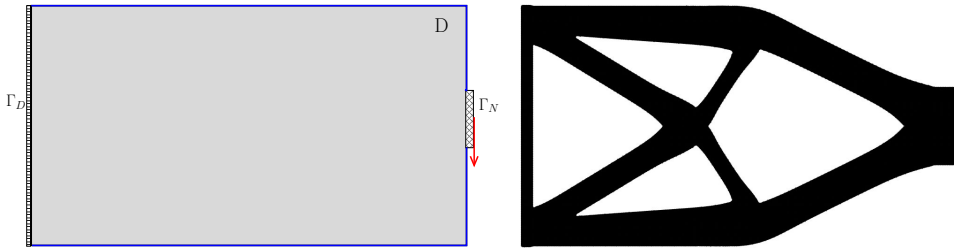


Figure 2.14: The configuration and the result from Fig. (2.9) is recaptured. This cantilever like structure is the most referred one in literature and serves well as a test setting. Here, we set the surface force to 5.5, volume constraint $\alpha = 1.4$, surface constraint $\beta = 0$ (this is always the case throughout this thesis) and threshold for the topological gradient $\tau_{top} = 0.05$. A topological change is considered every $n_{top} = 10$ iteration steps.

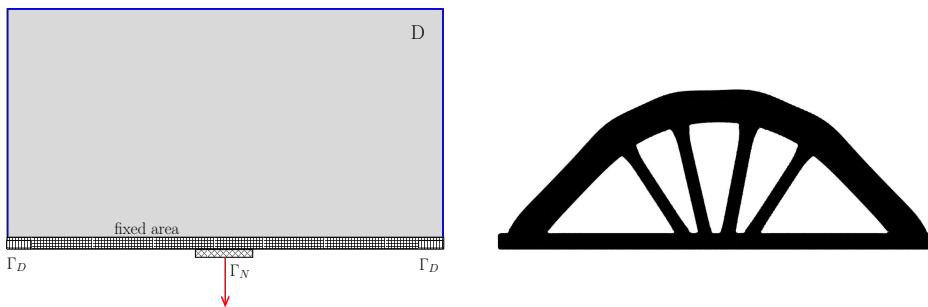


Figure 2.15: Here, we consider a bridge like configuration. Homogeneous Dirichlet boundary conditions are supposed downright and downleft. A force is applied down in the middle and the whole area at the bottom remains fixed during the optimization. It is the surface force $g = 20.0$, volume constraint $\alpha = 10.0$, surface constraint $\beta = 0$ and the threshold for the topological gradient $\tau_{top} = 0.05$. A topological change is considered every $n_{top} = 10$ iteration steps.

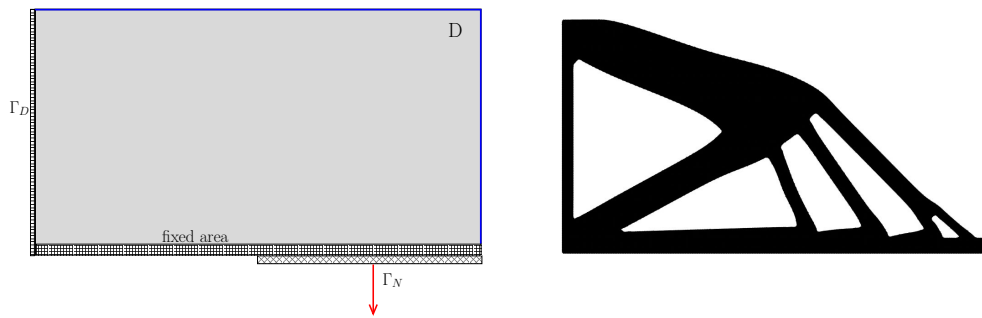


Figure 2.16: A different cantilever like configuration is examined. This time we consider the surface force g to act on a broader part of the boundary. We have $g = 5.5$, $\alpha = 10.0$, $\tau_{top} = 0.05$, and $n_{top} = 10.0$.

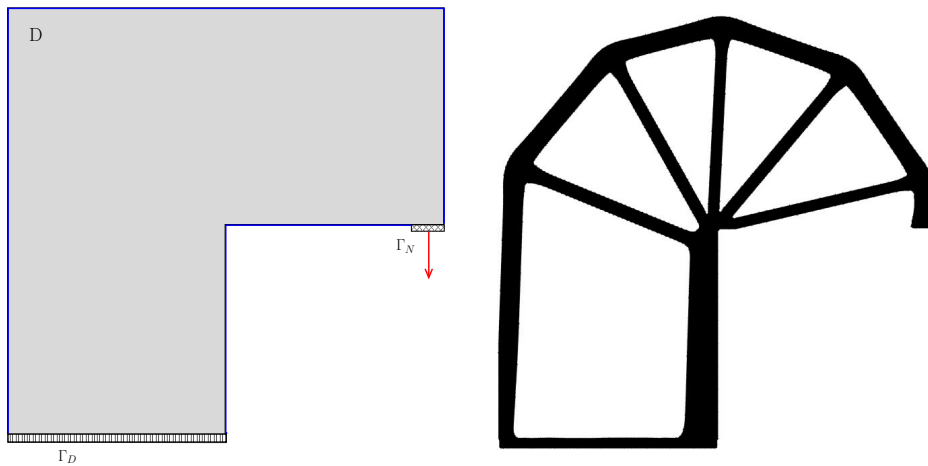


Figure 2.17: The last example shows a mast like configuration. Homogeneous Dirichlet boundary conditions are defined at the bottom left. The load is applied on the right. This time the working domain D has a corner which interrupts a direct connection between the Dirichlet and the Neumann boundary. This geometrical configuration is an additional restriction besides the volume constraint. In the examples before, obviously D was chosen large enough to have no effect on the optimization process. For this example we have $g = 20.5$, $\alpha = 10.0$, $\tau_{top} = 0.05$, and $n_{top} = 10.0$.

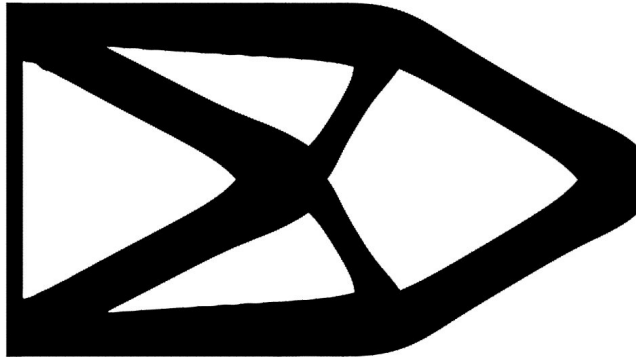


Figure 2.18: The cantilever structure that is obtained by solving the original problem. The surface force g is set to 1.8 and volume constraint $\alpha = 0.6$.

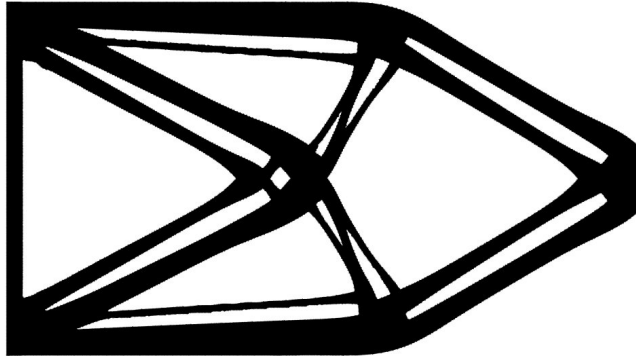


Figure 2.19: In the second scale, the cantilever shape in Fig. (2.18) is considered as the new working domain D_{new} . Then, an optimization with a bigger volume penalization is done. The surface force g maintains at an amount of 1.8 and the volume constraint α is increased to 0.8.

2.6.2 A Two-scale Approach

In many real-world applications, the structures used to design buildings, e.g. a bridge or a cantilever, are subjected to further restrictions. For instance, the construction of a bridge consisting of only one part, is not realistic. Such large-scale buildings are build up step by step out of smaller components. Here, we tried to detect such "sub-structures" by performing a two scale approach. We take the cantilever configuration as a test setting and proceed in the following way. First, the shape optimization problem defined in the working domain D , given as in Fig. (2.14) , is solved. Then, the resulting shape \mathcal{O} serves as the new working domain D_{new} . Doing so, reveals some "inner structure" of the cantilever.

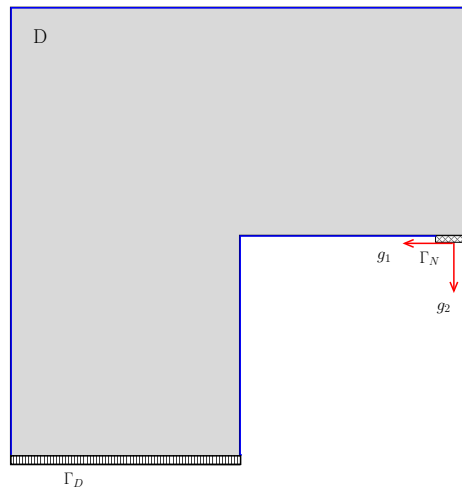


Figure 2.20: Configuration of a Two-load case. Forces g_1 and g_2 have the same amount (20.5) but differ in direction. Both occur with a probability of 0.5 .

2.6.3 A Hint to Stochastic: The Two-load Case

In most practical applications more than one single load is to consider. Forces applied can vary in direction, amount, or position on the boundary. The question arises, how to deal with this situation. Therefore, we will consider some basic approaches known from (stochastic programming) literature, and discuss a simple example which will give us a notion of the importance for models, which treat the involved uncertainties in an adequate way.

We consider a setting with two scenarios, each representing a surface force applied to the body \mathcal{O} with the same amount and position of the load, but different directions, as depicted in Fig. (2.20). Both scenarios occur with probability 0.5 . We take a view point inspired by stochastic programming theory and want to transfer knowledge and experience from that field to our considerations. There, a first approach is to replace computationally difficult problems by a simpler version. For example, instead of solving a complicated stochastic model, the deterministic model is considered which is obtained when all random variables are replaced by their expected value. Proceeding in this way ends up solving a single load case with a loading $g_{ev} = 0.5g_1 + 0.5g_2$. This results in the shape depicted in Fig. (2.21) on the right, which is called the *EV-solution* and denoted by \mathcal{O}_{ev} .

A more subtle but costlier approach is to minimize the expected-value of the shape functional $J(\mathcal{O})$. That is, we minimize $J_{ev}(\mathcal{O}) := 0.5J_1(\mathcal{O}) + 0.5J_2(\mathcal{O})$, where J_i is the corresponding functional for the load g_i . This is known as Multiload case in literature concerning shape or topology optimization. From a stochastic programming point of view, this will be the starting point for a two-stage formulation which serves as the

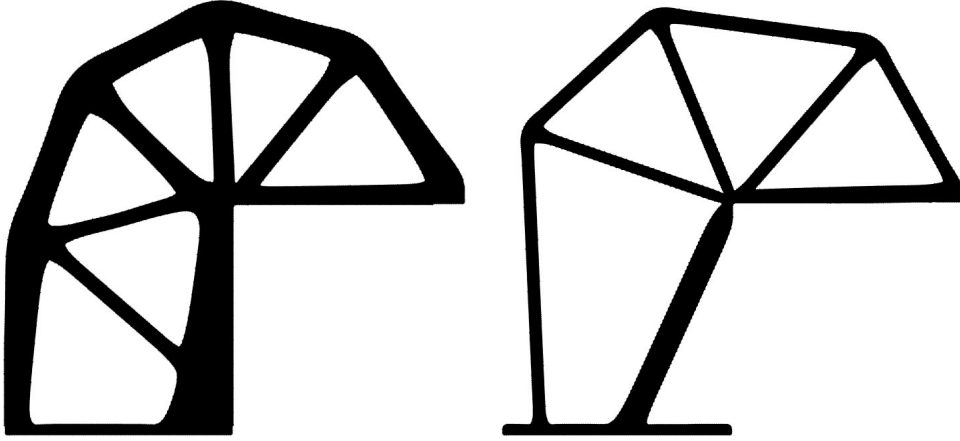


Figure 2.21: The shapes for the different approaches are depicted. On the left: the resulting shape corresponding to a minimization of the expected value of the shape functional $J(\mathcal{O})$ (Multiload case). On the right: the resulting shape obtained by minimization of the shape functional $J(\mathcal{O})$ only considering the expected value of the force g (EV-solution).

counterpart of a two-stage problem with fixed recourse. We will go into detail on that later in this thesis. This approach leads to the result shown in Fig. (2.21) on the left, and differs significantly from that one obtained from the first approach.

For assessment of these two different results, in stochastic programming literature, the concept of the *expected value of perfect information* (EVPI) and *value of the stochastic solution* (VSS) are employed, see [31] for instance. There, EVPI is defined as $EVPI := RP - WS$, where RP (recourse problem) is the optimum value of a two-stage stochastic linear program, whose counterpart here is $\arg \min_{\mathcal{O}} J_{ev}(\mathcal{O})$. WS is the so-called *wait-and-see* solution, which is calculated in the following way:

Suppose \mathcal{O}_i to be the solution to

$$\min\{J_i(\mathcal{O}) : \mathcal{O} \in \mathcal{U}_{ad}\}$$

where $i \in \{1, \dots, S\}$, S being the number of scenarios (here $S=2$). Then it holds $WS := \sum_{i=1}^S \pi_i J_i(\mathcal{O}_i)$ with π_i denoting the probability of each scenario.

In our case it is $WS = 0.5J_1(\mathcal{O}_1) + 0.5J_2(\mathcal{O}_2) = 0.5 (0.781928 + 3.38561) = 2.083769$ and $RP = 4.80335$. Thus $EVPI = 2.719581$.

The value of the stochastic solution is defined as $VSS := EEV - RP$. Where EEV is the *expected result using the EV solution*, $EEV := \sum_{i=1}^S \pi_i J_i(\mathcal{O}_{ev})$.

In our case $EEV = 0.5J_1(\mathcal{O}_{ev}) + 0.5J_2(\mathcal{O}_{ev}) = 0.5 (35.3106 + 33.2749) = 34.29275$. Thus $VSS = 29.4894$.

It can be proven that it holds

$$WS \leq RP \leq EEV$$

in the linear and in the non-linear case, see [31]. In that way, we can identify upper and lower bounds for the optimal values of our stochastic optimization model and assess the quality of those.

3 Stochastic Shape Optimization Models

Deterministic shape optimization has been developed and analyzed for a wide range of applications including aerospace engineering [88, 144, 145], structural mechanics [6, 29, 85, 111], geometrical inverse problems [38] and many more. When dealing with related mathematical and numerical models, uncertainties which arise from real world applications play an underrated role. This might be due to the fact that shape optimization, itself, is extremely challenging from the mathematical and numerical point of view. Additionally, quantification of uncertainties is no less problematic. There is plenty of possibilities to introduce uncertainties. They can be considered as a lack of knowledge of material properties, i.e., unknown coefficients or unknown geometry, think of microstructures, or the case we will deal with that is stochastic loadings. We have done first steps to bring together the latter type of uncertainty with shape optimization in [51, 52, 90]. Forces applied are considered to be of random character, that is the loadings f and g are becoming random variables $f(\omega), g(\omega)$, $\omega \in \Omega$ on some probability space $(\Omega, \mathcal{F}, \mathbb{P})$. The elasticity equation then reads

$$\begin{aligned} -\operatorname{div}(\mathcal{A}(\epsilon(u))) &= f(\omega) && \text{in } \mathcal{O} \\ u &= 0 && \text{on } \Gamma_D \\ \mathcal{A}(\epsilon(u)) \cdot n &= g(\omega) && \text{on } \Gamma_N \end{aligned} \tag{3.1}$$

The solution u of the state equation and the shape functional J then are random variables, too, denoted by $u(\mathcal{O}, \omega)$, $J(\mathcal{O}, u(\mathcal{O}, \omega))$. In this way, the following family of random variables arises

$$\{G(\mathcal{O}, \omega) : \mathcal{O} \in U_{ad}\} \tag{3.2}$$

where

$$G(\mathcal{O}, \omega) = \alpha \int_{\mathcal{O}} 1 \, dx + \beta \int_{\Gamma_N} 1 \, d\nu + J(\mathcal{O}, u(\mathcal{O}, \omega)) \tag{3.3}$$

and $J(\mathcal{O}, u(\mathcal{O}, \omega))$ takes the general form as in (2.16).

$$J(\mathcal{O}, u(\mathcal{O}, \omega)) = \int_{\mathcal{O}} j(x, u(\mathcal{O}, \omega)) dx + \int_{\Gamma_N} l(x, u(\mathcal{O}, \omega)) d\nu \quad (3.4)$$

From this perspective, \mathcal{O} can be seen as a 'parameter' defining a random variable $J(\mathcal{O}, \omega)$. "Optimizing" \mathcal{O} , hence, means finding an 'optimal' random variable. This raises the conceptual problem of how to rank random variables in (3.2).

The obvious fact, that under the above uncertainty the shape has to be fixed before knowing the outcome of the random problem ingredients requires that \mathcal{O} must not depend on ω . This is referred to as non-anticipativity of \mathcal{O} and becomes clear when looking at the following scheme of 'decision and observation' :

$$\text{decide } \mathcal{O} \longrightarrow \text{observe } f(\omega), g(\omega) \longrightarrow \text{decide } u = u(\mathcal{O}, \omega) \quad (3.5)$$

This view displays the non-anticipativity requirement, namely that the domain \mathcal{O} must be selected prior to observing random forces $g(\omega)$ and $f(\omega)$, according to the information constraint. From this perspectives we reformulate the shape optimization problem as

$$\min\{G(\mathcal{O}, \omega) : \mathcal{O} \in U_{ad}\} \quad (3.6)$$

Throughout this thesis, we set $\beta = 0$ and we will write $Vol(\mathcal{O})$ instead of $\int_{\mathcal{O}} 1 dx$, for sake of comprehension, so the problem becomes

$$\min\{\alpha Vol(\mathcal{O}) + J(\mathcal{O}, u(\mathcal{O}, \omega)) : \mathcal{O} \in U_{ad}\} \quad (3.7)$$

Reminding that the displacement u is the minimizer of the elastic energy $\mathcal{E}_{elast}(v)$ in (2.4),

$$\mathcal{E}_{elast}(v) := \int_{\mathcal{O}} \left[\frac{1}{2} \cdot \mathcal{A}(\epsilon(v)) : \epsilon(v) - f \cdot v \right] dx - \int_{\partial\mathcal{O}} g \cdot v d\nu$$

that is

$$u = \arg \min_v \mathcal{E}_{elast}(v)$$

and problem (3.7) becomes

$$\min\{\alpha Vol(\mathcal{O}) + J(\mathcal{O}, u(\mathcal{O}, \omega)) : u(\omega) = \arg \min_v \mathcal{E}_{elast}(v, \omega), \mathcal{O} \in U_{ad}\} \quad (3.8)$$

and finally, performing a last simple transformation, we obtain the formulation

$$\min \left\{ \alpha Vol(\mathcal{O}) + \min \left\{ J(\mathcal{O}, u(\mathcal{O}, \omega)) : u(\omega) = \arg \min_v \mathcal{E}_{elast}(v, \omega) \right\} \mid \mathcal{O} \in \mathcal{U}_{ad} \right\} \quad (3.9)$$

which emphasizes a two-stage character with an inner optimization problem for the random variable $J(\mathcal{O}, u(\mathcal{O}, \omega))$.

Admittedly, the inner optimization problem is fairly simple, because of the fact that there exist a unique minimizer of the elastic energy $\mathcal{E}_{elast}(v)$, but this new aspect stimulated further development of stochastic models. So, this underlying model problem will be briefly discussed in (3.1.1).

3.1 Mean Risk Models

Finding 'best' members in (3.2) for the problem formulated above calls for a proper ranking for this family of random variables. For a risk neutral setting, we proposed a stochastic programming model which ranked members of (3.2) according to their expected value. This choice completely ignores the variability of random variables in [51]. Thus, it may result in selecting an 'optimal' \mathcal{O} whose accompanying random variable $J(\mathcal{O}, \omega)$ takes big values 'too often'. To get around this lack of precaution, rankings according to risk measures are introduced. In a first approach, we have employed the expected excess and the excess probability. Thus, we focus on those three types of optimization problems

- Expected Value:

$$\min \{ \alpha Vol(\mathcal{O}) + \mathbb{E}_\omega [J(\mathcal{O}, u(\mathcal{O}, \omega))] \mid \mathcal{O} \in \mathcal{U}_{ad} \} \quad (3.10)$$

- Expected Excess:

$$\begin{aligned} \min \{ \alpha Vol(\mathcal{O}) + \mathbb{E}_\omega [\max\{J(\mathcal{O}, u(\mathcal{O}, \omega)) - \eta, 0\}] \mid \mathcal{O} \in \mathcal{U}_{ad} \} \\ \text{with preselected } \eta \in \mathbb{R} \end{aligned} \quad (3.11)$$

- Excess Probability:

$$\begin{aligned} \min \{ \alpha Vol(\mathcal{O}) + \mathbb{P}_\omega [J(\mathcal{O}, u(\mathcal{O}, \omega)) > \eta] \mid \mathcal{O} \in \mathcal{U}_{ad} \} \\ \text{with preselected } \eta \in \mathbb{R} \end{aligned} \quad (3.12)$$

Here, \mathbb{E} denotes the expected value of a random variable, thus it is a real number. The statistical parameter η quantifies the variability (risk) of a random variable. While for (3.12) it only matters whether $G(\mathcal{O}, \omega)$ exceeds η or not, (3.11) measures how much $G(\mathcal{O}, \omega)$ exceeds η in the mean. Such sort of optimization settings are referred to as mean-risk models and have been investigated for shape optimization in previous works [51, 52, 90].

We will enrich our selection of risk measures by stochastic dominance models, which rely on stochastic orders, also called integral orders, to rank random variables and offer a different way to assess the quality of those. In the mean-risk models considered above, risk aversion is accomplished by assigning a statistical parameter η , i.e., a real number, and evaluating the quality of the random variable $G(\mathcal{O}, \omega)$ by this. Our alternative to evaluate the quality of random variables is to compare it to a fixed benchmark random variable $b(\tilde{\omega})$, where b might have a different distribution as members in (3.2). To this end, we employ a partial order \preceq on the space of random variables and require that

$$G(\mathcal{O}, \omega) \preceq b(\tilde{\omega}).$$

Instead of heading for 'best' members in (3.2), this enables to identify a subset of 'acceptable' members:

$$\{\mathcal{O} : G(\mathcal{O}, \omega) \preceq b(\tilde{\omega}), \mathcal{O} \in \mathcal{U}_{\text{ad}}\} \quad (3.13)$$

From the modeling point of view, the benchmark allows for more flexibility in constructing requirements to the properties of random variables. For instance, rather than requiring that $G(\mathcal{O}, \omega)$ must not exceed the deterministic value of, say, 50, we might wish to allow for values up to 60, on the one hand, and to require that 35 not to be exceeded with 40% and 40 with 90% probability, on the other hand. In this way, risk aversion is not governed by 'just a real number' but by a benchmark which allows to include distribution information. Furthermore, we can select members in (3.13) being optimal with respect to a different criterion, e.g. minimal volume. Then, the optimization task would read as

$$\min\{Vol(\mathcal{O}) : G(\mathcal{O}, \omega) \preceq b(\tilde{\omega}), \mathcal{O} \in \mathcal{U}_{\text{ad}}\} \quad (3.14)$$

Subsequently, when we detail how constraints of type $G(\mathcal{O}, \omega) \preceq b(\tilde{\omega})$ can be implemented, we will see that aforementioned mean-risk models, the expected excess (3.11) and excess probability (3.12), are of eminent importance.

3.1.1 Stochastic Programming Perspective

As said, our implementation of stochastic shape optimization models is inspired by stochastic programming theory, which is a generic term for optimization problems involving uncertain parameters, for which stochastic models are available. Optimization problems involving stochastic models are found in wide areas of science and engineering, see for instance [171]. They address e.g. portfolio management and asset pricing in mathematical finance, production planning and scheduling under uncertainty or network planning in operations research. A main feature of this field of applications is decision making under uncertainty, for which stochastic programming provides a mathematical framework. Mathematical models issuing from that field depend on an underlying probability distribution, in detail, on information available on the uncertain problem components. For example, there are worst-case approaches, as in on-line or robust optimization [4,24], for the latter at least the ranges of the uncertain parameters have to be known, but no detailed distributional information. In the case when complete distributional information is available, as assumed throughout this thesis, different approaches are applicable. Of course, detailed distributional information can only be provided by statistical investigations of the involving uncertain parameters, and therefore is an aspect of modeling.

Taking notice of the information constraint (3.5) of our stochastic shape optimization model one observes a similarity with a special type of stochastic program. In fact, two-stage stochastic linear programming. The two-stage character of the arising shape optimization problem has been discussed detailed in [51,90].

3.1.2 Two-Stage Stochastic Programming Perspective

Let us gather some results we have obtained in previous works, starting with a short review of two-stage stochastic program and then drawing an analogy to shape optimization. Consider the random linear program

$$\min\{c^T x + q^T y : Tx + Wy = z(\omega), x \in X, y \in Y\} \quad (3.15)$$

for finite dimensional polyhedron X and Y in the Euclidian space together with the information constraint

$$\text{decide } x \mapsto \text{observe } \omega \mapsto \text{decide } y = y(x, \omega) \quad (3.16)$$

Assuming existence of a minimum, we rewrite (3.15) to emphasize the two-stage characteristic

$$\begin{aligned} & \min_x \{c^T x + \min_y \{q^T y : Wy = z(\omega) - Tx, y \in Y\} : x \in X\} \\ & = \min \{c^T x + \Phi(z(\omega) - Tx) : x \in X\} \end{aligned} \quad (3.17)$$

where $\Phi(v) := \min\{q^T y : Wy = v, y \in Y\}$ is a value function of a linear program with parameters on the right hand side. Then the task is to minimize the random cost functional $j(x, \omega) := c^T x + \Phi(z(\omega) - Tx)$. The two-stage character of this problem becomes clear when looking at (3.17) as one can interpret the search for a "best" non-anticipative decision x as the search for a "minimal" member in the family of random variables $\{j(x, \omega) : x \in X\}$. Choosing x means choosing a random variable $j(x, \omega)$, where randomness results from Φ ; x can be seen as an "index" varying in the set X . In that way, the two decisions on x and y become one decision on x ; y can be constructed after an "optimal" x is computed. But the price we have to pay is we have to deal with random variables $j(x, \omega)$, instead. That is, we need to assess the quality of random variables to find a 'best'. This is when risk measures come into play. For example, in a risk-neutral setting, random variables are ranked by their expectation, leading to the (nonlinear) optimization problem

$$\min \{\mathbb{E}_\omega(j(x, \omega)) : x \in X\} \quad (3.18)$$

This is the starting point for our shape optimization models.

Before we discuss results for these models, we will explain the structure of the random forces which underly our model problem.

3.1.3 Incorporating Stochastic Loadings

In order to set up a framework for the uncertainty in our considerations, we need to define a probability space, i.e., a triple $(\Omega, \mathcal{F}, \mathbb{P})$, for our optimization model. For the sake of completeness, we shortly recall the definition of a probability space.

In stochastic programming, uncertainty is represented in terms of random experiments with outcomes, called random elements. We say Ω is the universe of all possible outcomes, the sample space. A generic outcome of a random experiment is denoted by $\omega \in \Omega$. A subset F of Ω is called an event. The event F is said to have occurred if the outcome of the experiment is an element of F . Furthermore, the set of all events is represented by \mathcal{F} and is required to be a σ -algebra. Finally, $\mathbb{P} : \mathcal{F} \rightarrow [0, 1]$ is supposed to be a probability measure which assigns each event $F \in \mathcal{F}$ a value $\mathbb{P}(F) \in [0, 1]$ called probability of the event F .

We assume that ω follows a discrete distribution with finitely many realizations. That

is $\Omega = \{\omega_1, \dots, \omega_S\}$, $S \in \mathbb{N}^+$, each ω_i representing an event. Each scenario ω_i occurs with probability $\pi_i = \mathbb{P}(\{\omega_i\})$, for $i \in \{1, \dots, S\}$ and it is $\sum_i^S \pi_i = 1$.

We assume occurring forces to be random and suppose the set of realizations of these random forces consists of pairs $(f(\omega_i), g(\omega_i))$ of volume and surface loads. If we deal with K_1 realizations of $f(\omega)$, $K_1 \in \mathbb{N}^+$, and K_2 realizations of $g(\omega)$, $K_2 \in \mathbb{N}^+$, we observe that the number of possible scenarios is

$$S = |\{(f(\omega_i), g(\omega_i))\}| = K_1 \cdot K_2$$

One gets aware that increasing the number of realizations of f and g results in a fast growing number of scenarios, for which one has to solve the state equation, the elasticity model in (2.5). Solving systems of partial differential equations numerically is computationally expensive and therefore a high number of scenarios results in inadequate computational costs. To keep the numerical effort at an acceptable level, we will use an algorithmic shortcut.

First, due to linearity of the state equation, it is possible to compute the solutions for volume and surface forces separately. In detail, may u_f be the solution for the state equation with right hand side $f(\omega_i)$ for some realizations of ω . And let u_g be the solution for the state equation with right hand side $g(\omega_i)$. Then, a straight forward calculation yields that $u_f + u_g$ is the solution for the state equation with right hand side $(f(\omega_i), g(\omega_i))$. So, the number of equations to solve reduces to $K_1 + K_2$.

Second, our considerations are restricted to the case that all scenario forces are devised by a fixed number of so-called basis forces. In detail, scenario forces $f(\omega)$ and $g(\omega)$ are linear combinations of the basis forces.

$$f(\omega) = \sum_{n=1}^{L_1} \alpha_n(\omega) f^n, \quad g(\omega) = \sum_{m=1}^{L_2} \beta_m(\omega) g^m$$

In this way, the randomness is shifted to the coefficients, i.e., $\alpha_n(\omega)$ and $\beta_m(\omega)$. Now, we just have to handle a fixed number of deterministic basis forces the state equation has to be solved for, called basis scenarios. Doing so, a scenario solution $u(\omega_i)$ is obtained by linear combination of solutions of the basis scenarios u_n^f and u_m^g according to realizations of the random coefficients.

$$u(\omega_i) = \sum_{n=1}^{L_1} \alpha_n(\omega_i) u_n^f + \sum_{m=1}^{L_2} \beta_m(\omega_i) u_m^g \quad (3.19)$$

This, too, follows from the linearity of the elasticity model (2.5) using the same argumentation as above. So, the special construction of random forces enables to deal with a high number of scenarios at moderate computational costs by building on a reasonable number of basis forces. Say $L_1 \ll K_1$ and $L_2 \ll K_2$, then there are $L_1 + L_2$

equations of type (2.5) to solve for a stochastic shape optimization model concerning $K_1 \cdot K_2$ scenarios.

3.1.4 Results for Mean Risk Models

At this point, we discuss our numerical implementation of risk models introduced at the beginning of section 3.1. Comparing the optimal shapes for each respective risk model, will give us a notion of the impact of each model. This will be helpful in the succeeding chapter where we define stochastic dominance models as they rely on models for expected excess and excess probability.

As said before, the expected-value model

$$\min\{\alpha Vol(\mathcal{O}) + \mathbb{E}_\omega [J(\mathcal{O}, u(\mathcal{O}, \omega))] : \mathcal{O} \in \mathcal{U}_{ad}\} \quad (3.20)$$

is risk neutral in the sense that critical realizations of $J(\mathcal{O}, u(\mathcal{O}, \omega))$, say extremely high values occurring with marginal probability, are of no particular importance for the expected value. If this is not acceptable, we may refine assessment of risk by introducing a threshold, above which realizations of $J(\mathcal{O}, u(\mathcal{O}, \omega))$ are to be avoided. Our first implementation of risk aversion is given by the expected amount of which $J(\mathcal{O}, u(\mathcal{O}, \omega))$ exceeds that threshold. This model is called expected excess model:

$$\begin{aligned} \min\{\alpha Vol(\mathcal{O}) + \mathbb{E}_\omega [\max\{J(\mathcal{O}, u(\mathcal{O}, \omega)) - \eta, 0\}] : \mathcal{O} \in \mathcal{U}_{ad}\} \\ \text{with preselected } \eta \in \mathbb{R} \end{aligned} \quad (3.21)$$

Here, η is the intended threshold and the function $\max\{., 0\}$ ensures that only realizations $J(\mathcal{O}, u(\mathcal{O}, \omega))$ exceeding η are taken into account.

Another approach to design risk aversion arises when we ask for the probability that $J(\mathcal{O}, u(\mathcal{O}, \omega))$ exceeds threshold η . This is implemented by the excess probability model:

$$\begin{aligned} \min\{\alpha Vol(\mathcal{O}) + \mathbb{P}_\omega [J(\mathcal{O}, u(\mathcal{O}, \omega)) > \eta] : \mathcal{O} \in \mathcal{U}_{ad}\} \\ \text{with preselected } \eta \in \mathbb{R} \end{aligned} \quad (3.22)$$

Here, it only matters if threshold η is exceeded, in contrast to the expected excess model, which measures how much η is exceeded. Thus, we obtain the following identity

$$\mathbb{P}_\omega [J(\mathcal{O}, u(\mathcal{O}, \omega)) > \eta] = \mathbb{E}_\omega [\mathcal{H}(J(\mathcal{O}, u(\mathcal{O}, \omega)) - \eta)] \quad (3.23)$$

where $\mathcal{H}(x) : \mathbb{R} \rightarrow \mathbb{R}$ is the Heaviside function being 0 for $x \leq 0$ and 1 for $x > 0$. Note that this identity has no mathematical meaning, as the quantity on the left hand side

is probability, whereas the one on the right hand side is an expected value. But, it is easy to see that these real values coincide.

Altogether, we find that the above refined risk measures simply replace a minimization of the expected value of the objective $\mathbb{E}_\omega [J(\mathcal{O}, u(\mathcal{O}, \omega))]$ by a minimization of $\mathbb{E}_\omega [q(J(\mathcal{O}, u(\mathcal{O}, \omega)))]$. Where q is a nonlinear monotone increasing function $q : \mathbb{R} \rightarrow \mathbb{R}$, which reflects a specific aversion of risk. It is $q = \max\{., 0\}$ for the expected excess and $q = \mathcal{H}(\cdot)$ for the excess probability.

As differentiable approximations for q we use either

$$\max\{x, 0\} = \frac{\sqrt{x^2 + x}}{2} \approx \frac{\sqrt{x^2 + \epsilon + x}}{2} =: q_{max}^\epsilon(x) \quad \epsilon > 0 \quad (3.24)$$

or

$$\mathcal{H}(x) \approx \frac{1}{1 + e^{-2\epsilon}} =: q_H^\epsilon(x) \quad (3.25)$$

in accordance with the choice of q . Those we used in our numerical applications are depicted in Fig. (3.1). We denote \mathbf{Q}_{EE}^ϵ for the expected-excess model, \mathbf{Q}_{EP}^ϵ for the excess-probability model and \mathbf{Q}_{EV} for the expected-value model.

Thus, shape and topological derivatives of above functionals are simply obtained by the chain rule. Say $\mathbf{Q} = \mathbb{E}_\omega [q(J(\mathcal{O}, u(\mathcal{O}, \omega)))]$ and suppose ω has a finite number of realizations, we obtain

$$d\mathbf{Q}(\mathcal{O}, V) = \sum_{i=1}^{N_s} \pi_i q'(J(\mathcal{O}, \omega_i)) dJ(\mathcal{O}, \omega_i, V). \quad (3.26)$$

for the shape derivative and

$$D_T \mathbf{Q}(\mathcal{O}, x) = \sum_{i=1}^{N_s} \pi_i q'(J(\mathcal{O}, \omega_i)) D_T J(\mathcal{O}, \omega_i, x). \quad (3.27)$$

for the topological derivative. So, a slight modification of algorithm (2.17) for the evaluation of the cost functional, the shape and topological derivative needs to be done. We refer to [52] for a sketch of the resulting algorithm.

Let us now take a look at how this works in practice. Quoting from [90] we first describe the test setting and discuss results of risk neutral optimization. Then, we survey our own research published in [52] and focus on models with risk aversion. As a test setting, we suppose the situation illustrated in Fig. 3.2. There, two fixed areas on the top of the construction domain are affected by loadings in different directions. The bottom of the construction domain is considered to be firm ground, that is homogeneous Dirichlet boundary. We aim at optimizing the compliance of structures which support the areas under load. Two different instances are shown, each with

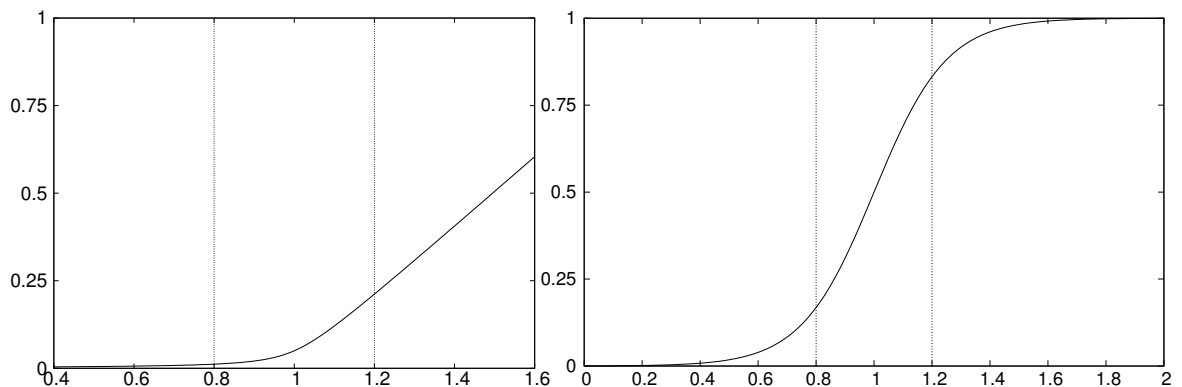


Figure 3.1: The profiles of q_{max}^ϵ with $\epsilon = 0.01$ for the expected excess model (left) and q_H^ϵ with $\epsilon = 0.25$ for the excess probability model (right) are depicted. In our applications below, we used $\eta = 1.0$. The dotted vertical lines (up to a shift) refer to dotted horizontal lines in the bar charts for the whole set of scenarios displayed in Fig. 3.6.

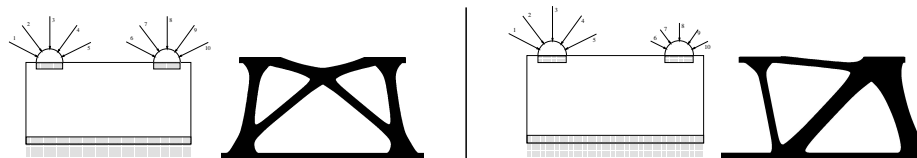


Figure 3.2: On the left side we see a symmetric stochastic load configuration which leads to symmetric structure, whereas a non-symmetric stochastic loading (on the right) results in a non-symmetric truss construction. These examples are quoted from [90].

ten scenarios forces. In the first one on the left, a symmetric setting of scenarios is considered. All scenario forces are equally strong and occur with the same probability. The second instance, on the right, pictures a non-symmetric setting. Forces applied on the left are twice as strong as those on the right. But each force on the left occurs with probability 1%, while those on the right do with 19%. To compute the scenario forces, 4 basis forces are required, two for each area under loading, respectively. As discussed in the previous section, the elasticity system only needs to be solved for these basis forces. Then, we benefit from the linearity of the elasticity model and compute scenario solutions from basis solutions, see section 3.1.3.

Optimization of the expected value leads to different structures depicted in Fig. (3.2). As we might expect, the symmetric load configuration results in a symmetric structure, whereas optimization in a non-symmetric load setting takes account of the fact that forces on the left, on average, play a minor role.

We now investigate how our risk averse models take impact on the resulting shape. The non-symmetric load configuration serves as our test setting. First, we focus on the expected excess model. Here, the threshold η plays a central role. Obviously, setting $\eta = 0$ results in an expected-value optimization, as we deal with the compliance

as shape functional, which is always nonnegative. In Fig. (3.3), we see a family of optimal shapes minimizing the expected excess for varying excess parameter η . One

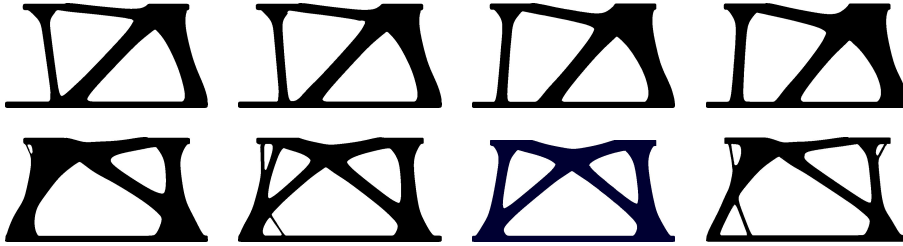


Figure 3.3: Results for an optimization for the expected-excess with different η . The displayed shapes correspond to the sequence $\eta = 0.1, 0.2, 0.3, 0.4, 0.6, 0.8, 1.0$ and 1.5 . Here, the load configuration shown in Fig. 3.2 (second right) is used.

observes that there exists a link between the parameter η and the resulting optimal shape, which appears to be continuous. For a better understanding which effect the scenario loadings take on different structures, the energy distribution (compliance) is illustrated for optimal shapes for three different values of η in Fig. (3.4). Forces applied on the left cause a significant higher compliance than those applied on the right. But, for a rather small threshold η , forces with a high probability, which are those on the right, contribute far more to the expected excess. With increasing threshold, this dominating effect vanishes, and forces on the right gain more attention. Thus, more support on the left is needed and results in a 'material shift' to the left side.

The situation is different in the case when optimizing the excess probability. Here, one observes a total 'material shift' to the right side. This is due to the fact that the excess probability model only detects if threshold η is exceeded. The amount by which η is exceeded has no impact. Thus, high forces on the left are de facto neglected, due to their low probabilities. Hence, forces on the right are the main focus. As a consequence, no support is needed for the left bearing and during the optimization process only thin trusses remain. Finally, these are removed via a topological optimization step to enable the optimization process to proceed. This very moment is illustrated in Fig. (3.5).

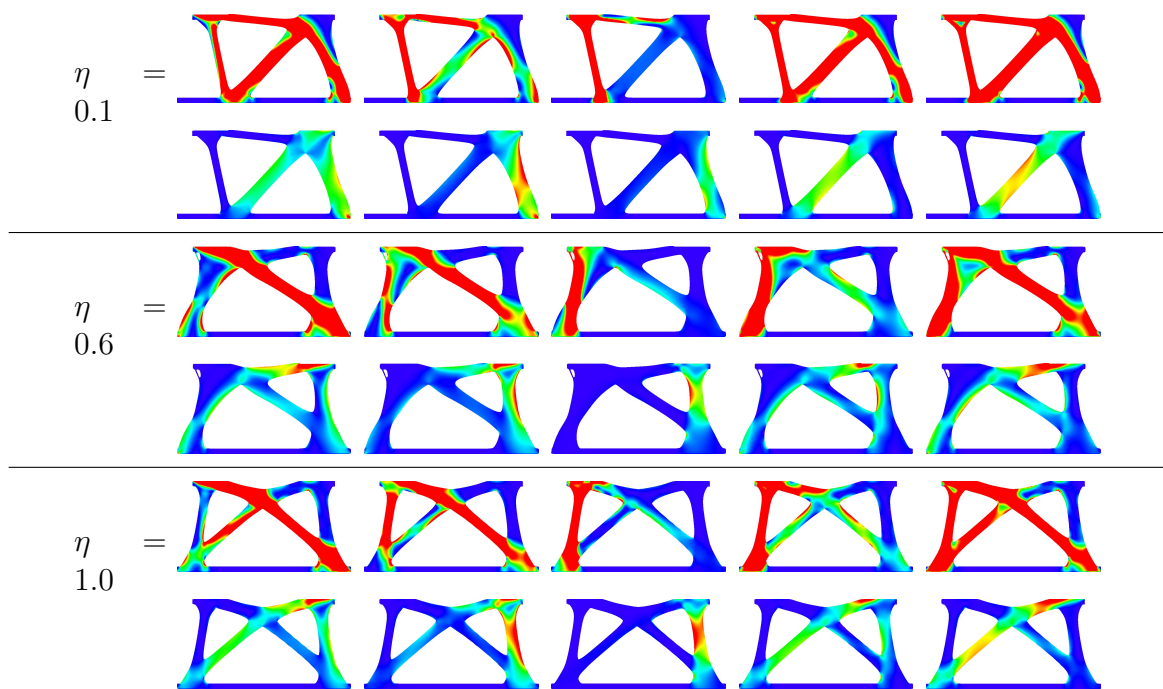


Figure 3.4: The energy distributions ($\mathcal{A}\epsilon(u) : \epsilon(u)$) for each scenario of the optimal shapes for the expected-excess model for different η are colorcoded as . The configuration of the loading is as in Fig. (3.2) (second right) and the set of realizations is taken from Fig. (3.3). The η values are shown on the left.



Figure 3.5: During the optimization process of the excess-probability model (for $\eta = 0.4$), a focus on the right bearing manifests itself. This is due to the fact, that loadings on the right are smaller than the ones on the left, but occur with higher probability. This leads to decreasingly thin structures on the left, until those are completely neglected by performing a topological optimization step. The final result is shown on the right.

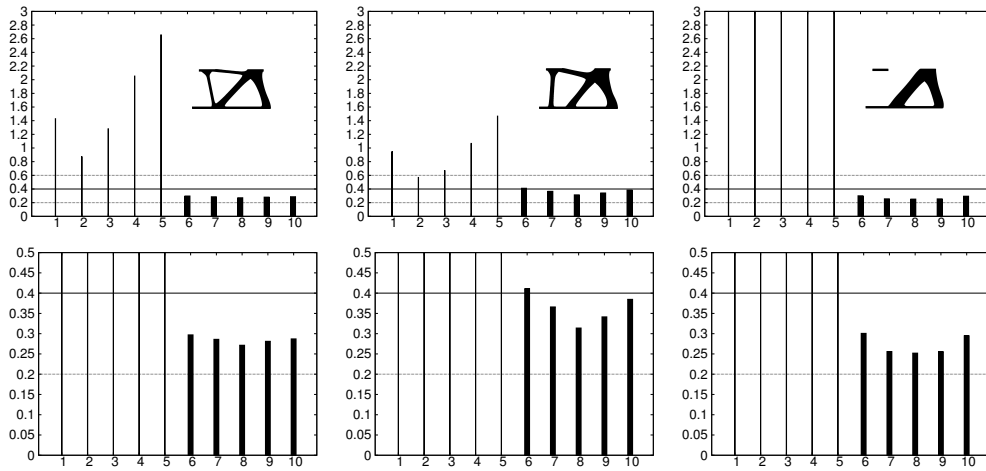


Figure 3.6: For optimal shapes corresponding to the stochastic cost functionals \mathbf{Q}_{EV} , $\mathbf{Q}_{EE}^{0.01}$ and $\mathbf{Q}_{EE}^{0.25}$ (with $\eta = 0.4$), the objective values for each scenario are displayed in a bar chart. The bar thickness is chosen proportional to the probability. The second row is a zoom into the diagrams.

Let us assemble the results for above risk averse functionals for a cross check. In the table below, the three risk functionals \mathbf{Q}_{EV} , $\mathbf{Q}_{EE}^{0.01}$, and $\mathbf{Q}_{EP}^{0.25}$ are each evaluated on the optimal shapes \mathcal{O}_{EE_η} (with respect to the expected value), \mathcal{O}_{EE_η} (with respect to the expected excess), and \mathcal{O}_{EP_η} (with respect to the excess probability), separately.

	\mathbf{Q}_{EV}	$\mathbf{Q}_{EE}^{0.01}$	$\mathbf{Q}_{EP}^{0.25}$
\mathcal{O}_{EV}	0.293	0.041	0.072
\mathcal{O}_{EE_η}	0.368	0.024	0.278
\mathcal{O}_{EP_η}	∞	∞	0.068

One main observation we made in practice is, that shape optimization problems with risk averse objectives are hard to tackle. This is because we have to deal with a nonlinear reformulation of risk averse optimization models, which are well studied in the linear case, but result in great challenges in the nonlinear case. For the ease of solvability, we therefore restrict the set of admissible shapes U_{ad} to those with a fixed topology, that is a structure of intersecting bars, see Fig. (3.8). The underlying grid resolution is illustrated in Fig. (3.10) and Fig. (3.14). The first setting picks up the idea in Fig. (3.2), a non-symmetric loading case and a rectangular working domain D , as illustrated in Fig. (3.7). Scenario forces and probabilities are chosen such that

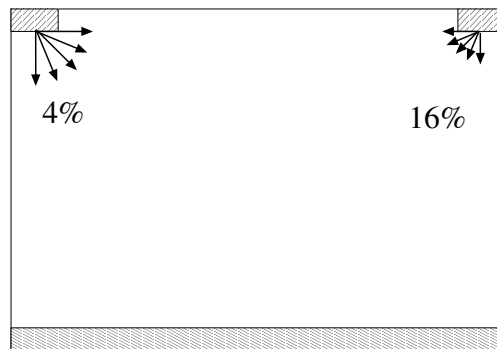


Figure 3.7: Nonsymmetric stochastic loading; loads on top left are set to 4 with probability 4%, whereas on the top right loads are set to 1 with probability 16%. Thus, the amount of the loads on the left and on the right have the same expected value.

the amount of the loads on both sides have the same expected values. Results shown in Fig. (3.8) demonstrate the preferences of the different risk measures.

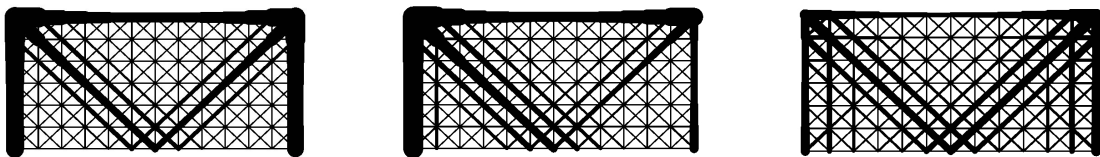


Figure 3.8: The results for Q_{EV} , $Q_{EE}^{0.01}$ and $Q_{EP}^{0.25}$; the threshold η is set to 12. We observe a symmetric structure for the expected-value model, whereas the expected-excess model leads to a structure with more support for the left loadings. The excess-probability model leads to a structure with more preference to right side.

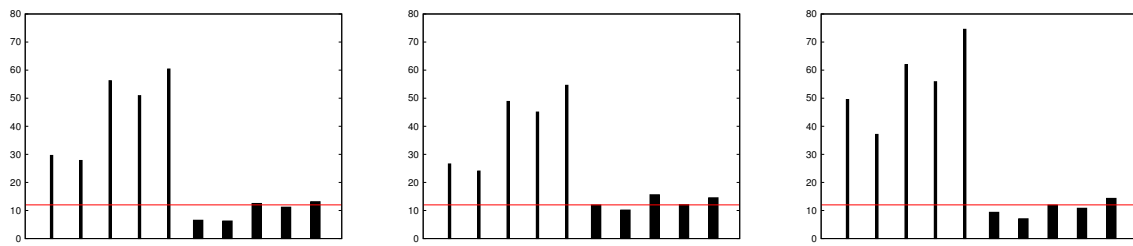


Figure 3.9: Sets of function values for the realizations of scenario forces for the expected-value (left), the expected-excess (middle) and the excess-probability model (right). Again the thickness of the bars is related to the scenario probabilities. We clearly see the different performances for the expected-excess and the excess-probability model.

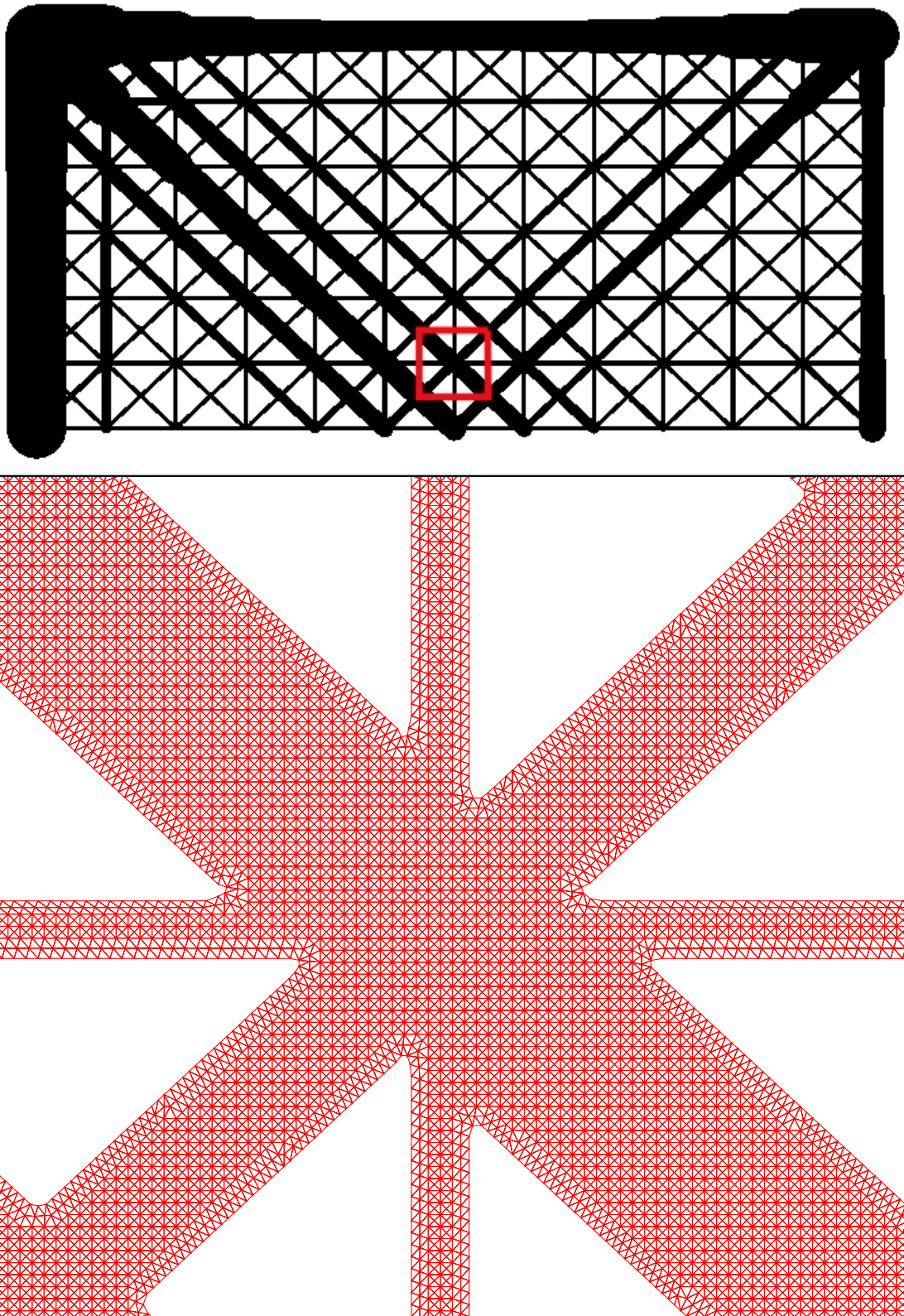


Figure 3.10: Here a detail of the triangular grid resolution is displayed (bottom). We see a zoom of the intersection of bars in the red marked area in the picture above.

In the second example, we consider a working domain similar to a mast. Again, we define a non-symmetric load setting corresponding to the configuration in Fig. (3.11).

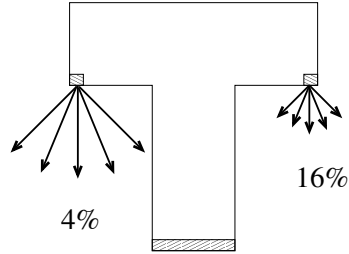


Figure 3.11: Non-symmetric stochastic loading; loads on top left are set to 4 with probability 4%, whereas on the top right loads are set to 1 with probability 16 %. This leads to, in the mean, equal strong amounts of loads on the left and on the right.

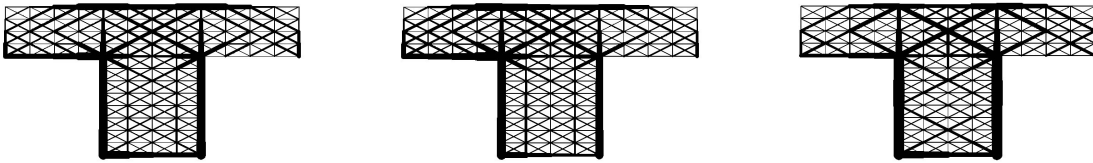


Figure 3.12: The results for $\mathbf{Q}_{EV}, \mathbf{Q}_{EE}^{0.01}$ and $\mathbf{Q}_{EE}^{0.25}$; the threshold η is set to 2. For the expected-value model, we obtain a structure with more support for the left loadings and even slight more for the expected-excess model. This time, the excess-probability model leads to a structure with symmetric support for both sides.

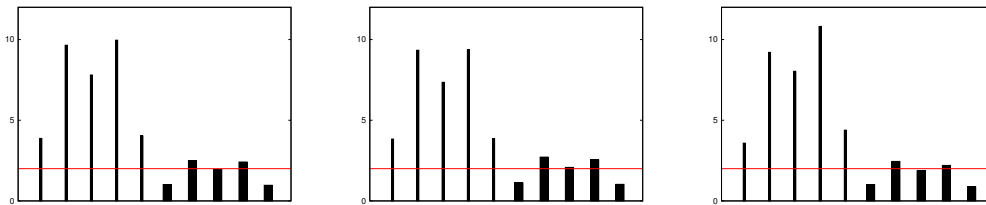


Figure 3.13: Sets of function values for the realizations of scenario forces for the expected-value (left), the expected-excess (middle) and the excess-probability model (right). The thickness of the bars is related to the scenario probabilities. We see the different performances for the expected-excess and the excess-probability model.

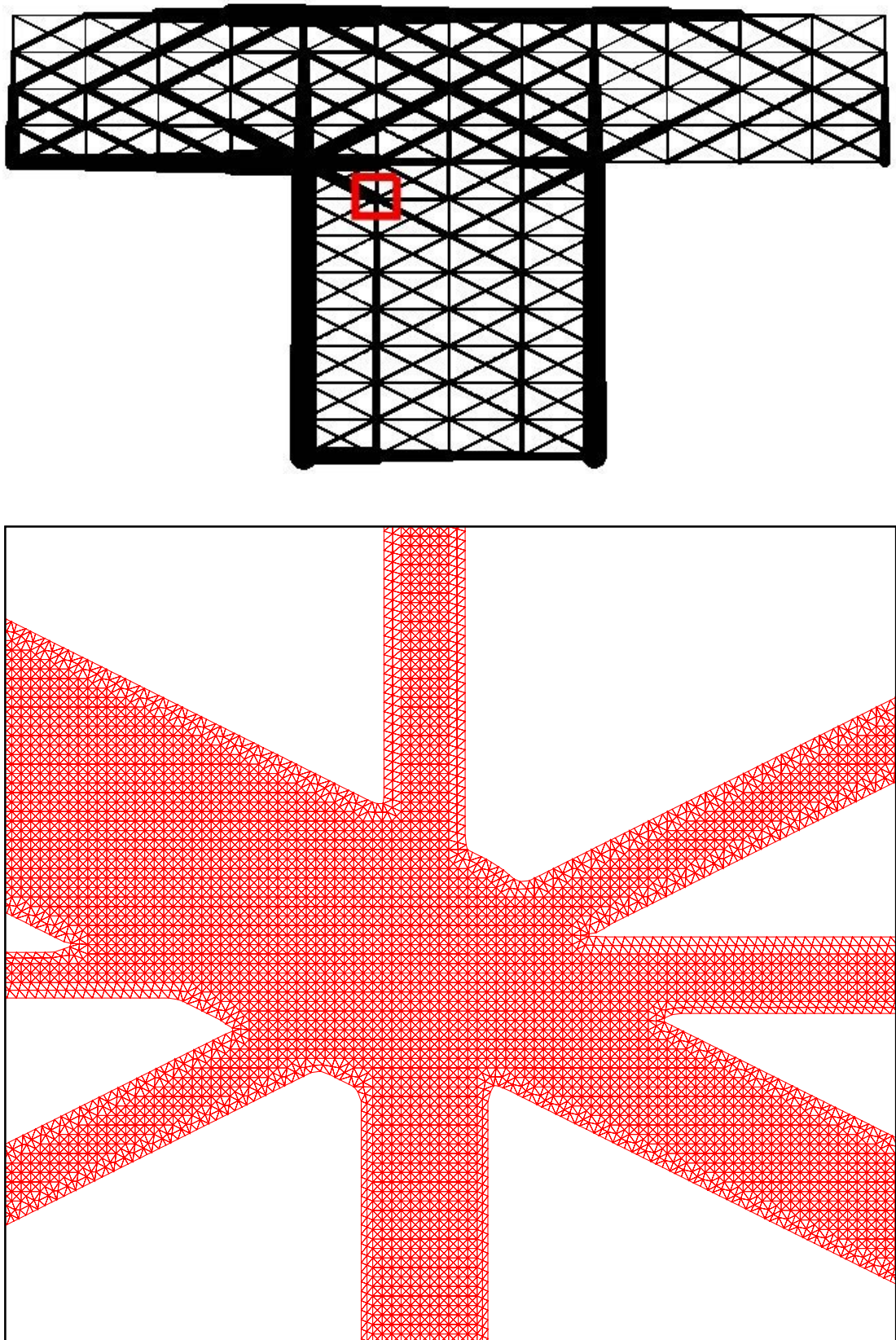


Figure 3.14: A detail of the triangular grid resolution is displayed (bottom). We see a zoom of the intersection of bars in the red marked area in the picture above.

3.2 Stochastic Dominance Models

As motivated above, we want to refine our methods for assessing the quality of random variables. Resuming the idea of comparing those to each other, the need for an order, or at least a partial order, on the space of random variables arises. In context of stochastic optimization, these are referred to as stochastic orders. Stochastic orders are an established issue in theory of decision making under risk. There, integral stochastic orders are employed for that purpose, and can be found under the key word *stochastic dominance rules*.

Following [114], we start with a descriptive and easy to understand definition of the so called *Usual Stochastic Order* to impart a very first notion of stochastic orders. For real-valued random variables X on \mathbb{R} , H_X denotes the associated cumulative distribution function.

$$H_X(t) := \mathbb{P}_X((-\infty, t]) = \mathbb{P}[X \leq t]$$

Then, a straight forward approach for comparing random variables X and Y is provided by pointwise comparison of the related distribution functions. If $H_X(t) \geq H_Y(t) \forall t \in \mathbb{R}$, then X assumes small values with higher probability than Y does, and vice versa, X assumes large values with smaller probability than Y does. This motivates for the definition of the following order relation.

Definition 3.1 (First Order Dominance). A real-valued random variable X is said to be smaller than a random variable Y with respect to usual stochastic order ($X \leq_{st} Y$), if

$$H_X(t) \geq H_Y(t) \quad \forall t \in \mathbb{R}.$$

Frequently, this stochastic order relation is also known just as *the stochastic order*. We adopt the notation used in economics and will this relation refer to as *first order stochastic dominance*. From our point of view, smaller realizations of a random variable X are preferred, so we say X dominates Y to first order (written $X \preceq_1 Y$), if $X \leq_{st} Y$.

The relation \preceq_1 fulfills the requirements for an (partial) order on the space of distribution functions, that is *Reflexivity*, *Transitivity* and *Antisymmetry*. But, since not all distribution functions can be set into relation it is not a total order.

At this point, it is important to call attention to the difference between comparison of distribution functions and comparison of random variables. Different random variables might have the same distribution even though when originating from different probability spaces. Thus, the relation \preceq_1 is antisymmetric as a relation among dis-

tributions, but not antisymmetric as a relation for random variables. A candidate to think of for a partial order that compares the size of random variables directly, would be the relation $X \preceq_{a.s.} Y$, that is $X(\omega) \leq Y(\omega)$ for P-almost all ω . This relation is much stronger as it does not only depend on the distribution function, i.e., taking a random variable X as entity, but also on the individual realizations of $\omega \in \Omega$. However, from a practical point of view, the relation \preceq_1 is much more useful.

To sum up the above considerations, comparing distribution functions means comparing classes of random variables with the same distribution. Now the following theorem reveals that for comparable classes of random variables, we find representative random variables and a suitable probability space, such that these are comparable to each other directly.

Theorem 3.2. For random variables X, Y with cumulative distribution functions H_X, H_Y the following statements are equivalent:

- (i) $H_X(\eta) \geq H_Y(\eta) \quad \forall \eta \in \mathbb{R}$.
- (ii) There exist a probability space $(\hat{\Omega}, \hat{\mathcal{A}}, \hat{\mathbb{P}})$ and random variables \hat{X} and \hat{Y} on it with distribution functions H_X and H_Y , respectively, such that $\hat{X}(\hat{\omega}) \leq \hat{Y}(\hat{\omega}) \quad \forall \hat{\omega} \in \hat{\Omega}$.

For a proof of this fundamental statement we refer the reader to [114].

From now on, whenever $X \preceq_1 Y$ holds for random variables X and Y , it can be assumed without loss of generality that $X \leq Y$ almost surely, as relation \preceq_1 only depends on the distributions on \mathbb{R} and not on the underlying probability spaces of X and Y .

In what follows, a crucial characterization for relation \preceq_1 in terms of expectations of increasing functions will be introduced. This different perspective will offer further possibilities for defining order relations.

Lemma 3.3. The following statements are equivalent.

- (i) X dominates Y to first order ($X \preceq_1 Y$).
- (ii) The inequality

$$\mathbb{E}(h(X)) \leq \mathbb{E}(h(Y))$$

holds for all nondecreasing functions h for which both expectations exist.

Proof :

(i) \Rightarrow (ii) : With the above consideration, it can be assumed without loss of generality that $X(\omega) \leq Y(\omega)$ for all $\omega \in \Omega$. For h nondecreasing, it follows $h(X(\omega)) \leq h(Y(\omega))$

for all $\omega \in \Omega$. And this implies $\mathbb{E}(h(X)) \leq \mathbb{E}(h(Y))$.

(ii) \Rightarrow (i) : For arbitrary η fixed, define h as :

$$h(t) := \begin{cases} 0 & t < \eta \\ 1 & \text{otherwise} \end{cases}$$

h is nondecreasing, which implies $\mathbb{E}(h(X)) \leq \mathbb{E}(h(Y))$. Since it is $\mathbb{E}(h(X)) = \mathbb{P}[X > \eta]$ and likewise for Y , one obtains $\mathbb{P}[X > \eta] \leq \mathbb{P}[Y > \eta]$. □

This characterization of first order stochastic dominance relation \preceq_1 is of eminent importance in context of decision making under risk. Here, the function h is considered as the utility or disutility function of a rational decision maker. This depends on whether one is dealing with random gains and related prospects, or dealing with random losses. As we are concerned with finding shapes with minimal compliance, that is maximal stiffness, our viewpoint will be treating disutility functions. For sake of completeness, it should be mentioned that we assume gains or losses being described by random variables with distributions which are known to the decision maker. Following the notation in [114], this situation is called *decision under risk* in contrast to *decision under uncertainty*, where the decision maker is not aware of the underlying distributions. Furthermore, we assume decisions to depend on the distribution as a whole and not on concrete realizations of the random variable.

The idea of employing a utility function to describe the behavior of a rational decision maker originates from von Neumann and Morgenstern detailed in the book *Theory of Games and Economic Behavior* [119]. There, they define axioms for the behavior of rational decision maker, which imply the so-called *expected utility hypothesis*. It predicates that for a rational decision maker there exists a utility function h such that prospect Y is preferable to prospect X if and only if $\mathbb{E}(h(X)) \leq \mathbb{E}(h(Y))$. That means that the behavior of a decision maker is prescribed by his utility function. With attention to losses instead of gains, as in our case, X is preferable and from now on we will use the term disutility function.

Of course, in practice it is not possible to know a decision makers disutility function in detail, as it is based on fairly subjective assessment. Therefore, a more promising approach arises when considering classes of disutility functions \mathcal{F} , say

$$X \preceq Y \quad \text{if} \quad \mathbb{E}(h(X)) \leq \mathbb{E}(h(Y)) \quad \text{for all } h \in \mathcal{F}.$$

Replacing a concrete function with a class of functions can be interpreted as analyzing the behavior of a group of decision makers or, as aforementioned, a vaguely known function. From our point of view, losses are greater when realizations of random variables are greater. Thus, a disutility function should be nondecreasing. Defining \mathcal{F} as the set of all nondecreasing functions then leads to the above characterization

of first order dominance relation \preceq_1 .

A further *stochastic integral order* is obtained by choosing a different class \mathcal{F} of disutility functions. Therefore, let us take into account decision maker's attitude to risk to get an additional property of disutility functions under consideration. If we assume decision makers to be risk averse in the sense that the certain amount $\mathbb{E}(X)$ is preferred to the risky (in the sense of volatility) amount X irrespectively of the distribution of X , then we obtain that disutility functions comply with the inequality $h(\mathbb{E}(X)) \leq \mathbb{E}h(X)$. An immediate conclusion, by contemplating Jensen's inequality, is convexity of disutility functions h . This leads to the definition of *second order stochastic dominance*.

Definition 3.4 (Second Order Dominance). The real-valued random variable $X(\omega)$ is said to be stochastically smaller than $Y(\omega)$ in increasing convex order ($X \preceq_{icx} Y$) if and only if $\mathbb{E}h(X) \leq \mathbb{E}h(Y)$ for all nondecreasing convex functions h for which both expectations exist. In this case we say that $X(\omega)$ dominates $Y(\omega)$ to second order.

Remark 3.5. As a direct consequence of the definitions of both order relations, we observe that *first order dominance* implies *second order dominance*. This is easy to understand when looking at the classes of disutility functions \mathcal{F} which underlie both definitions. The set of all nondecreasing convex functions, relevant for *second order dominance*, is a sub set of all nondecreasing functions utilized for *first order dominance*. Thus, *first order dominance* is a stronger relation than *second order dominance*.

In what follows, an alternative characterization of *second order dominance* will be derived. This will give us a more comprehensible notion, similar to the definition of *first order dominance*, and it will offer methods for an efficient numerical treatment.

Lemma 3.6. It holds $X \preceq_{icx} Y$ if and only if $\mathbb{E}[X - \eta]_+ \leq \mathbb{E}[Y - \eta]_+$ for all $\eta \in \mathbb{R}$.

Proof :

(i) \Rightarrow (ii) : With $h(t) := [t - \eta]_+$ being convex and nondecreasing for all $\eta \in \mathbb{R}$ the implication is obvious.

(ii) \Rightarrow (i) : Let $h : \mathbb{R} \rightarrow \mathbb{R}$ be convex and nondecreasing. Then there occur three cases to be dealt with :

1. $\lim_{t \rightarrow -\infty} h(t) = 0$
2. $\lim_{t \rightarrow -\infty} h(t) = \alpha \in \mathbb{R}$
3. $\lim_{t \rightarrow -\infty} h(t) = -\infty$

The case when $\lim_{t \rightarrow -\infty} h(t) = \infty$ is trivial because this would imply $h \equiv \infty$ which yields $\mathbb{E}h(\cdot) = \infty$.

Case 1 : h can be presented as the point wise maximum of a countable family of non-decreasing affine functions $h(t) = \max\{l_1(t), l_2(t), l_3(t), \dots\}$. We define the sequence of functions $h_n(t) := \max\{0, l_1(t), l_2(t), l_3(t), \dots\}$. The sequence h_n is pointwise non-decreasing and converges to h pointwise. Since h_n is piecewise linear with a finite number of kinks, it can be represented as

$$h_n(t) = \sum_{i=1}^n a_{i_n} [t - b_{i_n}]_+$$

with certain $a_{i_n} \geq 0$ and $b_{i_n} \in \mathbb{R}$. Hence,

$$\mathbb{E}h_n(X) = \sum_{i=1}^n a_{i_n} \mathbb{E}[X - b_{i_n}]_+ \leq \sum_{i=1}^n a_{i_n} \mathbb{E}[y - b_{i_n}]_+ = \mathbb{E}h_n(Y)$$

Applying the Monotone Convergence Theorem yields $\mathbb{E}(h(X)) \leq \mathbb{E}(h(Y))$.

Case 2 : Replacing h with $h - \alpha$ the same argumentation as in *Case 1* yields $\mathbb{E}(h(X)) \leq \mathbb{E}(h(Y))$.

Case 3 : For each $n \in \mathbb{N}$ fixed, the function $h_n(t) := \max\{h(t), -n\}$ complies with the requirements for *Case 2*. As h_n converges monotonically to h the statement follows with the Monotone Convergence Theorem. □

The shown equivalence reveals that $X \preceq_{icx} Y$ if and only if X exceeds thresholds $\eta \in \mathbb{R}$ by less than Y does, in the mean.

Remark 3.7. As a consequence of Definition 3.1 and Lemma 3.6 we can equate first-order stochastic dominance with a continuum of probabilistic constraints and second-order dominance with a continuum of expected-value constraints. This view links to semi-infinite optimization, e.g. [78, 133], where continua of constraints are the objects of study.

However, continua of constraints are hard to tackle, especially in our case. Furthermore, in order to keep computational cost at an acceptable level, it would make things easier if just a finite number of constraints would have to be checked. We will show in the following, subject to the condition that the underlying probability distributions are discrete and finite, the continua of constraints reduce to finite sets.

Proposition 3.8. Assume random variables X and Y have discrete distributions, that is $X(\omega) \in \{x_i : 1 \leq i \leq S_X, x_i \in \mathbb{R}\}$ with $\Omega^X = \{\omega_1^X, \omega_2^X, \dots, \omega_{S_X}^X\}$, $S_X \in \mathbb{N}^+$ and similar $Y(\omega) \in \{y_i : 1 \leq i \leq S_Y, y_i \in \mathbb{R}\}$ with $\Omega^Y = \{\omega_1^Y, \omega_2^Y, \dots, \omega_{S_Y}^Y\}$, $S_Y \in \mathbb{N}^+$. Without loss of generality, we assume $x_1 \leq x_2 \leq \dots \leq x_{S_X}$ and $y_1 \leq y_2 \leq \dots \leq y_{S_Y}$. Then it holds :

- (i) $X \preceq_1 Y$ if and only if $\mathbb{P}[X \leq \eta] \geq \mathbb{P}[Y \leq \eta]$ for all $\eta \in \{Y(\omega_i^Y) : 1 \leq i \leq S_Y\}$

(ii) $X \preceq_{icx} Y$ if and only if $\mathbb{E}[X - \eta]_+ \leq \mathbb{E}[Y - \eta]_+$ for all $\eta \in \{Y(\omega_i^Y) : 1 \leq i \leq S_Y\}$

That means, to probe whether X dominates Y to first or second order it is sufficient to check the inequalities on the right hand side just for the finite number of realizations of Y instead for all $\eta \in \mathbb{R}$.

Proof : We follow [114],

(i) :

The implication " \Rightarrow " is obvious.

To show " \Leftarrow " we consider three cases:

Case 1 : Let $\eta \in [y_{n-1}, y_n[$ for $2 \leq n \leq S_Y$. Then it holds:

$$\mathbb{P}[Y \leq \eta] = \mathbb{P}[Y \leq y_{n-1}] \leq \mathbb{P}[X \leq y_{n-1}] \leq \mathbb{P}[X \leq \eta]$$

The first identity follows from the fact that Y is discrete and that there are no mass points in between y_{n-1} and y_n . The second relation is just the assumption, and the last relation is valid due to the monotonicity of the cumulative distribution function.

Case 2 : Let $\eta < y_1$. Then it is $\mathbb{P}[Y \leq \eta] = 0 \leq \mathbb{P}[X \leq \eta]$.

Case 3 : Let $\eta > y_{S_Y}$. Due to monotonicity of the distribution function it holds $\mathbb{P}[X \leq y_{S_Y}] \leq \mathbb{P}[X \leq \eta]$. Together with the assumption we obtain $1 = \mathbb{P}[Y \leq y_{S_Y}] \leq \mathbb{P}[X \leq y_{S_Y}]$ and thus $\mathbb{P}[X \leq \eta] = 1 \geq \mathbb{P}[Y \leq \eta]$.

(ii) :

The implication " \Rightarrow " is obvious due to definition (3.1).

To show " \Leftarrow ", define $F(\eta)$ as

$$F(\eta) := \mathbb{E}[X - \eta]_+ = \sum_{n=1}^{S_X} \pi_n^X [x_n - \eta]_+$$

where $\pi_n^X = \mathbb{P}[X = x_n] \geq 0$, and $A(\eta)$ as

$$A(\eta) := \mathbb{E}[Y - \eta]_+ = \sum_{n=1}^{S_Y} \pi_n^Y [y_n - \eta]_+$$

with $\pi_n^Y = \mathbb{P}[Y = y_n] \geq 0$.

According to the assumption it holds

$$F(y_n) \leq A(y_n) \tag{3.28}$$

for $n = 1, \dots, S_Y$. Obviously, the function A is convex and piecewise linear on each of the intervals $\eta \leq y_1$, $y_{n-1} \leq \eta \leq y_n$ ($2 \leq n \leq S_Y$), and $y_{S_Y} \leq \eta$. First, we consider $\eta \leq y_1$. Choose $\eta_0 \leq \eta$ such that $\eta_0 \leq x_1$.

We denote $S' := \{n \in \{1, \dots, S_X\} : x_n < y_1\}$ and we obtain

$$\begin{aligned}
F(\eta_0) - F(y_1) &= \sum_{n=1}^{S_X} \pi_n^X x_n - \eta_0 - \sum_{n \notin S'} \pi_n^X x_n + \sum_{n \notin S'} \pi_n^X y_1 \\
&= \sum_{n \notin S'} \pi_n^X y_1 - \eta_0 + \sum_{n \in S'} \pi_n^X x_n \\
&\leq \sum_{n \notin S'} \pi_n^X y_1 - \eta_0 + \sum_{n \in S'} \pi_n^X y_1 \\
&= y_1 - \eta_0.
\end{aligned} \tag{3.29}$$

Moreover, $A(\eta) = \sum_{n=1}^{S_Y} \pi_n^Y y_n - \eta$ for $\eta \leq y_1$, and thus

$$A(\eta_0) - A(y_1) = \sum_{n=1}^{S_Y} \pi_n^Y y_n - \eta_0 - \sum_{n=1}^{S_Y} \pi_n^Y y_n + y_1 = y_1 - \eta_0 \tag{3.30}$$

Let $\eta = \lambda\eta_0 + (1 - \lambda)y_1$ for suitable $\lambda \in \mathbb{R}$ with $0 \leq \lambda \leq 1$. Since F is convex as a finite sum of convex functions we find

$$\begin{aligned}
F(\eta) &\leq \lambda F(\eta_0) + (1 - \lambda)F(y_1) \\
&= F(y_1) + \lambda(F(\eta_0) - F(y_1)) \\
&\leq F(y_1) + \lambda(y_1 - \eta_0) \\
&\leq A(y_1) + \lambda(y_1 - \eta_0) \\
&= A(y_1) + \lambda(A(\eta_0) - A(y_1)) \\
&= A(\lambda\eta_0 + (1 - \lambda)y_1) \\
&= A(\eta)
\end{aligned}$$

We used (3.29) to justify the third relation, (3.28) for the fourth, (3.30) for the fifth, and eventually the linearity of A on the considered interval.

In case that $y_{n-1} \leq \eta \leq y_n$ ($2 \leq n \leq S_Y$), we take into account the convexity of F , (3.28), and the linearity of A on the particular interval and obtain that for suitable λ ($0 \leq \lambda \leq 1$)

$$\begin{aligned}
F(\eta) &\leq \lambda F(y_{n-1}) + (1 - \lambda)F(y_n) \\
&\leq \lambda A(y_{n-1}) + (1 - \lambda)A(y_n) \\
&= A(\lambda y_{n-1} + (1 - \lambda)y_n) \\
&= A(\eta)
\end{aligned}$$

Finally, let $y_{S_Y} \leq \eta$. Since F and A are non-increasing and non-negative (3.28) yields

$$0 \leq F(\eta) \leq F(y_{S_Y}) \leq A(y_{S_Y}) = 0$$

and thus $F(\eta) = A(\eta) = 0$.

□

As introduced in section 3.1.3, our approach for quantifying uncertainty provides that the loads acting on elastic structures are random and follow a discrete distribution. Of course, this holds for random variables $G(\mathcal{O}, \omega)$ in (3.2) as well (as they directly result from the loadings $f(\omega)$ and $g(\omega)$), and the above proposition is appropriate. Reminding the viewpoint emphasized in the beginning of chapter 3, i.e., identifying \mathcal{O} as a parameter defining the random variable $G(\mathcal{O}, \omega)$, comparing shapes to each other means comparing the associated random variables $G(\mathcal{O}, \omega)$ to each other.

Now, the set of all admissible shapes \mathcal{U}_{ad} can be separated into two subsets, the first one U_{acc} containing 'acceptable' shapes, which dominate a given benchmark with respect to the chosen order relation, and the second one containing those, which do not dominate this benchmark and are 'not acceptable'. Going further, we aim for a shape in U_{acc} , which is optimal according to some criterion. As a natural choice, we seek for a member of U_{acc} with minimal volume.

Then our ultimate goal reads as follows: For a given reference shape \mathcal{O}_{ref} , find a different shape \mathcal{O}_{opt} , whose associated random variable $G(\mathcal{O}_{opt}, \omega)$ dominates the random variable $G(\mathcal{O}_{ref}, \omega)$ (associated with the initial shape \mathcal{O}_{ref}) to first or second order, but whose volume is as small as possible.

Note, since the objective we are dealing with, here in this context, is the volume of \mathcal{O} , the volume penalization in (3.3) is redundant, and therefore α (the Lagrange Multiplier for the volume) is set to zero. So is β (Lagrange Multiplier for the surface), for sake of simplicity. Then, $G(\mathcal{O}, \omega)$ simply reduces to $J(\mathcal{O}, \omega)$ and we obtain the optimization task

$$\min\{Vol(\mathcal{O}) : J(\mathcal{O}, \omega) \preceq_i J(\mathcal{O}_{ref}, \omega) \text{ with } \mathcal{O} \in \mathcal{U}_{ad}\} \quad i = 1, 2 \quad (3.31)$$

that is

$$\min\{Vol(\mathcal{O}) : \mathcal{O} \in U_{acc}\} \quad (3.32)$$

Using (3.8), stochastic dominance is verifiable by checking a finite number of inequalities.

For **First Order Dominance** we rely on the following equivalence

$$\begin{aligned} & J(\mathcal{O}_{opt}, \omega) \preceq_1 J(\mathcal{O}_{ref}, \omega) \\ \Leftrightarrow & \mathbb{P}[J(\mathcal{O}, \omega) \leq \eta] \geq \mathbb{P}[J(\mathcal{O}_{ref}, \omega) \leq \eta] \quad \text{for all } \eta \in \mathbb{B} \end{aligned} \quad (3.33)$$

where \mathbb{B} is the finite set of realizations of $J(\mathcal{O}_{ref}, \omega)$, i.e., $\mathbb{B} = \{b_i = J(\mathcal{O}_{ref}, \omega_i), 1 \leq i \leq S\}$, S being the number of realizations. The right hand side of the second inequality can be computed a priori for each $\eta \in \mathbb{B}$ and remains fixed during the optimization process. We obtain constraints of the form

$$\mathbb{P}[J(\mathcal{O}, \omega) \leq b_i] \geq \underbrace{\mathbb{P}[J(\mathcal{O}_{ref}, \omega) \leq b_i]}_{:=B_i} \quad \text{for all } 1 \leq i \leq S$$

As ω has finitely many realizations ω_j , $1 \leq j \leq S$, we obtain for B_i

$$B_i = \sum_{j=1}^S \pi_j \mathcal{H}(b_i - J(\mathcal{O}_{ref}, \omega_j)) \quad (3.34)$$

where $\mathcal{H}(x)$ denotes the Heaviside function being 0 for $x < 0$ and 1 for $0 < x$. So (3.31) becomes

$$\min\{Vol(\mathcal{O}) : \mathbb{P}[J(\mathcal{O}, \omega) \leq b_i] \geq B_i, 1 \leq i \leq S, \mathcal{O} \in \mathcal{U}_{ad}\} \quad (3.35)$$

As above, we observe

$$\mathbb{P}[J(\mathcal{O}, \omega) \leq b_i] = \sum_{j=1}^S \pi_j \mathcal{H}(b_i - J(\mathcal{O}, \omega_j))$$

and replace \mathcal{H} with the differentiable approximation

$$\mathcal{H}(x) \approx \frac{1}{1 + e^{-2\epsilon}} =: \tilde{\mathcal{H}}(x) \quad \epsilon > 0$$

Our intention is to employ a penalty function to formulate an optimization task, which itself is then solved by a gradient descent method. Therefore, we rewrite the above constraints as a penalty term to be added to the objective $Vol(\mathcal{O})$

$$\min_{\mathcal{O} \in \mathcal{U}_{ad}} Vol(\mathcal{O}) + \alpha_0 \left[\sum_{i=1}^S \alpha_i \left(B_i - \sum_{j=1}^S \pi_j \tilde{\mathcal{H}}(b_i - J(\mathcal{O}, \omega_j)) \right)^2 \right] \quad (3.36)$$

and choose Lagrange Multipliers $\alpha_i > 0$, $0 \leq i \leq S$, for the penalty terms.

For **Second Order Dominance** we use

$$J(\mathcal{O}_{opt}, \omega) \preceq_{icx} J(\mathcal{O}_{ref}, \omega)$$

$$\Leftrightarrow \mathbb{E}[J(\mathcal{O}, \omega) - \eta]_+ \leq \mathbb{E}[J(\mathcal{O}_{ref}, \omega) - \eta]_+ \quad \text{for all } \eta \in \mathbb{B}$$

where \mathbb{B} is the set in (3.33). In the same manner as above, we can calculate the right hand side of the inequalities beforehand,

$$B_i = \sum_{j=1}^S \pi_j \max \{J(\mathcal{O}_{ref}, \omega_j) - b_i, 0\} \quad (3.37)$$

So, (3.31) becomes

$$\min \{Vol(\mathcal{O}) : \mathbb{E}[J(\mathcal{O}, \omega) - b_i]_+ \leq B_i, \quad 1 \leq i \leq S, \quad \mathcal{O} \in \mathcal{U}_{ad}\} \quad (3.38)$$

We identify the left hand side as

$$\mathbb{E}[J(\mathcal{O}, \omega) - \eta]_+ = \sum_{j=1}^S \pi_j \max \{J(\mathcal{O}, \omega_j) - b_i, 0\}$$

and replace $\max\{x, 0\}$ with the differentiable approximation $\text{Max}(x)$.

$$\max\{x, 0\} = \frac{\sqrt{x^2} + x}{2} \approx \frac{\sqrt{x^2 + \epsilon} + x}{2} =: \text{Max}(x) \quad \epsilon > 0$$

with $\epsilon \ll 1$. We end up with the penalty function to minimize

$$\min_{\mathcal{O} \in \mathcal{U}_{ad}} Vol(\mathcal{O}) + \alpha_0 \left[\sum_{i=1}^S \alpha_i \left(\sum_{j=1}^S \pi_j \text{Max}(J(\mathcal{O}, \omega) - b_i) - B_i \right)^2 \right] \quad (3.39)$$

$\alpha_i > 0$, $0 \leq i \leq S$, being Lagrange Multipliers to choose.

3.2.1 Solution Algorithm

The algorithm follows the principle of (2.17) except that we have to set additional parameters for the penalty function.

Algorithm 3.9.

Parameters to be set:

- Specify the function J (here just the compliance without volume penalization α and surface penalization β).
- Define a maximal number of iterations $0 < Num_{iter} \in \mathbb{N}$.
- Set parameters q and b for the Armijo step size control, and an initial step size t_0 .
- Determine the frequency of topological changes n_{top} .
- As initial shape choose the working domain D .
- Finally set parameters for the penalty function to be optimized $\alpha_i > 0$, $0 \leq i \leq S$.

For $k = 0$ until $k = Num_{iter}$ do :

1. Solve the elasticity system (2.5) (and if necessary its adjoint system) for ϕ_k to obtain u_k .
2. Compute B_i according to (3.34) for the first order model or according to (3.37) for the second order model.
3. (a) For $(k \bmod n_{top}) \neq 0$: Compute the gradient direction $grad_{\mathcal{G}}J(\phi^k)$ according to (2.31), where derivatives $dJ(\phi, \psi)$ of the penalty function in (3.36) or (3.39) are obtained by the chain rule. Generate ϕ_{k+1} as described in (2.32) and find an acceptable step size t_k in (2.33).
 (b) For $(k \bmod n_{top}) = 0$: Compute the topological gradient of the penalty function using (2.14) and the chain rule and check whether or not a change of topology decreases the objective J , see (2.16).
4. Re-initialized the updated level set function ϕ_{k+1} according to (2.29).
 Set $k := k + 1$ and return to step 1 unless $k = Num_{iter}$.

3.2.2 Results for Optimization with Stochastic Dominance Constraints

Before we start with concrete examples, we define the set \mathcal{U}_{ad} of admissible shapes. As we have seen in section 2.6, for deterministic settings the optimization process works fairly stable. The investigation of risk-models in section 3.1.4, however, revealed a fundamental problem compared to the situation in traditional finite-dimensional linear stochastic programming. For models with finite discrete distributions equivalent formulas exist, which can be written as large-scale linear programs. In our situation, there are no such equivalents and we have to work with the original nonlinear objective functions directly. In particular, the evaluation whether the functional J exceeds the threshold η , or not, can not be tackled as efficient as in finite linear stochastic programming. Regularization according to (3.24) or (3.25) just leads to a nonlinear optimization problem, with high fluctuations of the function value near to the threshold. Additionally, without significant restrictions, the set of admissible shapes \mathcal{U}_{ad} does not have a vector space structure.

With regard to our *Stochastic Dominance Models*, we are confronted with a set of difficult side constraints, originating from the underlying risk-models. To this end, we will restrict the class of admissible shapes to those, which are described by a finite number of geometric parameters, in order to reduce the complexity of the optimization problem. So, the set \mathcal{U}_{ad} is a vector space.

In a first approach, we construct different types of shapes by inserting holes, which are simply parametrized in the following way: Each hole has a center and a fixed number of facets. The geometric parameters are the distances of the facets to the center.

Now, we discuss a practical application of *Stochastic Dominance Models*. We will recap the fundamental ideas from previous chapters and formulate our optimization problem step by step. As a motivation, let us consider a mechanical structure, which may, for instance, originate from an industrial application. This structure is subject to a range of varying loads and meets some given requirements. We proceed from the assumption that we are able to set up a framework of stochastic loads, according to our model presented in section 3.1.3, that approximates the actual loads with sufficient accuracy. Then, we can identify a set of acceptable shapes \mathcal{U}_{acc} by employing *stochastic dominance constraints*. These acceptable shapes are said to have a better or at least the same qualitative behavior under uncertainty.

So let us assume we are in the following situation: We consider a given structure, which we will refer to as the benchmark shape, and a load scenario as shown in Fig. (3.15). We consider a configuration with four scenario forces, each force denoted by a red arrow, shown in the lower picture. The load decreases from the left to the right, while the probability for each scenario remains fixed. Now, when forces act on

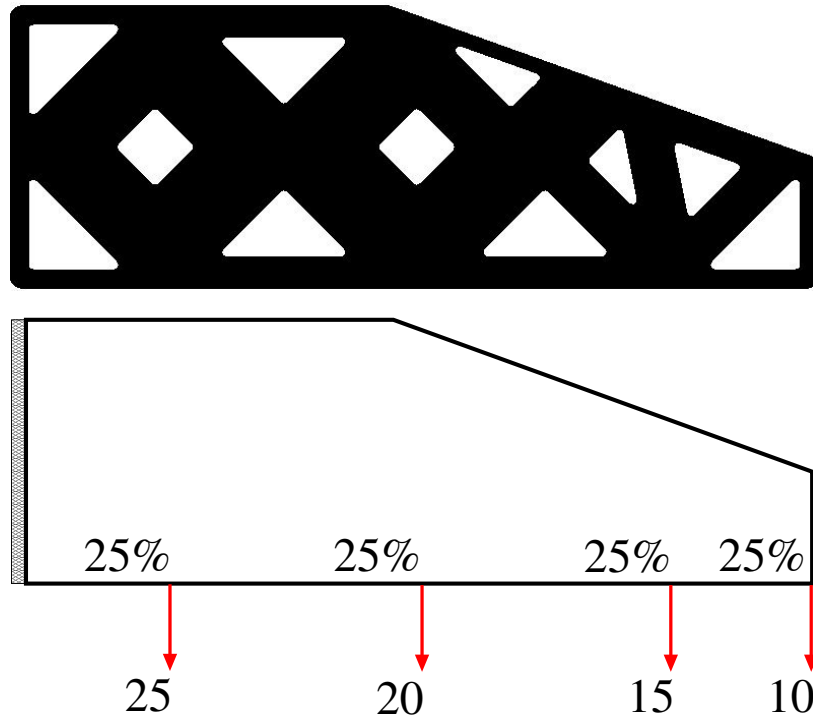


Figure 3.15: The configuration for the first example is depicted. On top: Benchmark shape with volume 0.134496 . Below: The load scenario under consideration. The scenario forces are numbered from the left to the right (1-4).

the benchmark shape \mathcal{O}_b , its elastic response in terms of deformations is measured by the shape functional $J(\mathcal{O}_b)$. Here, we consider the compliance as the objective $J(\mathcal{O}_b)$, which, as said before, is the overall elastic energy contained in the shape \mathcal{O}_b , see (2.9), and is a value on the reals. As discussed previously in this thesis, due to the randomness of the forces, the objective $J(\mathcal{O}_b)$ becomes a random variable $J(\mathcal{O}_b, \omega)$, too. According to the known probabilities of the realizations of the forces, we can generate the distribution function of the objective $J(\mathcal{O}_b, \omega)$. This is illustrated in Fig. (3.16). There, the distribution function of the benchmark shape is colored in black. Now, we can identify this distribution function with a certain qualitative behavior under uncertainty (when forces are applied). Then, we seek for shapes with the same or even better behavior under uncertainty. For this purpose, we employ the presented principles of stochastic dominance of first and second order. On the basis of these criteria we can decide whether a shape has the same or better behavior under uncertainty. In terms of our preparations in section 3.2, we say, the shape \mathcal{O} has a better, or at least the same, qualitative behavior under uncertainty than the benchmark shape \mathcal{O}_b , if and only if the corresponding random variable $J(\mathcal{O}, \omega)$ dominates $J(\mathcal{O}_b, \omega)$ to the chosen order (first or second order). In that sense, first order dominance and second order dominance are two different ways to assess the

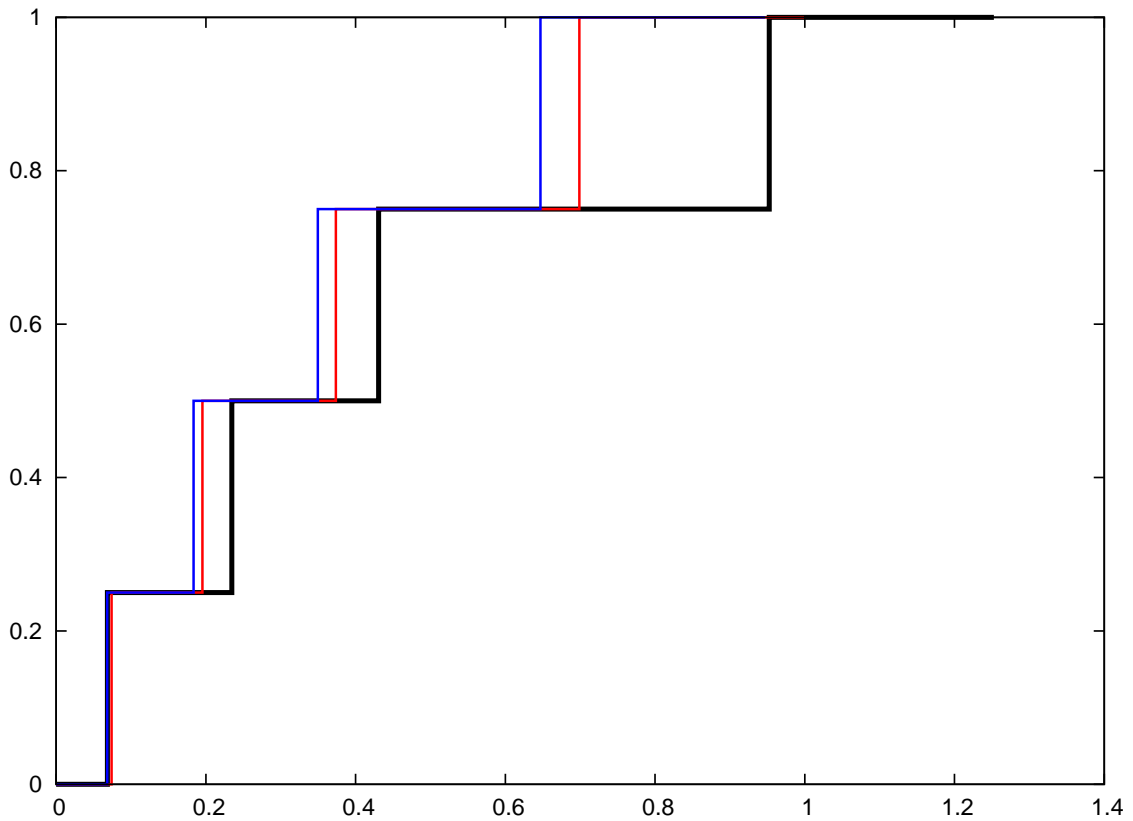


Figure 3.16: The cumulative distribution functions of random variables generated by the benchmark shape (black) and the shapes obtained by optimization with dominance constraints of first (blue) and second order (red). Probability is plotted on the vertical axis, while evaluations of $J(\mathcal{O}, \omega)$ in \mathbb{R} are displayed on the horizontal axis.

behavior under uncertainty of shapes. Remark 3.5 reveals that first order dominance implies second order dominance, as it is a stronger relation. Thus, according to our requirements concerning the qualitative behavior under uncertainty, we can identify two different sets of acceptable shapes, U_{acc}^{SD1} for first order dominance and U_{acc}^{SD2} for second order dominance, where it holds

$$U_{acc}^{SD1} \subset U_{acc}^{SD2}.$$

We prefer shapes with small volume, thus, we seek for shapes in U_{acc}^{SD1} or U_{acc}^{SD2} with minimal volume. This offers the choice between two approaches. Either we put more emphasis on the behavior under uncertainty, or on the amount of material (volume of the shape) that is used. Explicitly, optimizing shapes with respect to *Second Order Dominance Constraints* leads to shapes with less volume which are infeasible with respect to *First Order Dominance Constraints*.

For the optimization we employed penalty functions according to (3.36) and (3.39),

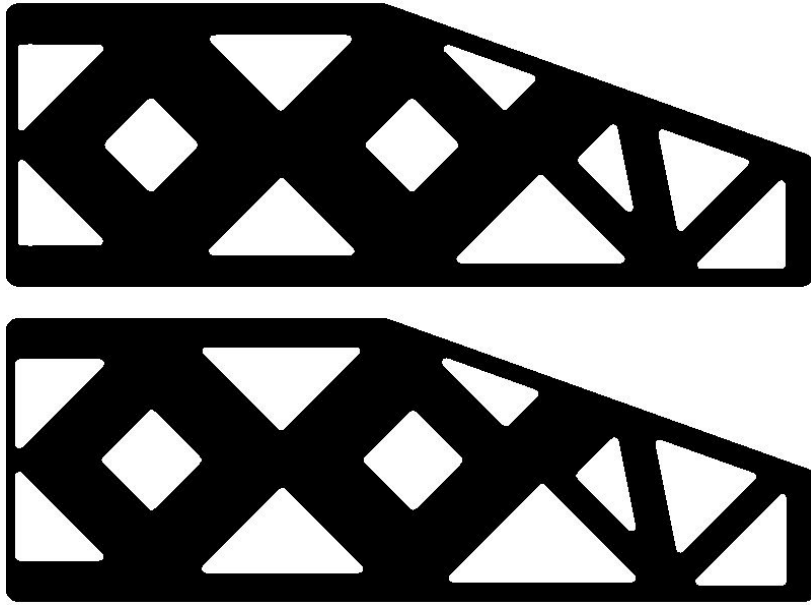


Figure 3.17: Shapes obtained by optimization with first order constraints (top), the volume has decreased to 0.123998, and optimization with second order constraints (bottom), the volume has decreased to 0.11714.

where the Parameters $(\alpha_0, \dots, \alpha_4)$ are set to 60.0 . The different shapes obtained by optimizing the volume under consideration of *First Order Dominance Constraints* and *Second Order Dominance Constraints* respectively are displayed in Fig. (3.17). The shape on the left dominates the benchmark shape \mathcal{O}_b to first order and has a reduced volume of around 92% of the benchmark shape. If we can relax the requirements concerning the behavior under uncertainty, for instance, the requirements for first order are usually rather strong, then we would prefer the shape in the lower picture. This dominates the benchmark shape \mathcal{O}_b to second order and has a reduced volume of around 87% of the benchmark shape. Of course, the two approaches do not lead to completely different shapes and only slightly differ in the geometry. But the performance in terms of the distribution function in Fig. (3.16) clearly shows the difference of the two approaches.

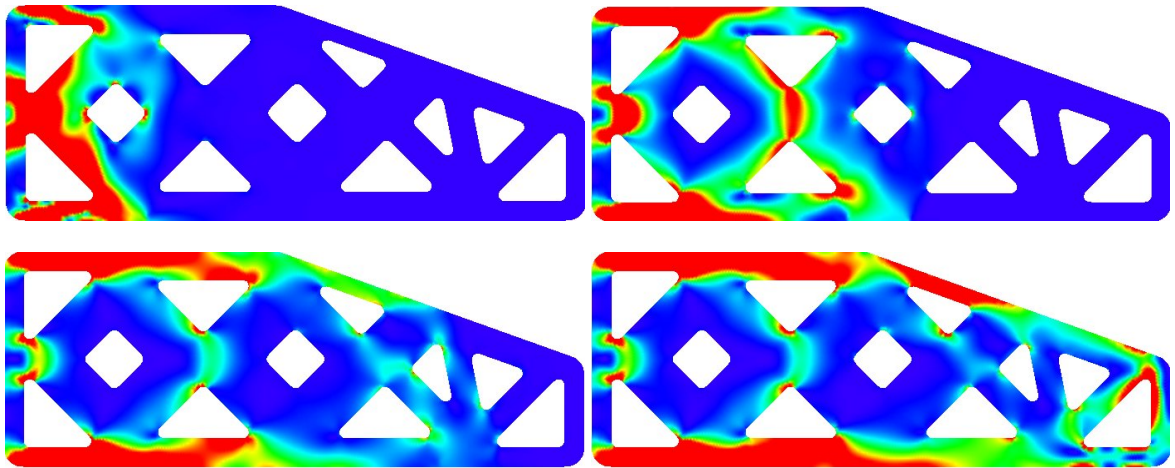



Figure 3.18: Visualization of the elastic energy for each scenario force for the benchmark shape. Values are arranged according to the colorbar , where blue corresponds to zero and red corresponds to the maximum. The maximum is set to 10 for the first scenario (upper left) and the second one (upper right), 30 for the third (lower left) and 50 for the fourth scenario (lower right).

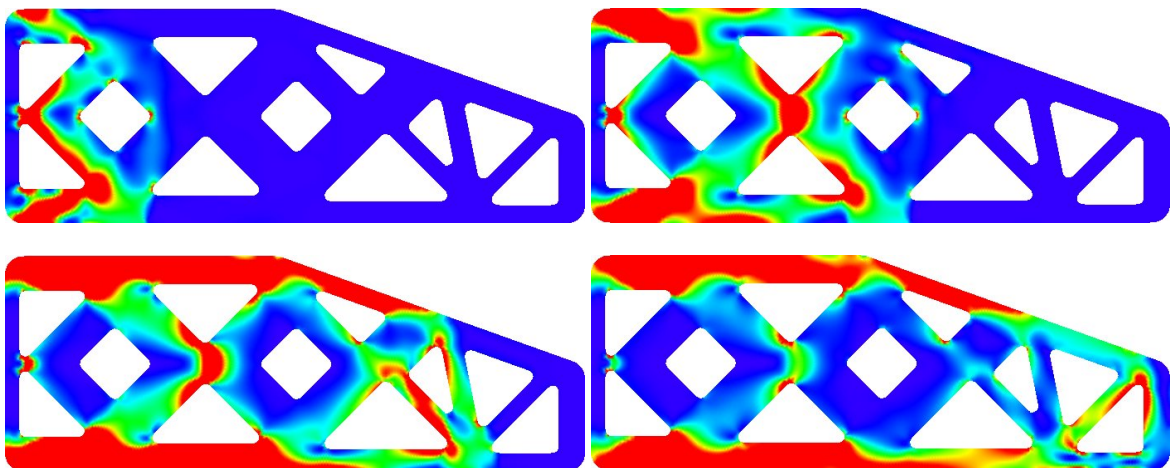


Figure 3.19: Visualization of the elastic energy for the four scenario forces (from top left to bottom right) for the shape obtained by optimization with first order constraints. Values are arranged with the same specification as in Fig. (3.18).

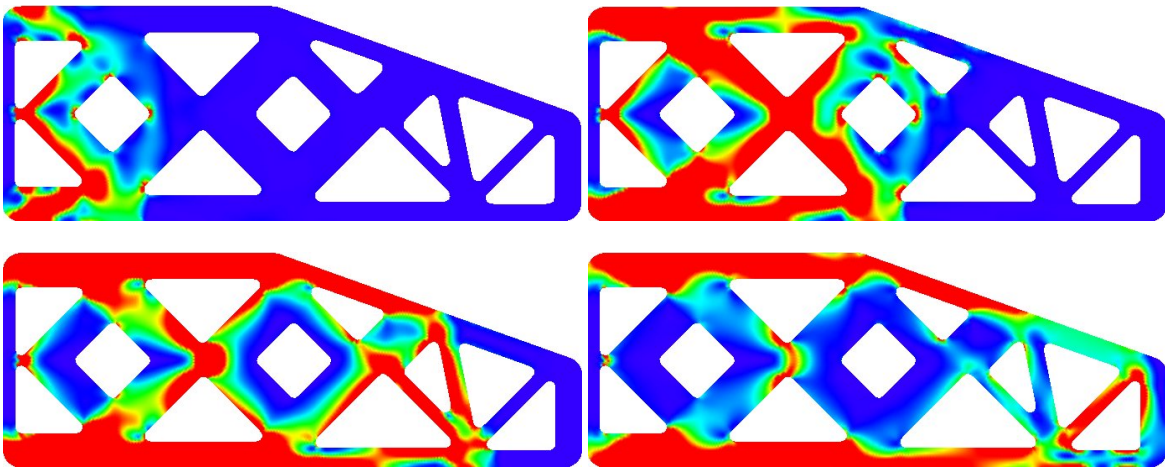


Figure 3.20: Similar to Fig. (3.18) and Fig. (3.19), the visualization of the elastic energy for each scenario force for the shape obtained by optimization with second order constraints is displayed.

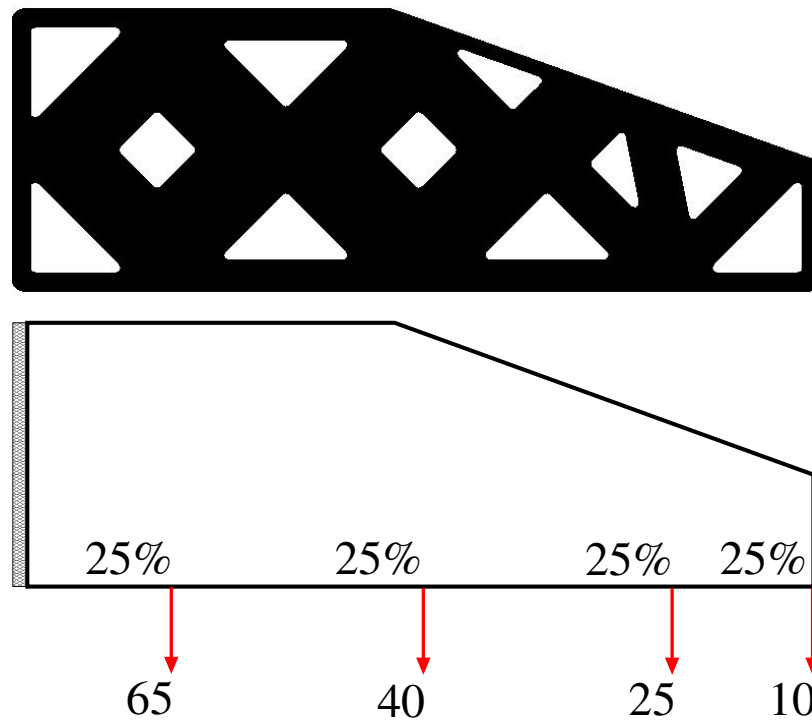


Figure 3.21: The configuration of the second example. We consider the same class of shapes as in the first example and the same benchmark shape (volume 0.134496), but a different configuration of the load scenarios.

In the next example, we see how the solutions for the different approaches behave when we modify the distribution of forces applied, see the configuration in Fig. (3.21). Here, we suppose the load of random forces to decrease from left to right, while the benchmark shape remains fixed. This yields a change of the distribution function (colored in black) associated with the benchmark shape as displayed in Fig. (3.22). In this situation, difference among the optimal shapes for the two dominance models become more apparent, see their distribution functions depicted in Fig. (3.23). The one colored in red is associated with the optimization of the volume under consideration of the *Second Order Constraints* model. It shows a clear violation of the *First Order Constraints* as it drops below the benchmark distribution function. The corresponding shapes for both approaches are depicted in Fig. (3.23). We observe a 25% drop in volume for the model concerning *First Order Constraints* and a 32% drop in volume for the model concerning *Second Order Constraints*.

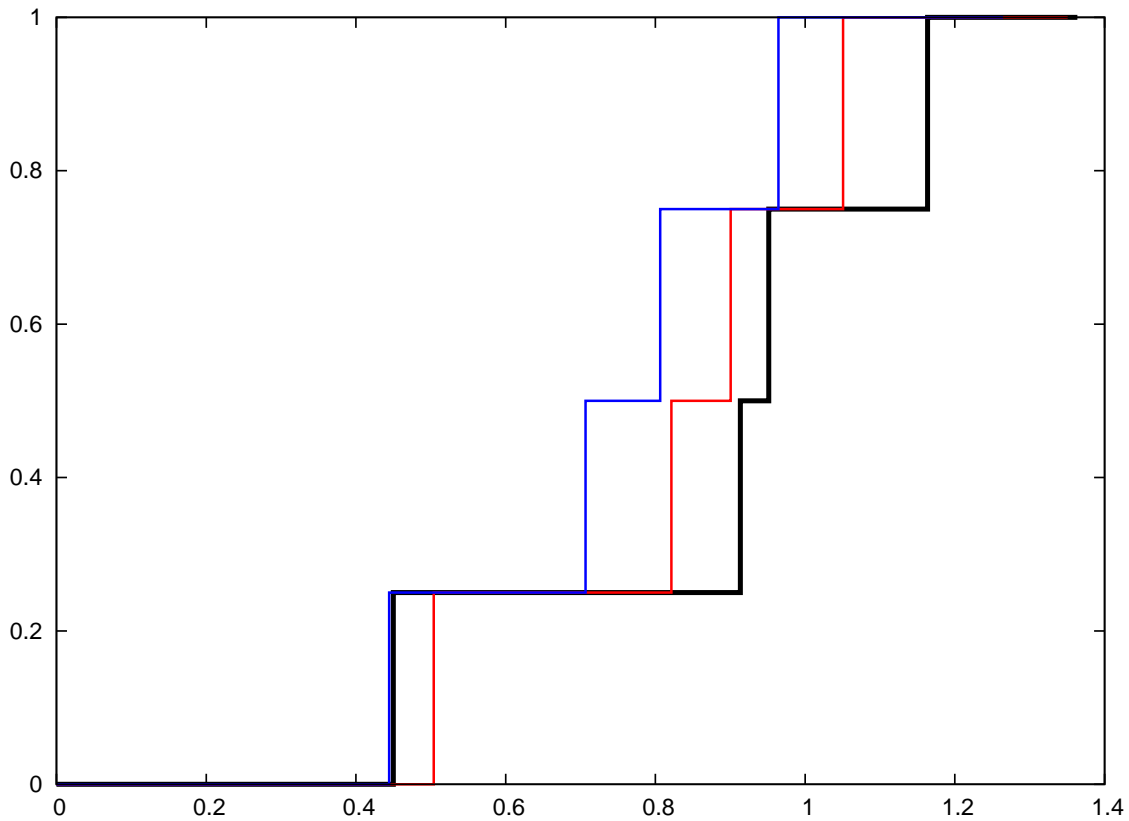


Figure 3.22: Distribution functions for the random variables associated with the benchmark shape (black), the resulting shapes for optimization with first order constraints (blue) and for optimization with second order constraints (red). Probability is plotted on the vertical axis, while evaluations of $J(\mathcal{O}, \omega)$ in \mathbb{R} are displayed on the horizontal axis.

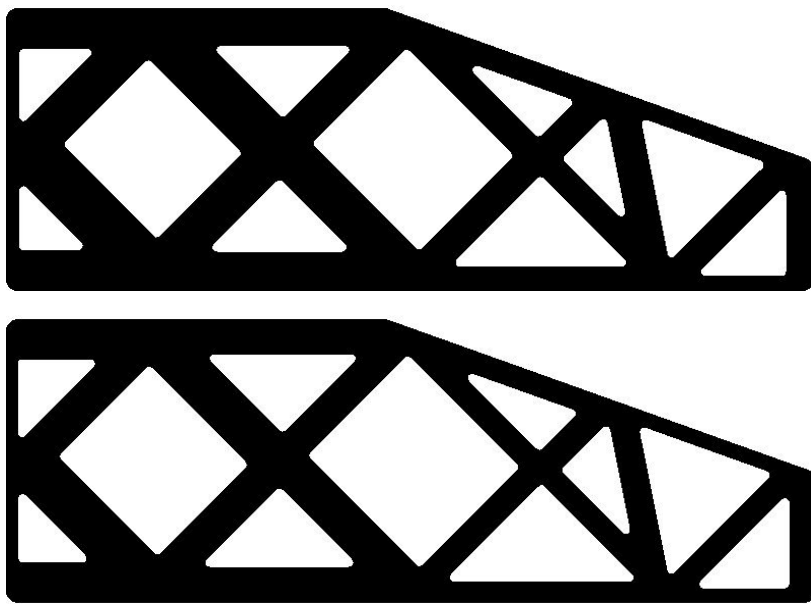


Figure 3.23: Shapes obtained by optimization with first order constraints (top), the volume has decreased to 0.100702, and optimization with second order constraints (bottom), the volume has decreased to 0.0916096.

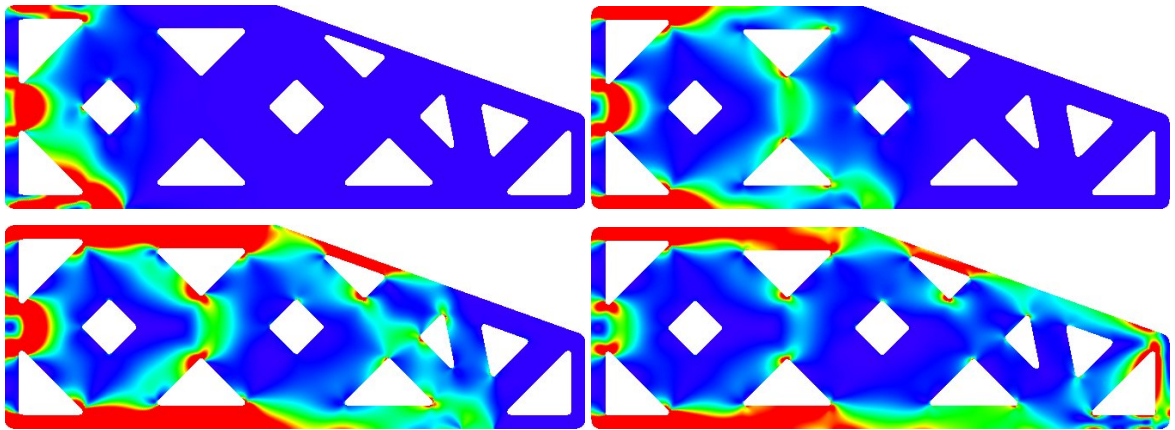



Figure 3.24: Visualization of the elastic energy for each scenario force for the benchmark shape. Values are arranged according to the color bar , where blue corresponds to zero and red corresponds to the maximum. The maximum is set to 15 for the first scenario (upper left) and the second one (upper right), 20 for the third (lower left) and 25 for the fourth scenario (lower right).

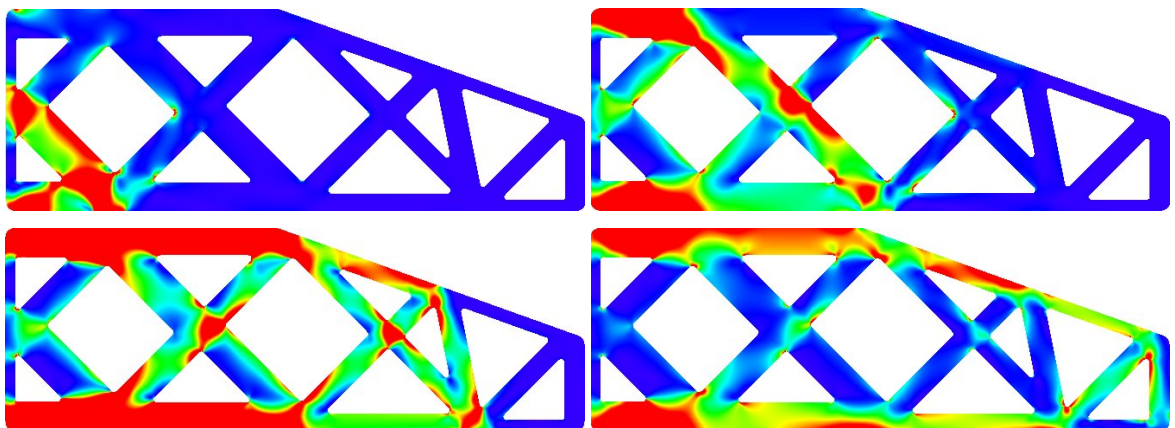


Figure 3.25: Visualization of the elastic energy for the four scenario forces (from top left to bottom right) for the shape obtained by optimization with first order constraints. Values are arranged with the same specification as in Fig. (3.24).

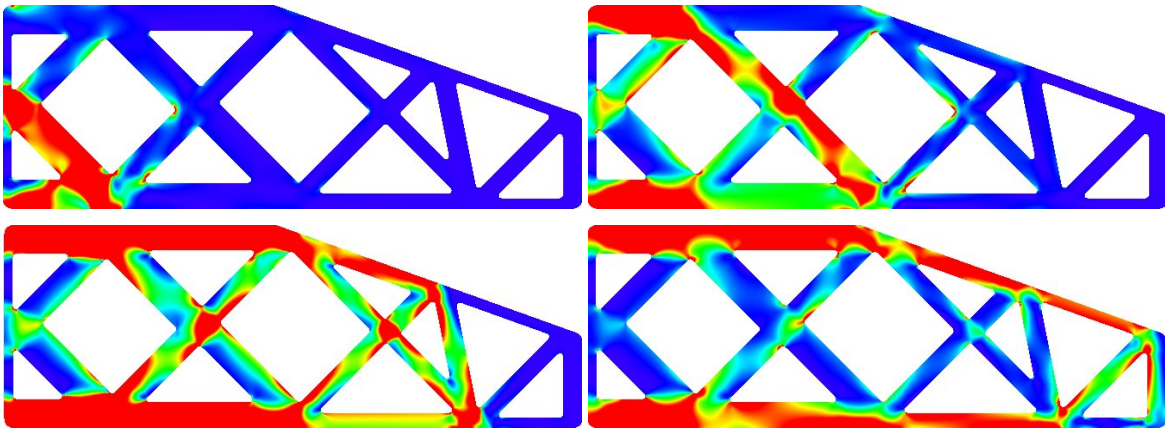


Figure 3.26: Similar to Fig. (3.24) and Fig. (3.25), the visualization of the elastic energy for each scenario force for the shape obtained by optimization with second order constraints is displayed.

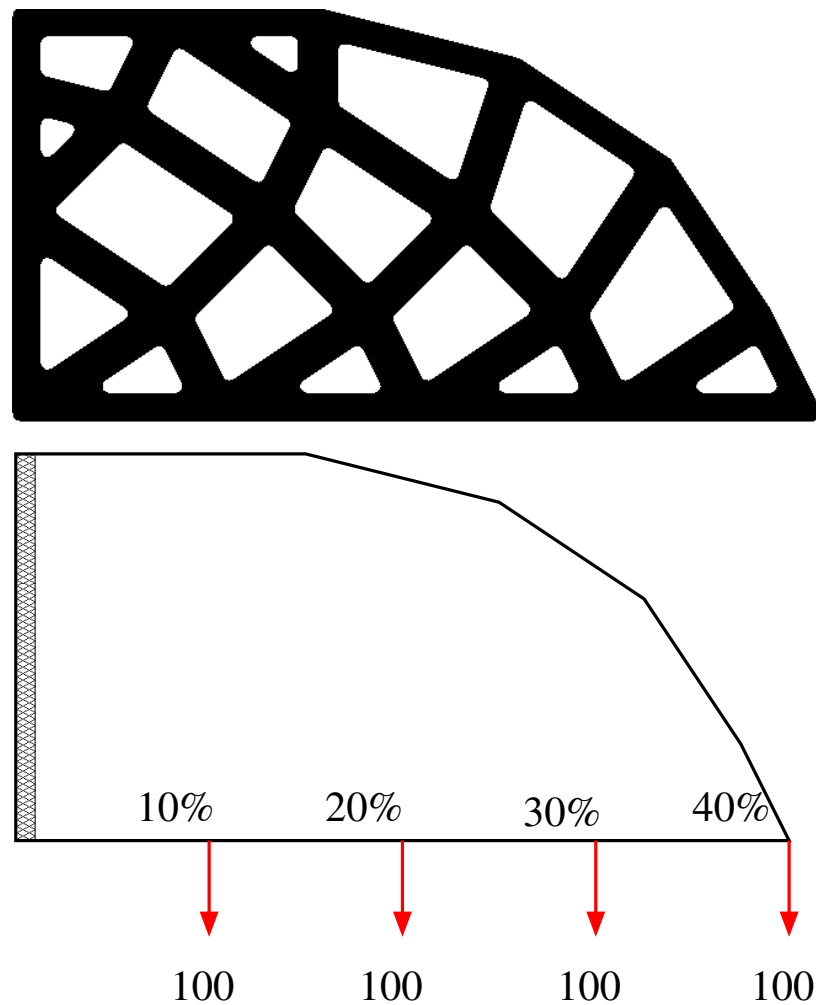


Figure 3.27: The configuration of the scenario loads for the third example. Here we consider a class of shapes with a different topology to those in the first and second example. We see the benchmark shape (top) with volume 0.22039 and the scenario loads under consideration (below).

In the third example, we consider a modified fundamental structure with a different topology. Fig. (3.27) shows the benchmark shape \mathcal{O}_b on the left and the underlying configuration of random forces on the right. In the same manner as before, we can identify the distribution function of $J(\mathcal{O}_b, \omega)$ which reflects the stochastic behavior of the benchmark shape. See Fig. (3.28). Here, we find shapes with a reduction of the volume by 5.1% for *First Order Dominance Constraints* and by 9.5% for *Second Order Dominance Constraints*, depicted in Fig. (3.29).

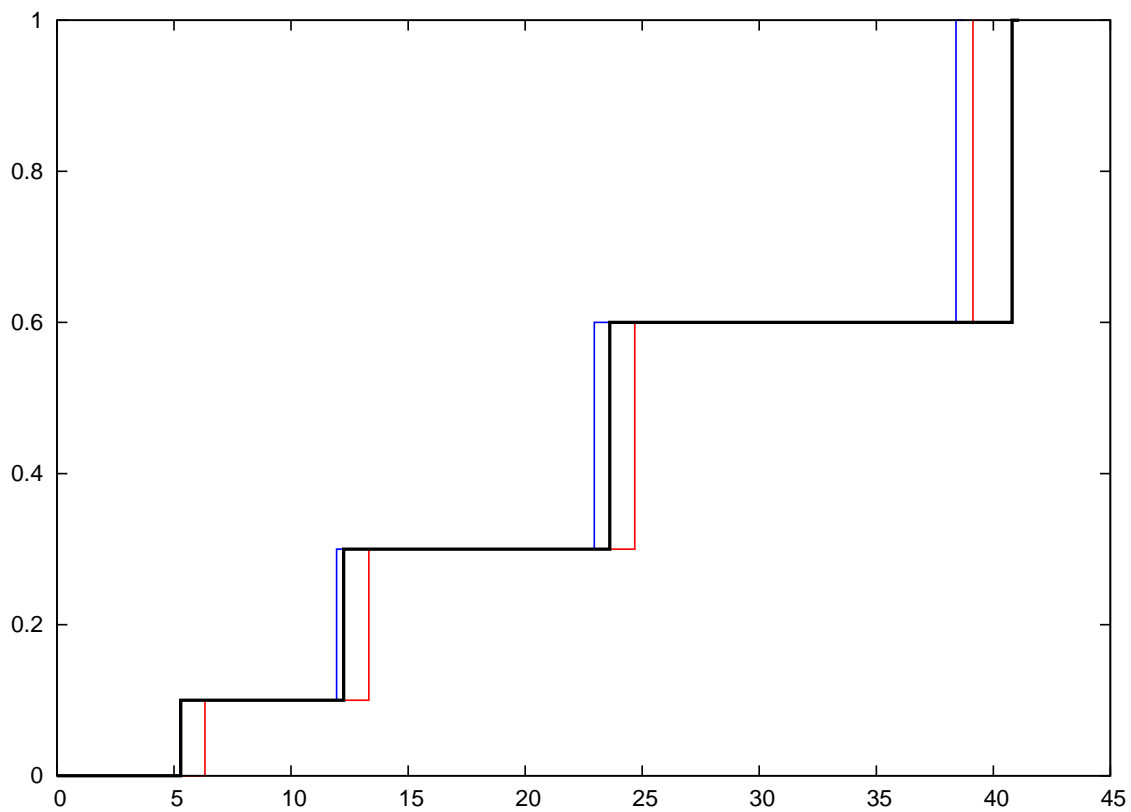


Figure 3.28: Distribution functions for the random variables associated with the benchmark shape (black), the resulting shapes for optimization with first order constraints (blue) and for optimization with second order constraints (red). Probability is plotted on the vertical axis, while evaluations of $J(\mathcal{O}, \omega)$ in \mathbb{R} are displayed on the horizontal axis.

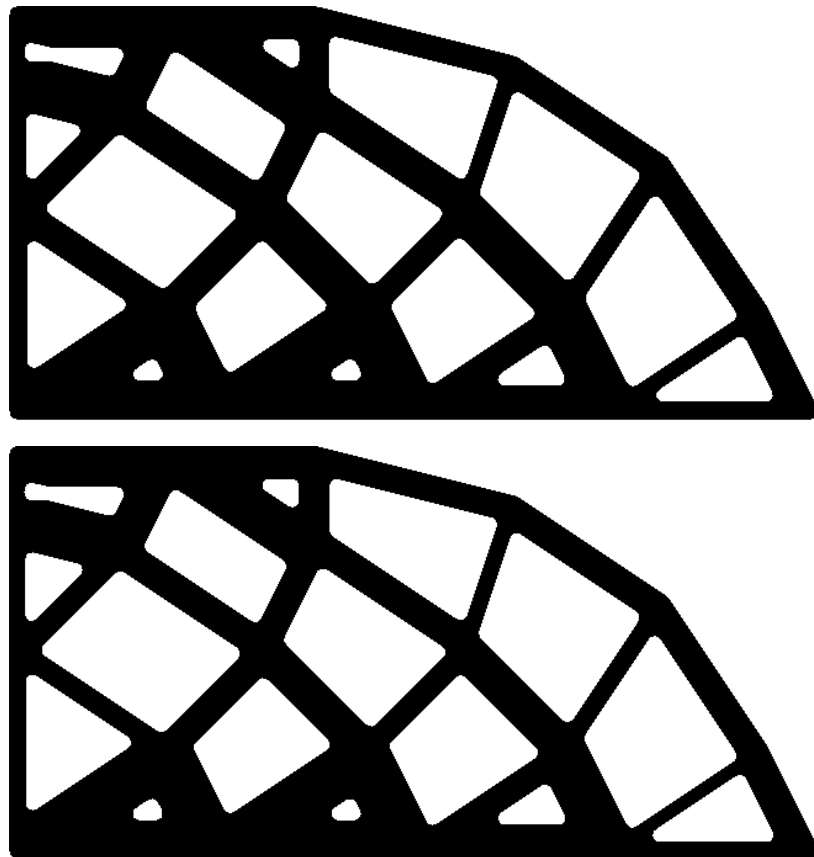


Figure 3.29: Shapes obtained by optimization with first order constraints (top), the volume has decreased to 0.20913, and optimization with second order constraints (bottom), the volume has decreased to 0.199525

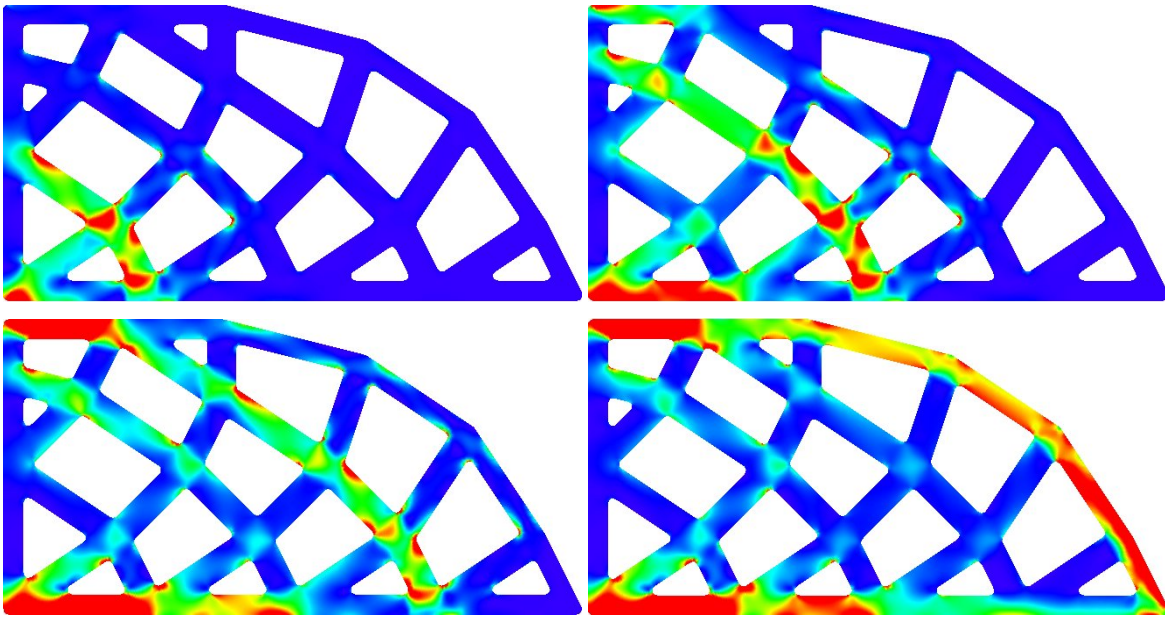



Figure 3.30: Visualization of the elastic energy for each scenario force for the benchmark shape. Values are arranged according to the color bar , where blue corresponds to zero and red corresponds to the maximum. The maximum is set to 250 for the first scenario (upper left) and the second one (upper right), 350 for the third (lower left) and 500 for the fourth scenario (lower right).

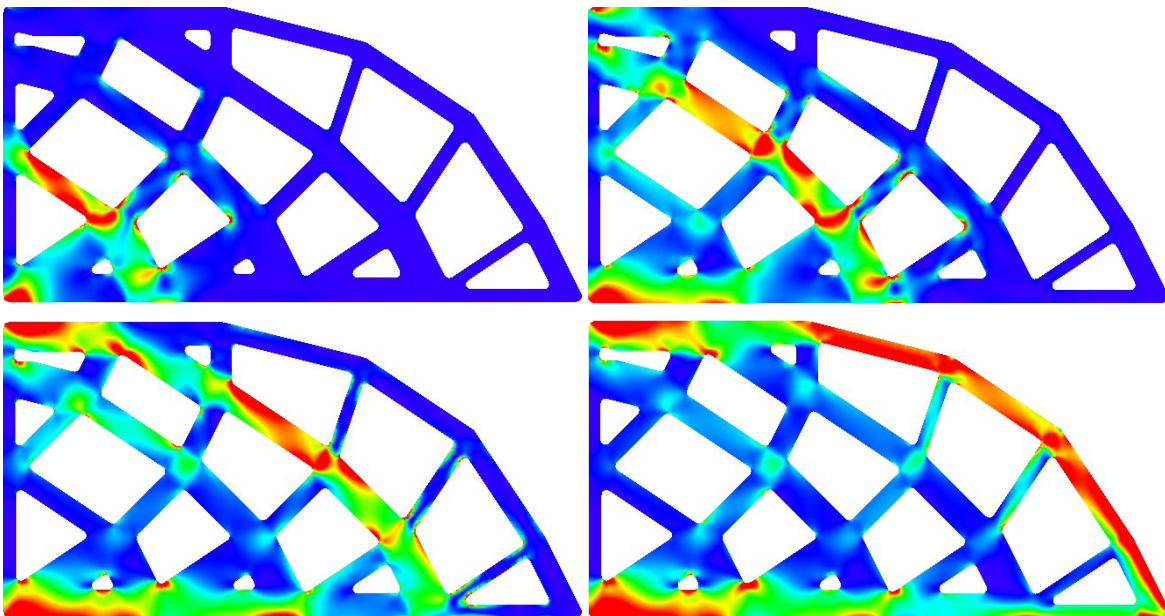


Figure 3.31: Visualization of the elastic energy for the four scenario forces (from top left to bottom right) for the shape obtained by optimization with first order constraints. Values are arranged with the same specification as in Fig. (3.30).

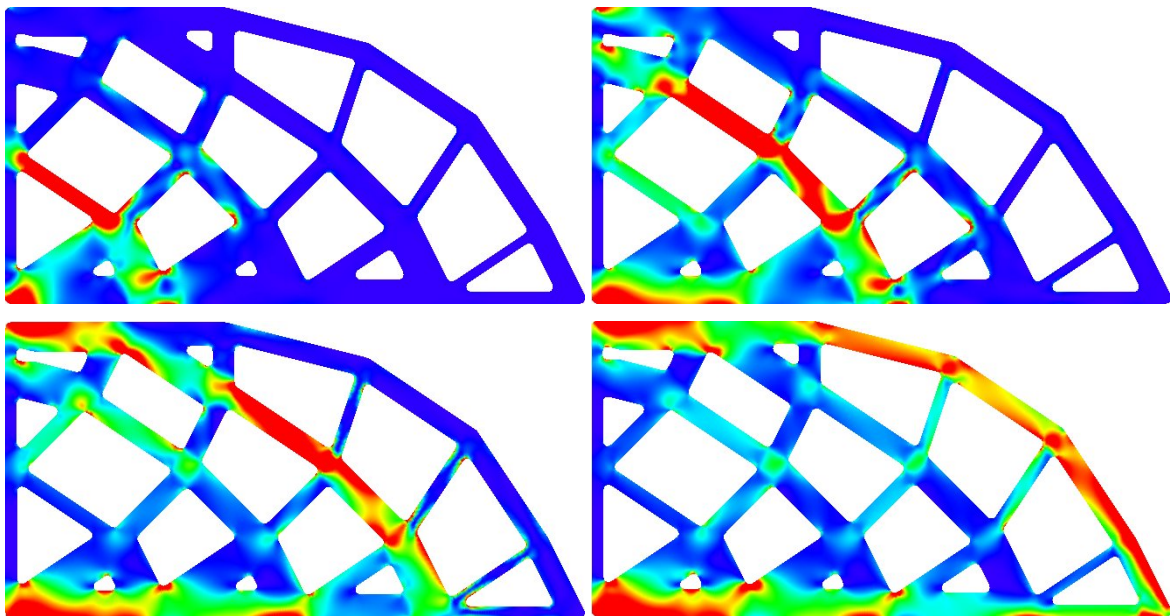


Figure 3.32: Similar to Fig. (3.30) and Fig. (3.31), the visualization of the elastic energy for each scenario force for the shape obtained by optimization with second order constraints is displayed.

4 Final Remarks - State of the Art

Shape optimization in general

Within the last decade, methods for solving shape optimization problems have undergone considerable improvements. Sensitivity analysis has been done for a wide range of problems with different underlying state equation [13, 15, 16, 46, 84, 103, 162] or variational inequalities [76, 95] as well as different objectives, for instance, image processing (or image registration) [91, 94, 96, 106] and structural design [164, 166]. Results regarding shape and topology sensitivity provide an analytical framework for adequate solution approaches. In some rare cases, even existence can be proven although subject to strong restrictions [12, 34, 35, 40–44, 71, 165]. Despite the fact that in most situations, existence, in general, can not be proven for the analytical model, the results obtained by solving the discretized model are applicable for real-world problems. A great challenge remains the numerical implementation for advanced applications. For common settings, see for instance section 2.6.1, we can rely on fairly robust methods to solve shape optimization problems, using level set methods [6, 14, 36, 92], the SIMP method [27–29, 87], or alternative methods [26, 69, 105, 111, 168].

The situation becomes more tricky when we go beyond this basic settings. For example, the investigation of micro structures requires further effort concerning modeling, analysis, and implementation [5, 18, 116]. Incorporating uncertainty, the way we do, results in nonlinear optimization problems with side constraints that are hard to tackle. There are excellent solvers available (e.g. [170]) for nonlinear problems, but due to the high computational costs (for each evaluation of the objective, a partial differential equation needs to be solved), the performance becomes almost inoperative.

Therefore, adapted solution approaches exploiting the special structure of the problems need to be developed.

Uncertainty

Recently, incorporating uncertainty in shape and topology optimization has attracted more and more attention. Identification and classification of uncertainties have become an issue, for instance, in aerodynamic shape optimization, see [98, 143]. There, aleatory uncertainties, e.g. atmospheric turbulences or geometrical uncertainties, are considered and incorporated in a robust optimization setting.

In structural mechanics, unknown material properties, geometrical uncertainties, and stochastic loadings are an issue. Different approaches were employed for treatment of each special type of uncertainty.

Perturbation techniques are used to deal with geometrical uncertainties, which are modeled via stochastic fields in [108]. Stochastic collocation methods are used to model material and geometrical uncertainties in [107]. Stochastic loadings, based on a known probability distribution, are considered in the so-called Multiload case,

see [7, 11, 80, 109, 113, 176] for instance. Optimization approaches, without known distribution of the random forces, have been investigated in [1, 20, 25, 48, 49, 137]. In [8], a perturbation of the loads is considered and identifying a worst case perturbation enables to optimize the compliance functional in a robust (or worst case) sense. For a rather broad survey on modeling uncertainties, see the recently published monograph [118].

Robust optimization assumes that range information on the uncertain data is available, in stochastic programming, in addition, distributional information is present. Typical examples are the Multiload case (with distributional information) [7], and the robust approach in [25]. In this thesis, stochastic optimization approaches have been discussed. For a comprehensive survey on robust optimization the reader is referred to [4, 23, 24].

Two-Stage stochastic shape optimization

The perspective in this thesis links shape optimization under uncertainty to the field of stochastic programming. There, treatment of uncertainties has been a big issue in the past decades, as documented in the monographs [31, 47, 55, 60, 102, 127, 139], and a wide selection of models for handling risk is available for practical applications, see [21, 64, 126, 135, 136, 140, 171]. We emphasized models, for which we already had experiences from previous applications. It remains a future task to select further adequate 'risk-models' for shape optimization.

For example, besides incorporating uncertainty via random forces one could consider geometrical uncertainties such as microstructures.

Our investigation of the *expected-excess* and *excess-probability* models, motivated the step towards models with *stochastic dominance constraints*. First examples have been successfully investigated, but they suggest, that further investigations on method for solving the underlying nonlinear optimization problem are crucial for advanced applications, such as incorporation of microstructures. In this context, we aim at refined models concerning the optimization of local structures, for instance, as indicated in section 2.6.2 .

References

- [1] ADALI, S., BRUCH, J.C., SADEK, I., AND SLOSS, J. Robust shape control of beams with load uncertainties by optimally placed piezo actuators. *Structural and Multidisciplinary Optimization* 19, 4 (2000), 274–281.
- [2] ADALSTEINSSON, D., AND SETHIAN, J. A. The fast construction of extension velocities in level set methods. *Journal of Computational Physics* 148 (1999), 2–22.
- [3] ADAMS, R. *Sobolev Spaces*. No. Bd. 65 in Pure and Applied Mathematics. Academic Press, 1975.
- [4] ALBERS, S. Online algorithms: a survey. *Math. Programming* 97 (2003), 3–26.
- [5] ALLAIRE, G. *Shape Optimization by the Homogenization Method*, vol. 146. Springer Applied Mathematical Sciences, 2002.
- [6] ALLAIRE, G., DE GOURNAY, F., JOUVE, F., AND TOADER, A.-M. Structural optimization using topological and shape sensitivity via a level set method. *Control and Cybernetics* 34 (2005), 59–80.
- [7] ALLAIRE, G., AND JOUVE, F. A level-set method for vibration and multiple loads structural optimization. *Comput. Methods Appl. Mech. Engrg.* 194 (2005), 3269–3290.
- [8] ALLAIRE, G., JOUVE, F., AND DE GOURNAY, F. Shape and topology optimization of the robust compliance via the level set method. *ESAIM Control Optim. Calc. Var.* 14 (2008), 43–70.
- [9] ALLAIRE, G., JOUVE, F., AND TOADER, A. M. A level-set method for shape optimization. *C. R. Acad. Sci. Paris Sér. I* 334 (2002), 1125–1130.
- [10] ALT, H. W. *Lineare Funktionalanalysis: Eine anwendungsorientierte Einführung*. Springer, 2002.
- [11] ALVAREZ, F., AND CARRASCO, M. Minimization of the expected compliance as an alternative approach to multiload truss optimization. *Struct. Multidiscip. Optim.* 29 (2005), 470–476.
- [12] AMBROSIO, L., AND BUTTAZZO, G. An optimal design problem with perimeter penalization. *Calc. Var.* 1 (1993), 55–69.

- [13] AMSTUTZ, S. The topological asymptotic for the navier-stokes equation. *ESAIM:COCV* 11, 3 (2005), 401–425.
- [14] AMSTUTZ, S., AND ANDRÄ, H. A new algorithm for topology optimization using a level-set method. *Journal of Computational Physics* 216 (2006), 573–588.
- [15] AMSTUTZ, S., MASMOUDI, M., AND SAMET, B. The topological asymptotic for the helmholtz equation. *SIAM J. Control Optim.* 42, 5 (2003), 1523–1544.
- [16] AMSTUTZ, S., TAKAHASHI, T., AND VEXLER, B. Topological sensitivity analysis for time dependent problems. *ESAIM: Control, Optimisation and Calculus of Variations* 14 (2008), 427–455.
- [17] APEL, T. Anisotropic finite elements: Local estimates and applications, 1999.
- [18] AZ, D., AND BUTTAZZO, G. Some remarks on the optimal design of periodically reinforced structures. *Math. Mod. Num. Anal.* 23, 1 (1989), 53–61.
- [19] BABUSKA, I., AND AZIZ, A. K. On the angle condition in the finite element method. *SIAM J. Numer. Anal.* 13, 2 (1976), 214–226.
- [20] BANICHUK, N. V., AND NEITTAANMÄKI, P. On Structural Optimization with Incomplete Information. *Mechanics Based Design of Structures and Machines* 35 (2007), 75–95.
- [21] BASTIN, F., CIRILLO, C., AND TOINT, P. Convergence theory for nonconvex stochastic programming with an application to mixed logit. *Math. Program.* 108 (2006), 207–234.
- [22] BELYTSCHKO, T., MÖES, N., USUI, S., AND PARIMI, C. Arbitrary discontinuities in finite elements. *Int. J. Numer. Meth. Engng* 50, 4 (2001), 993–1013.
- [23] BEN-TAL, A., GHAOUI, L., AND NEMIROVSKI, A. *Robust Optimization*. Princeton Series in Applied Mathematics. Princeton University Press, 2009.
- [24] BEN-TAL, A., AND NEMIROVSKI, A. Robust optimization - methodology and applications. *Mathematical Programming* 92 (2002), 453–480.
- [25] BEN-TAL, A., NEMIROVSKI, A., KOČVARA, M., AND ZOWE, J. Free material design via semidefinite programming: the multiload case with contact conditions. *SIAM J. Optim.* 92 (1999), 813–832.
- [26] BENDSØE, M., AND KIKUCHI, N. Generating optimal topologies in structural design using homogenization methods. *Comput. Methods Appl. Mech. Engrg.* 71 (1988), 197–224.

- [27] BENDSØE, M., AND SIGMUND, O. *Topology optimization*. Springer-Verlag, Berlin, 1998.
- [28] BENDSØE, M. P. *Optimization of structural topology, shape, and material*. Springer-Verlag, Berlin, 1995.
- [29] BENDSØE, M. P., AND SIGMUND, O. *Topology Optimization: Theory, Methods and Applications*. Springer, 2003.
- [30] BERN, M., EPPSTEIN, D., AND GILBERT, J. Provably good mesh generation. In *Proceedings of the 31st Annual Symposium on Foundations of Computer Science* (Washington, DC, USA, 1990), SFCS '90, IEEE Computer Society, pp. 231–241 vol.1.
- [31] BIRGE, J. R., AND LOUVEAUX, F. *Introduction to Stochastic Programming*. Springer Series in Operations Research, 1997.
- [32] BORZÌ, A., AND SCHULZ, V. *Computational Optimization of Systems Governed by Partial Differential Equations*, vol. 8 of *Computational science and engineering*. SIAM, 2012.
- [33] BRAESS, D. *Finite Elemente - Theorie, schnelle Löser und Anwendungen in der Elastizitätstheorie*. Springer, 2007.
- [34] BUCUR, D. How to prove existence in shape optimization. *Control and Cybernetics* 34, 1 (2005), 103–116.
- [35] BUCUR, D., AND BUTTAZZO, G. *Variational Methods in Shape Optimization Problems*. Progress in Nonlinear Differential Equations and Their Applications, Birkhäuser, 2005.
- [36] BURGER, M. A framework for the konstruktion of level set methods for shape optimization and reconstruction. *Interfaces and Free Boundaries* 5 (2003), 301–329.
- [37] BURGER, M., HACKL, B., AND RING, W. Incorporating Topological Derivatives into Level Set Methods. *J. Comp. Phys.* 194 (2004), 344–362.
- [38] BURGER, M., AND OSHER, S. A Survey on Level Set Methods for Inverse Problems and Optimal Design. *European Journal of Applied Mathematics* 16 (2005), 263–301. Under consideration for publication in Euro. J. Appl. Math.
- [39] BUTTAZZO, G. Some Relaxation Problems in Optimal Control Theory. *J. Math. Anal. Appl.* 125 (1987), 273–287.

- [40] BUTTAZZO, G. On the existence of minimizing domains for some shape optimization problems. vol. 3, ESAIM, pp. 51–64.
- [41] BUTTAZZO, G., AND GUASONI, P. Shape Optimization Problems over Classes of Convex Domains. *J. Conv. Anal.* 4, 2 (1997), 343–351.
- [42] BUTTAZZO, G., AND MASO, G. D. Shape Optimization for Dirichlet Problems: Relaxed Formulation and Optimality Conditions. *Appl. Math. Optim.* 23 (1991), 17–49.
- [43] BUTTAZZO, G., AND MASO, G. D. An Existence Result for a Class of Shape Optimization Problems. *Arch. Rational Mech. Anal.* 122 (1993), 183–195.
- [44] BUTTAZZO, G., AND TREBESCHI, P. The role of monotonicity in some shape optimization problems. *nn* 122 (1993), 183–195.
- [45] CÉA, J. Conception optimale ou identification de formes, calcul rapide de la dérivée directionnelle de la fonction coût. *Math. Model. Num. Anal.* 20 (1986), 371–402.
- [46] CARDONE, G., NAZAROV, S. A., AND SOKOLOWSKI, J. Asymptotic analysis, polarization matrices, and topological derivatives for piezoelectric materials with small voids. *SIAM J. Control and Optimization* 48, 6 (2010), 3925–3961.
- [47] CHANG, F. R. *Stochastic Optimization in Continuous Time*. Cambridge University Press, Cambridge, 2004.
- [48] CHERKAEV, A., AND CHERKAEV, E. Stable optimal design for uncertain loading conditions. In *Homogenization*, V. B. et al., Ed., vol. 50 of *Series on Advances in Mathematics for Applied Sciences*. World Scientific, Singapore, 1999, pp. 193–213.
- [49] CHERKAEV, A., AND CHERKAEV, E. Principal Compliance and Robust Optimal Design. *Journal of Elasticity* 72 (2003), 71–98.
- [50] CIARLET, P. G. *Mathematical Elasticity, Volume I: Three-Dimensional Elasticity*. North-Holland, Amsterdam, 1988.
- [51] CONTI, S., HELD, H., PACH, M., RUMPF, M., AND SCHULTZ, R. Shape Optimization Under Uncertainty – A Stochastic Programming Perspective. *SIAM J. Optim.* 19 (2009), 1610–1632.
- [52] CONTI, S., HELD, H., PACH, M., RUMPF, M., AND SCHULTZ, R. Risk Averse Shape Optimization. *SIAM J. Control and Optimization* 49, 3 (2011), 927–947.

- [53] CORREA, R., AND SEEGER, A. Directional derivative of a minimax function. *Nonlinear Anal. Vol 9* (1985), 13–22.
- [54] DAMBRINE, M., AND VIAL, G. On the influence of a boundary perforation on the dirichlet energy. *Control and Cybernetics 34*, 1 (2005), 117–136.
- [55] DANTZIG, G. B. Linear programming under uncertainty. *Management Science 1* (1955), 197–206.
- [56] DE, G. F. Velocity extension for the level-set method and multiple eigenvalues in shape optimization. *SIAM J. Control and Optimization 45*, 1 (2006), 343–367.
- [57] DELFOUR, M. C., AND ZOLÉSIO, J.-P. Structure of shape derivatives for nonsmooth domains. *J. Funct. Anal. 104* (1992), 1–33.
- [58] DELFOUR, M. C., AND ZOLÉSIO, J.-P. *Shapes and Geometries. Analysis, Differential Calculus, and Optimization*. Siam, Philadelphia, 2001.
- [59] DENTCHEVA, D., AND RUSZCZYŃSKI, A. Optimization with stochastic dominance constraints. *SIAM J. Optim. 14*, 2 (2003), 548–566.
- [60] DENTCHEVA, D., RUSZCZYŃSKI, A., AND SHAPIRO, A. *Lectures on Stochastic Programming: Modeling and Theory*. MPS-SIAM Series on Optimization. Siam, 2009.
- [61] DEUFLHARD, P., AND HOHMANN, A. *Numerical Analysis: A First Course in Scientific Computation*. Walter de Gruyter, 1995.
- [62] DU, Q., AND WANG, D. Tetrahedral mesh generation and optimization based on centroidal Voronoi tesselations. *International Journal for Numerical Methods in Engineering 56* (2003), 1355–1373.
- [63] ECKHAUS, W. *Asymptotic analysis of singular perturbations*. North-Holland, Amsterdam, 1979.
- [64] EICHHORN, A., AND RÖMISCH, W. Polyhedral Risk Measures in Stochastic Programming. *SIAM J. on Optimization 16*, 1 (2005), 69–95.
- [65] EKELAND, I., AND TEMAN, R. *Convex Analysis and Variation Problems. Studies in Mathematics and its Applications Vol 1* (1976).
- [66] ELLIOTT, C., HINTERMÜLLER, M., LEUGERING, G., AND SOKOLOWSKI, J. Special issue on advances in shape and topology optimization: theory, numerics and new applications areas. *Optimization Methods and Software 26*, 4-5 (2011), 511–512.

- [67] EPPLER, K. On Hadamard representation of shape gradients — a computational guide. *Preprint SPP 1253-79*.
- [68] EPPLER, K. On Hadamard shape gradient representations in linear elasticity. *Deutsche Forschungsgemeinschaft, Preprint 1253-104, Schwerpunktprogramm 1253 “Optimization with Partial Differential Equations”* (2010).
- [69] EPPLER, K., AND HARBRECHT, H. Compact gradient tracking in shape optimization. *Comp. Opt. and Appl.* 39, 3 (2008), 297–318.
- [70] EPPLER, K., AND HARBRECHT, H. On a kohn-vogelius like formulation of free boundary problems. *Comp. Opt. and Appl.* 52, 1 (2012), 69–85.
- [71] EPPLER, K., HARBRECHT, H., AND SCHNEIDER, R. On convergence in elliptic shape optimization. *SIAM J. Control and Optimization* 46, 1 (2007), 61–83.
- [72] ESCHENAUER, H., SCHUMACHER, A., AND KOBOLEV, V. V. Bubble method for topology and shape optimization of structures. *Structural optimization* 8 (1994), 42–51.
- [73] EVANS, L. C. *Partial Differential Equations*, vol. 19. AMS Graduate Studies in Mathematics, 2002.
- [74] FEIJÓO, R. A., NOVOTNY, A. A., PADRA, C., AND TAROCO, E. O. The Topological-Shape Sensitivity Analysis and its Applications in Optimal Design. *Mecánica Computacional XXI*, 30 (2002), 2687–2711.
- [75] FRAENKEL, L. E. On the method of matched asymptotic expansions. *Proc. Cambridge Phil. Soc.* 65, I II III (1969), 209–231, 233–261 and 263–284.
- [76] FULMANSKI, P., LAURAIN, A., SCHEID, J., AND SOKOLOWSKI, J. A level set method in shape and topology optimization for variational inequalities. *Applied Mathematics and Computer Science* 17, 3 (2007), 413–430.
- [77] GARREAU, S., GUILLAUME, P., AND MASMOUDI, M. The Topological Asymptotic for PDE Systems: The Elasticity Case. *SIAM J. Control Optim.* 39, 6 (2001), 1756–1778.
- [78] GOBERNA, M., AND LÓPES, M. Linear Semi-Infinite Optimization.
- [79] GUEDES, J., RODRIGUES, H. C., AND BENDSØE, M. A material optimization model to approximate energy bounds for cellular materials under multiload conditions. *Struct. Multidiscip. Optim.* 25 (2003), 446–452.

- [80] GUEDES, J. M., RODRIGUES, H. C., AND BENDSØE, M. P. A material optimization model to approximate energy bounds for cellular materials under multiload conditions. *Struct. Multidiscip. Optim.* 25 (2003), 446–452.
- [81] HACKBUSCH, W. *Multi-Grid Methods and Applications*. Springer Series in Computational Mathematics, 1985.
- [82] HACKBUSCH, W., AND SAUTER, S. Composite Finite Elements for the approximation of PDEs on domains with complicated micro-structures. *Numerische Mathematik* 75 (1997), 447–472.
- [83] HAN, X., XU, C., AND PRINCE, J. L. A Topology Preserving Level Set Method for Geometric Deformable Models. *IEEE Transactions on Pattern Analysis and Machine Intelligence* 25, 6 (2003), 755–768.
- [84] HARBRECHT, H., AND TAUSCH, J. On the numerical solution of a shape optimization problem for the heat equation. *SIAM J. Scientific Computing* 35, 1 (2013).
- [85] HASLINGER, J., KOCVARA, M., LEUGERING, G., AND STINGL, M. Multi-disciplinary free material optimization. *SIAM Journal of Applied Mathematics* 70, 7 (2010), 2709–2728.
- [86] HASLINGER, J., AND MÄKINEN, R. *Introduction to Shape Optimization: Theory, Approximation, and Computation*. Advances in Design and Control. SIAM, 2003.
- [87] HASLINGER, J., AND NEITTAANMÄKI, P. *Finite Element Approximation for Optimal Shape, Material and Topology Design*. Wiley, 1997.
- [88] HAZRA, S. B., AND SCHULZ, V. Simultaneous pseudo-timestepping for aerodynamic shape optimization problems with state constraints. *SIAM J. Scientific Computing* 28, 3 (2006), 1078–1099.
- [89] HE, L., KAO, C., AND OSHER, S. Incorporating topological derivatives into shape derivatives based level set methods. *J. Comp. Phys.* 225, 1 (2007), 891–909.
- [90] HELD, H. *Shape optimization under uncertainty from a stochastic programming point of view*. PhD thesis, Universität Duisburg-Essen, 2008.
- [91] HINTERMÜLLER, M. A combined shape-newton and topology optimization technique in real-time image segmentation, 2004.
- [92] HINTERMÜLLER, M. Fast level-set based algorithms using shape and topological sensitivity information. *Control and Cybernetics* 34, 1 (2005), 305–324.

- [93] HINTERMÜLLER, M., AND LAURAIN, A. Where to place a hole? *European Consortium for Mathematics in Industry, ECMI Newsletter 41* (2007).
- [94] HINTERMÜLLER, M., AND LAURAIN, A. Multiphase image segmentation and modulation recovery based on shape and topological sensitivity. *Journal of Mathematical Imaging and Vision 35*, 1 (2009), 1–22.
- [95] HINTERMÜLLER, M., AND LAURAIN, A. Optimal shape design subject to elliptic variational inequalities. *SIAM J. Control and Optimization 49*, 3 (2011), 1015–1047.
- [96] HINTERMÜLLER, M., LAURAIN, A., AND NOVOTNY, A. A. Second-order topological expansion for electrical impedance tomography. *Adv. Comput. Math. 36*, 2 (2012), 235–265.
- [97] HINTERMÜLLER, M., AND RING, W. An inexact newton-cg-type active contour approach for the minimization of the mumford-shah functional. *Journal of Mathematical Imaging and Vision 20* (2004), 19–42.
- [98] HUYSE, L. *Free-form airfoil shape optimization under uncertainty using maximum expected value and second-order second-moment strategies*. ICASE report ; no. 2001-18. ICASE, NASA Langley Research Center Available from NASA Center for Aerospace Information, Hampton, VA, 2001.
- [99] IGUERNANE, M., NAZAROV, S. A., ROCHE, J. R., SOKOLOWSKI, J., AND SZULC, K. Topological derivatives for semilinear elliptic equations. *Applied Mathematics and Computer Science 19*, 2 (2009), 191–205.
- [100] IL’IN, A. *Matching of asymptotic expansions of solutions of boundary value problems*, translation of mathematical monographs ed., vol. 102. AMS, Providence, 1992.
- [101] ITO, K., KUNISCH, K., SCHULZ, V., AND GHERMAN, I. Approximate nullspace iterations for kkt systems. *SIAM J. Matrix Analysis Applications 31*, 4 (2010), 1835–1847.
- [102] KALL, P., AND WALLACE, S. W. *Stochastic Programming*. Wiley-Interscience Series in Systems and Optimization, 1994.
- [103] KOWALEWSKI, A., LASIECKA, I., AND SOKOLOWSKI, J. Sensitivity analysis of hyperbolic optimal control problems. *Comp. Opt. and Appl. 52*, 1 (2012), 147–179.
- [104] KUNISCH, K., AND ITO, K. *Lagrange Multiplier Approach to Variational Problems and Applications*. Advances in Design and Control. SIAM, 2008.

- [105] LAPORTE, E., AND TALLEC, P. L. *Numerical Methods in Sensitivity Analysis and Shape Optimization*. Birkhäuser, 2003.
- [106] LARRABIDE, I., FELJÓO, R., NOVOTNY, A., AND TAROCO, E. Topological derivative: A tool for image processing. *Computers & Structures* 86, 13-14 (2008), 1386–1403.
- [107] LAZAROV, B. S., AND SCHEVENELS, M. Topology optimization considering material and geometric uncertainties using stochastic collocation methods. *Structural and Multidisciplinary Optimization* 46, 4 (2012), 597–612.
- [108] LAZAROV, B. S., SCHEVENELS, M., AND SIGMUND, O. Topology optimization with geometric uncertainties by perturbation techniques. *International Journal for Numerical Methods in Engineering* 90, 11 (2012), 1321–1336.
- [109] LEUGERING, G., KOČVARA, M., AND STINGL, M. A sequential convex semidefinite programming algorithm with an application to multiple-load free material optimization. *SIAM Journal on Optimization* 20, 1 (2009), 130–155.
- [110] LIEHR, F., PREUSSER, T., RUMPF, M., SAUTER, S., AND SCHWEN, L. Composite finite elements for 3d image based computing. *Computing and Visualization in Science* 12 (2009), 171–188.
- [111] MAAR, B., AND SCHULZ, V. Interior point multigrid methods for topology optimization. *Struct Multidisc Optim* 19 (2000), 214–224.
- [112] MAZ’YA, V., NAZAROV, S., AND PLAMENEVSKIJ, B. *Asymptotic theory of elliptic boundary value problems in singularly perturbed domains*, vol. 1 and 2. Birkhäuser Verlag, 2000.
- [113] MELCHERS, R. Optimality-criteria-based probabilistic structural design. *Structural and Multidisciplinary Optimization* 23, 1 (2001), 34–39.
- [114] MÜLLER, A., AND STOYAN, D. *Comparison Methods for Stochastic Models and Risks*. Wiley, 2002.
- [115] MURAT, F., AND SIMON, S. Etudes de problèmes d’optimal design. vol. 41, Springer, pp. 54–62.
- [116] MURAT, F., AND TARTAR, L. *Calcul des variations et homogénéisation, in Les Méthods de l’homogénéisation: Théorie et Applications en Physique*. Coll. Dir Etudes et Recherches EDF, Eyrolles, 1985, pp. 319–369. (engl. translation A. Cherkaev & R. V. Kohn eds. (1994), pp. 139-173).

- [117] NAZAROV, S. A., AND SOKOLOWSKI, J. The topological derivative of the dirichlet integral due to formation of a thin ligament. *Siberian Math. J.* 45, Issue 2 (March-April 2004), 341–355.
- [118] NEITTAANMÄKI, P., AND BANICHUK, N. V. *Structural Optimization with Uncertainties*, vol. 162 of *Solid Mechanics and Its Applications*. 2010.
- [119] NEUMANN, J., AND MORGENSTERN, O. *Theory of games and economic behavior*. Princeton University Press, 1944.
- [120] OGRYCZAK, W., AND RUSZCZYŃSKI, A. From stochastic dominance to mean-risk models: Semideviations as risk measures. *European Journal of Operational Research* 116 (1999), 33–50.
- [121] OGRYCZAK, W., AND RUSZCZYŃSKI, A. On consistency of stochastic dominance and mean–semideviation models. In *Mathematical Programming* (2001), vol. 89, pp. 217–232.
- [122] OGRYCZAK, W., AND RUSZCZYŃSKI, A. Dual stochastic dominance and related mean-risk models. *SIAM J. on Optimization* 13, 1 (2002), 60–78.
- [123] OSHER, S., AND FEDKIW, R. *Level set methods and dynamic implicit surfaces*, vol. 153 of *Applied Mathematical Sciences*. Springer-Verlag, New York, 2003.
- [124] OSHER, S., AND FEDKIW, R. P. Level Set Methods : An Overview and Some Recent Results. *J. Comput. Phys.* 169 (2001), 463–502.
- [125] OSHER, S. J., AND SETHIAN, J. A. Fronts propagating with curvature dependent speed. Algorithms based on the Hamilton-Jacobi formulation. *J. Comput. Phys.* 79 (1988), 12.
- [126] PENNANEN, T. Epi-convergent discretizations of multistage stochastic programs. *Mathematics of Operations Research* 30 (2005), 245–256.
- [127] PFLUG, G. C., AND RÖMISCH, W. *Modeling, Measuring and Managing Risk*. World Scientific, Singapore, 2007.
- [128] PIRONEAU, O. *Optimal shape design for elliptic systems*. Springer-Verlag, New York, 1984.
- [129] PRANDTL, L. *Über Flüssigkeitsbewegungen bei sehr kleiner Reibung*. Proc. Internat. Congr. Math. (Heidelberg 1904). Leipzig, 1905, pp. 484–491.
- [130] PRECHTEL, M., LEUGERING, G., STEINMANN, P., AND STINGL, M. Optimal design of brittle composite materials: a nonsmooth approach. *J. Optimization Theory and Applications* 155, 3 (2012), 962–985.

- [131] PRÉKOPA, A. *Stochastic Programming*. Kluwer, Dordrecht, 1995.
- [132] RECH, M., SAUTER, S., AND SMOLIANSKI, A. Two-scale composite finite element method for the dirichlet problem on complicated domains. *Numer. Math.* 102, 4 (2006), 681–708.
- [133] REEMTSEN, R., AND RÜCKMANN, J.-J. E. *Semi-Infinite Programming*.
- [134] RIIS, M., AND SCHULTZ, R. Applying the Minimum Risk Criterion in Stochastic Recourse Programs. *Comput. Optim. Appl.* 24, 2-3 (2003), 267–287.
- [135] RIIS, M., AND SCHULTZ, R. Applying the Minimum Risk Criterion in Stochastic Recourse Programs. *Computational Optimization and Applications* 24 (2003), 267–287.
- [136] ROCKAFELLAR, R. T., URYASEV, S., AND ZABARANKIN, M. Generalized deviations in risk analysis. *Finance and Stochastics* 10, 1 (01 2006), 51–74.
- [137] RUMIGNY, N., PAPADOPOULOS, P., AND POLAK, E. On the use of consistent approximations in boundary element-based shape optimization in the presence of uncertainty. *Comput. Methods Appl. Mech. Engrg.* 196 (2007), 3999–4010.
- [138] RUPPERT, J. A delaunay refinement algorithm for quality 2-dimensional mesh generation. *J. Algorithms* 18, 3 (May 1995), 548–585.
- [139] RUSZCZYŃSKI, A., AND SHAPIRO, A. *Handbooks in Operations Research and Management Science: Stochastic Programming*, vol. 10. Elsevier Science & Technology, 2003.
- [140] RUSZCZYŃSKI, A., AND SHAPIRO, A. Optimization of Convex Risk Functions. *Math. Oper. Res.* 31, 3 (2006), 433–452.
- [141] SAAD, Y. *Iterative Methods for Sparse Linear Systems*, 2nd ed. Society for Industrial and Applied Mathematics, Philadelphia, PA, USA, 2003.
- [142] SAUTER, S. A., AND WARNKE, R. Composite finite elements for elliptic boundary value problems with discontinuous coefficients. *Computing* 77, 1 (2006), 29–55.
- [143] SCHILLINGS, C., SCHMIDT, S., AND SCHULZ, V. Efficient shape optimization for certain and uncertain aerodynamic design. *Computers and Fluids* 46, 1 (2011), 78–87.
- [144] SCHMIDT, S., ILIC, C., GAUGER, N., AND SCHULZ, V. Airfoil design for compressible inviscid flow based on shape calculus. *Optimization and Engineering* 12, 3 (2011), 349–369.

- [145] SCHMIDT, S., AND SCHULZ, V. Impulse response approximations of discrete shape Hessians with application in CFD. *SIAM J. Control and Optimization* 48, 4 (2009), 2562–2580.
- [146] SETHIAN, J. A. Curvature and the evolution of fronts. *Commun. Math. Phys.* 101 (1985), 487.
- [147] SETHIAN, J. A. Numerical algorithms for propagating interfaces: Hamilton–Jacobi equations and conservation laws. *J. Diff. Geom.* 31 (1990), 131.
- [148] SETHIAN, J. A. A fast marching level set method for monotonically advancing fronts. *Proc. Nat. Acad. Sci.* 93, 4 (1996).
- [149] SETHIAN, J. A. *Level Set Methods: Evolving Interfaces in Geometry, Fluid Mechanics, Computer Vision and Materials Sciences*. Cambridge Univ. Press, 1996.
- [150] SETHIAN, J. A. *Level-Set Methods and fast marching methods: evolving interfaces in computational geometry, fluid mechanics, computer vision and materials science*. Cambridge University Press, 1999.
- [151] SETHIAN, J. A. Evolution, implementation, and application of level set and fast marching methods for advancing fronts. *J. Comput. Phys.* 169, 2 (2001), 503–555.
- [152] SETHIAN, J. A., AND WIEGMANN, A. Structural boundary design via level-set and immersed interface methods. *J. Comp. Phys.* 163 (2000), 489–528.
- [153] SHAKED, M., AND SHANTIKUMAR, J. G. *Stochastic Orders*. Springer Series in Statistics. Springer, 2007.
- [154] SHEWCHUK, J. R. Tetrahedral mesh generation by delaunay refinement. Proceeding of the 14th Annual ACM Symposium on Computational Geometry, ACM Press, pp. 86–95.
- [155] SHEWCHUK, J. R. An introduction to the conjugate gradient method without the agonizing pain, 1994.
- [156] SHEWCHUK, J. R. Triangle: Engineering a 2d quality mesh generator and delaunay triangulator. In *Applied Computational Geometry: Towards Geometric Engineering*, (1996), vol. 1146 of *Lecture Notes in Computer Science*, Springer-Verlag, pp. 203–222.
- [157] SHEWCHUK, J. R. What is a good linear element? interpolation, conditioning, and quality measures. In *Proceedings of the 11th International Meshing Roundtable* (2002), pp. 115–126.

- [158] SIMON, J. Differentiation with respect to the domain in boundary value problems. *Num. Funct. Anal. Optimz.* 2 (1980), 649–687.
- [159] SKINNER, L. A. Matched asymptotic expansions of integrals. *IMA J. Appl. Math* 50 (1993), 77–90.
- [160] SMITH, D. R. *Singular-perturbation theory*. Cambridge University Press, Cambridge, 1985.
- [161] SOKOŁOWSKI, J., AND NOVOTNY, A. *Topological Derivatives in Shape Optimization*. Interaction of Mechanics and Mathematics. Springer, 2013.
- [162] SOKOŁOWSKI, J., AND STEBEL, J. Shape sensitivity analysis of incompressible non-newtonian fluids. In *System Modelling and Optimization* (2011), pp. 427–436.
- [163] SOKOŁOWSKI, J., AND ŻOCHOWSKI, A. On the Topological Derivative in Shape Optimization. *SIAM J. Control Optim.* 37, 4 (1999), 1251–1272.
- [164] SOKOŁOWSKI, J., AND ŻOCHOWSKI, A. Topological Derivatives of Shape Functionals for Elasticity Systems. *Mech. Struct. & Mach.* 29, 3 (2001), 331–349.
- [165] SOKOŁOWSKI, J., AND ŻOCHOWSKI, A. Optimality Conditions for Simultaneous Topology and Shape Optimization. *SIAM Journal on Control and Optimization* 42, 4 (2003), 1198–1221.
- [166] SOKOŁOWSKI, J., AND ZOCHOWSKI, A. *IUTAM Symposium on Topological Design Optimization of Structures, Machines and Materials*, vol. 137 of *Solid Mechanics and its Applications*. springer, 2006, pp. 479–491.
- [167] SOKOŁOWSKI, J., AND ZOLÉSIO, J. P. *Introduction to Shape Optimization: Shape Sensitivity Analysis*. Springer Series in Computational Mathematics. Springer, 1992.
- [168] STOLPE, M., AND SVANBERG, K. Modelling topology optimization problems as linear mixed 0-1 programs. *Int. J. Numer. Meth. Engng* 57 (2003), 723–739.
- [169] TARTAR, L. An introduction to the homogenization method in optimal design. In *Lecture Notes in Mathematics* (2001), vol. 1740 of *Optimal shape design*, Springer, pp. 47–156.
- [170] WÄCHTER, A., AND BIEGLER, L. T. On the Implementation of a Primal-Dual Interior Point Filter Line Search Algorithm for Large-Scale Nonlinear Programming. *Mathematical Programming* 106, 1 (2006), 25–57.

- [171] WALLACE, S. W., AND ZIEMBA, W. T. *Applications of Stochastic Programming*. MPS-SIAM Series on Optimization. SIAM and MPS, 2005.
- [172] WANG, M., WANG, X., AND GUO, D. A level-set method for structural topology optimization. *Comput. Methods Appl. Mech. Engrg.* 192 (2003), 227–246.
- [173] WARNKE, R. *Schnelle Löser für elliptische Randwertprobleme mit springenden Koeffizienten*. PhD thesis, Zürich, 2003. Dissertation.
- [174] WIEGMANN, A., AND BUBE, K. P. The explicit-jump immersed interface method: Finite difference methods for pde with piecewise smooth solutions. *Siam J. Numer. Anal* 37, 3 (2000), 827–862.
- [175] ZHAO, H.-K., CHAN, T., MERRIMAN, B., AND OSHER, S. A variational level set approach to multiphase motion. *Journal of Computational Physics* 127 (1996), 179–195.
- [176] ZHUANG, C., XIONG, Z., AND DING, H. A level set method for topology optimization of heat conduction problem under multiple load cases. *Comput. Methods Appl. Mech. Engrg.* 196 (2007), 1074–1084.